Polyester functionalisation for mycobacterial capture

by
Benjamin Jacobus Cillié van der Westhuizen

Department of Chemistry and Polymer Science

University of Stellenbosch

Thesis presented in fulfilment of the requirements for the degree of Master of Science in Chemistry and Polymer Science in the Faculty of Science at Stellenbosch University

M.Sc (Chemistry and Polymer Science)

Supervisor: Prof A.J. van Reenen
Co-supervisor: Dr Lizl Cronje

March 2018

Declaration

By submitting this thesis electronically, I declare that the entirety of the work contained therein is my own, original work, that I am the sole author thereof (save to the extent explicitly otherwise stated), that reproduction and publication thereof by Stellenbosch University will not infringe any third party rights and that I have not previously in its entirety or in part submitted it for obtaining any qualification.

Date: March 2018

Acknowledgements

I would like to hereby acknowledge and give thanks to the following people. Without their support, directing and assistance this thesis would not have been possible.

Firstly, I would like to thank my supervisor, Professor van Reenen for his unfaltering support and guidance throughout this project.

The polyolefin research group, for their inputs and assistance. Mrs Adine Gericke, for her extensive knowledge of materials.

The staff of the Department of Chemistry and Polymer Science, for their kindness and support. The staff of the Central Analytical Facility for their time and expertise.

Prof Dicks, for the use of his laboratory facilities and especially Anton du Preez Van Staden for culturing the BCG bacteria which was used in this thesis.

My friends and family, for their encouragement.

Finally, I would like to thank Alta-Marié Bruwer for her tolerance and enduring support.

Abstract

Tuberculosis (TB) is one of the deadliest diseases known to man and ranks among the top ten global causes of fatalities. This stems from the fact that *Mycobacterium tuberculosis* (*Mtb*), the causative pathogenic bacterial species responsible for TB, has developed extensive mechanisms to elude detection and eradication by the human immune system. While its diagnosis in adults with a negative human immunodeficiency virus (HIV) status is commonplace, paediatric diagnosis can be arduous even with the aid of sophisticated techniques. Therefore, paediatric cases often do not receive the priority they deserve. This problem is further amplified in developing countries, since they are most affected by the disease and also do not have access to sophisticated diagnostic techniques.

Diagnosis of TB in developing countries is primarily based on sputum smear microscopy, a proficient but limited technique. Children often develop a paucibacillary form of TB, in which case the concentration of bacteria in their sputum falls below the lowest limit of detection for microscopic detection. If the TB bacilli can be concentrated within the specimen collected from patients, the detection limit can likely be met, allowing for rapid detection. Since the bacilli are prone to adhere to polymeric surfaces, a high surface to volume, fibrous matrix is of interest.

In this study, various means of surface functionalising poly(ethylene terephthalate) (PET) microfibres with a biological entity was investigated. The entity of interest was a lectin based ahesin, namely Concanavalin A (Con A). Con A has an affinity for the mannose groups on the *Mtb* cell wall. By functionalising these fibres, a substrate was created which could potentially act as a concentrating and capturing platform for the *Mtb* bacilli. It follows that since these types of fibres are commonly used for specimen collection swabs, an *Mtb* specific buccal swab could be created. This would allow bacilli collection by means of their entrapment upon wiping the oral mucosa of a patient with the swab.

Affinity studies between the modified PET microfibres and an attenuated strain of Mycobacterium bovis namely the bacillus of Calmette-Guérin (BCG) were conducted. The strain of BCG used, possessed a fluorescent protein reporter gene, namely mCherry-BCG. These studies were also conducted as a function of serial dilutions, to evaluate the *Mtb* capture ability of the modified substrates. The successful capture of BCG by the substrates was confirmed by the aid of confocal fluorescence microscopy (CFM) and scanning electron microscopy (SEM). These studies revealed that all of the surface functionalised substrates were able to successfully capture the bacteria. This was possible down to culture concentrations which fell well below the detection threshold of sputum smear microscopy. The surface modification, which proved most

successful at BCG capture, was a cross-linked protein aggregate (CLPA) derivative. CLPA was covalently bound to the surface of the fibres, by means of glutaraldehyde (GA).

Opsomming

Tuberkulose (TB) is een van die dodelikste siektes bekend aan die mens, en word beskou as op die ranglys van die top tien oorsake van sterftes wêreldwyd. Dit is vanweë die feit dat *Mikobakterium tuberkulose* (*Mtb*), die patogene bakteriese spesie wat verantwoordelik is vir TB, omvattende meganismes ontwikkel het, wat sy opsporing en uitwissing deur die menslike immuunstelsel te fnuik. Terwyl TB allerdaag by volwassenes met 'n negatiewe menslike immuniteitsgebreksvirus (MIV)-status gediagnoseer word, kan pediatriese diagnose moeilik wees selfs met behulp van gesofistikeerde tegnieke. Pediatriese gevalle ontvang dus dikwels nie die prioriteit wat hulle toekom nie. Hierdie probleem word verder vergroot in ontwikkelende lande, aangesien hulle die meeste deur die siekte geraak word en nie toegang het tot gesofistikeerde diagnostiese tegnieke nie.

Diagnose in ontwikkelende lande word hoofsaaklik gebaseer op sputum-smeer-mikroskopie, 'n toereikende, maar beperkte tegniek. Kinders ontwikkel dikwels TB met 'n geringe bacilli telling (paucibacillary TB), in welke geval die konsentrasie van bakterieë in hul sputum onder die laagste opsporingsperk vir mikroskopiese opsporing val. As die TB-bacilli gekonsentreer kan word binne die monster wat by pasiënte versamel word, kan die opsporingsperke waarskynlik bereik word, wat vinnige diagnose moontlik maak. Aangesien die bacilli geneig is om aan polimeriese oppervlaktes te heg, is 'n hoë oppervlak tot volume, veselagtige, matriks van belang.

In hierdie studie is verskeie metodes ondersoek om die oppervlak van politileentereftalaat (PET) mikrovesels met 'n biologiese entiteit doelgerig te maak, om so die konsentrasie van TB bacilli in 'n monster te konsentreer.

Die entiteit van belang was 'n lektien gebaseerde bindingsgroep, naamlik Concanavalin A (Con A). Con A het 'n affiniteit vir die mannose groepe op die *Mtb* selwand. Deur hierdie funktionalisering van die vesels is 'n substraat geskep wat potensieël kan dien as 'n konsentrasie- en vasvang- platform vir die *Mtb*-bacilli. Dit volg dat, aangesien hierdie soort vesels algemeen gebruik word as deppers om monster te neem, 'n *Mtb*-spesifieke depper geskep kan word vir gebruik in die wangholte. Dit sal die bacilli-versameling bemiddel, wanneer 'n monster van die mondslymvlies van 'n pasiënt geneem word.

Affiniteitstudies tussen die gemodifiseerde PET-mikrovesels en 'n verswakte stam van Mikobakterium bovis, naamlik die basil van Calmette-Guérin (BCG) is uitgevoer. Die BCG stam wat gebruik is, het n fluoresserende proteïen-indikator bevat, naamlik mCherry-BCG. Hierdie studies is ook uitgevoer as n funksie van reeks verdunnings, om die *Mtb*-onderskeppingsvermoë van die aangepaste substrate te evalueer. Die suksesvolle verstrengeling van BCG deur

die substrate is bevestig met behulp van konfokale fluoressensiemikroskopie en skandering-elektronmikroskopie. Hierdie studies het bevestig dat al die oppervlak gefunksioneerde substrate daartoe in staat was om die bakterieë suksesvol vas te vang. Dit was moontlik selfs tot en met kultuurkonsentrasies wat ver onder die opsporingsdrempel van sputum-smeer-mikroskopie val. Die oppervlak-modifikasie wat die beste resultate gelewer het vir BCG-onderskepping was 'n kruisgekoppelde proteïen-aggregaat afgeleide, wat kovalent gebind was aan die oppervlak van die vesel, deur middel van Pentaan-1,5-dialdehied.

Table of Contents

List of Figures

List of Schemes

List of Tables

Acronyms and Abbreviations

Mtb	*Mycobacterium tuberculosis*
ABTS	2,2'-azino-bis(3-ethylbenzthiazoline-6-sulfonic acid)
ATR-FTIR	Attenuated total reflectance Fourier transform infrared
ATR	Attenuated total reflectance
BCG	Bacillus of Calmette-Guérin
CFM	Confocal fluorescence microscopy
CFU/mL	Colony-forming units per milliletre
CLEM	Correlative light-electron microscopy
CLPA	Cross-linked protein aggregate
Con A	Concanavalin A
DIEA	Diisopropylethylamine
DNA	Deoxyribonucleic acid
DSC	N,N'-disuccinimidyl carbonate
EDX	Energy dispersive X-ray spectroscopy
FITC	Fluorescein isothiocyanate
GA	Glutaraldehyde
HIV	Human immunodeficiency virus
HRP	Horseradish peroxidase
KCN	Potassium cyanide

LAM	Lipoarabinomannan
LED	Light-emitting diode
ManLAM	Mannose-capped lipoarabinomannan
NHS	N-hydroxysuccinimide
OD_{600}	Optical density measured at 600 nm
PBS	Phosphate buffered saline
PET	Poly(ethylene terephthalate)
PIMs	Phosphatidylinositol mannosides
SEM	Scanning electron microscopy
T PMT	Transmitted photomultiplier tube
TB	Tuberculosis
THF	Tetrahydrofuran
WHO	World Health Organisation
CIE	International Commission on Illumination

Chapter 1

Prologue

1.1 Introduction

Tuberculosis (TB) is amongst the oldest of humankind's plagues, as even the earliest of humanoids suffered from its onslaught millennia ago[1]. The bacterial agents responsible for this disease belong to the *Mycobacterium tuberculosis* (*Mtb*) complex, and may be ranked amidst the most successful human pathogens[2]. It follows that the incessant struggle of humans and the pathogen throughout the ages, has led to it developing extensive mechanisms to prevent its detection and eradication by the immune system[3].

The disease is most prevalent in developing countries, with over 95% of deaths occurring in low- and mid-range income countries[4]. A repetitive cycle is caused by the fact that the most sensitive methods for TB diagnosis are not available to the countries most burdened by the disease[5]. As such, sputum smear microscopy remains to be the workhorse of diagnosis in these settings[6]. Consequently, this technique has seen several improvements over the years, leading to increases in sensitivity and diagnostic rate, while decreasing the strain on analysts[7]. The advent of fluorescence microscopy alone led to a 10% increase in sensitivity, compared to conventional microscopy[8-10]. The lowest limit of detection achievable is in the vicinity of 10^4 colony-forming units per milliletre (CFU/mL)[11,12]. This sensitivity further decreases as sample quality deteriorates, which is typically the case with paediatric and human immunodeficiency virus (HIV)-coinfected patients[13]. The eventual outcome of this limited sensitivity is a large number of undiagnosed or even misdiagnosed patients[14]. In addition, diagnosis in children is even further hampered, owing to the absence of a diagnostic gold standard[15]. This entails detection of *Mtb* by means of either culture or molecular methods[6]. Accordingly, the disease in children often goes undiagnosed and ultimately forms the reservoir for future infections[16].

A means of addressing these issues is to incorporate a device, which is capable of increasing the sensitivity of the most prevalent detection method in poverty stricken countries, namely sputum smear microscopy.

This holds that the best quality of sample possible, needs to be collected from the patients[17]. Using sputum as a sample for this type of analysis is however challenging, due to several factors which include its production and composition[18,19]. Hence, there is scope for a means of sample collection and concentration which is safe, rapid, uniform, nonintrusive and yields high bacterial loading. The intended device should therefore be able to extract *Mtb* bacteria predominantly, with little other material.

Fibrous polymeric materials are a logical basis for amplification, since they readily form the foundation of several specimen collection swabs[20]. A typical sampling swab, exhibiting a microfibrous polyester bud, is an ideal precursor for this intent. Also, its flocked structure and hydrophobic nature creates a suitable adhesion surface for the mycobacterium bacilli[21-23]. In addition, polyester is an inert polymer, and does not interfere with samples[20]. Its chemical structure, however, makes it favourable for subsequent chemical modification[24].

The repetitive ester and therefore carbonyl moiety of the polymer makes it susceptible to chemical modification by nucleophilic attack[25]. This can be exploited to facilitate the covalent attachment of adhesion entities to the fibre surface. These entities can sequentially be utilised for selectively binding to target components on the *Mtb* cell wall. In this way, an *Mtb* cell binding ability can be imparted onto a well-established means of sample collection.

1.2 Objectives

The rationale of this work, was to develop and evaluate the efficiency of a polyester based affinity substrate for *Mtb*. The substrate was intended for use as a buccal swab, with the ability to capture and concentrate the pathogenic bacteria from the sputum or oral mucosa of patients. For this purpose, poly(ethylene terephthalate) (PET) microfibers were chosen as precursor polymeric scaffolds for the attachment of the adhesin protein, Concanavalin A (Con A). Con A was chosen as a functionality, due to its known affinity for the cell wall of the virulent members of the *Mtb* complex[26]. The *Mtb* capture potential of the modified fibres were to be evaluated by means of affinity towards mycobacterium bovis bacillus Calmette-Guérin (BCG).

The objectives for this study can, therefore, be summarised as follows:

1. To generate and characterise surface functionalities on PET parent polymer, by means of selective degradation reactions:
   (a) Amination of PET (PET-NH_2)
   (b) Glycolysis of PET (PET-OH)

2. The activation of functionalised surfaces with bifunctional bioconjugate molecules glutaraldehyde (GA) and N,N'-Disuccinimidyl carbonate (DSC).
   (a) Aminated PET treated with GA (PET-NH-GA)
   (b) Aminated PET treated with DSC (PET-NH-DSC)
3. To immobilise the adhesin molecule Con A onto the activates surfaces, along with sequential treatment to form cross-linked protein aggregate derivatives.
   (a) Con A immobilised onto GA activated PET-NH_2 (PET-NH-GA-Con A)
   (b) Cross-linked protein derivative of PET-NH-GA-Con A (PET-NH-GA-CLPA)
   (c) Con A immobilised onto DSC activated PET-NH_2 (PET-NH-DSC-Con A)
   (d) Cross-linked protein derivative of PET-NH-DSC-Con A (PET-NH-DSC-CLPA)
4. To evaluate *Mtb* capture ability of the adhesin functionalised fibres against a suitable control. BCG would be used as a non-pathogenic *Mtb*-mimic.

1.3 Layout of thesis

Chapter 1 - Prologue

A brief introduction to the study is provided, along with an overview of the specific aims. The presented objectives in this study are also discussed.

Chapter 2 - Historical and theoretical background

A literature based overview is provided, discussing the theoretical and historical background of some of the aspects covered in this thesis.

Chapter 3 - Surface functionalisation and characterisation of PET microfibres

In this chapter PET surface functionalisation techniques are introduced, and the difficulties of imparting functionalities to fibrous media are discussed. Following this, glycolysis and amination of PET fibres are discussed and the detection of the new functionalities is described.

Chapter 4 - Aminated PET microfibre activation for Concanavalin A immobilisation

The use of bioconjugate molecules to activate solid substrates is described. This is followed by a discussion on the activation of amine functionalised PET fibres, and subsequent protein immobilisation onto these fibres. Finally, the characterisation of the various fibre derivatives is discussed.

Chapter 5 - Affinity studies between microfibrous substrates and mycobacteria

A concise background is given of the adhesion type interactions between bacteria and material surfaces. Following this, the *Mtb* capture ability of the fibres is evaluated and discussed with regards to their affinity towards BCG.

Chapter 6 - Conclusions and recommendations

An overview of the conclusions reached throughout this study is given, in addition to the challenges encountered and possible solutions for future work.

1.4 References

1. Daniel, T. M. The history of tuberculosis. Respiratory Medicine 100, 1862-1870 (2006).

2. Marmiesse, M., Gutierrez, M. C., Brisse, S., Brosch, R., Fabre, M., Oma, B., Supply, P. & Vincent, V. Ancient Origin and Gene Mosaicism of the Progenitor of *Mycobacterium tuberculosis*. PLOS Pathogens 1, 55-61 (2005).

3. Pieters, J. & Mckinney, J. D., editors. Current Topics in Microbiology and Immunology: Pathogenesis of *Mycobacterium tuberculosis* and its Interaction with the Host Organism. New York: Springer. 2013.

4. Tuberculosis. WHO Media centre (2017). Available at: http://www.who.int/mediacentre/factsheets/fs104/en/. (Accessed: 11th November 2017)

5. Parsons, L. M., Gutierrez, C., Lee, E., Paramasivan, C. N., Abimiku, A., Spector, S., Roscigno, G. & Nkengasong, J. Laboratory Diagnosis of Tuberculosis in Resource-Poor Countries: Challenges and Opportunities. Clinical Microbiology Reviews 24, 314-350 (2011).

6. Achkar, J. M., Lawn, S. D., Moosa, M. S., Wright, C. A. & Kasprowicz, V. O. Adjunctive Tests for Diagnosis of Tuberculosis: Serology, ELISPOT for Site-Specific Lymphocytes, Urinary Lipoarabinomannan, String Test, and Fine Needle Aspiration. The Journal of Infectious Diseases 204, S1130-S1141 (2017).

7. Mcnerney, R., Cunningham, J., Hepple, P. & Zumla, A. New tuberculosis diagnostics and rollout. International Journal of Infectious Diseases 32, 81-86 (2015).

8. Steingart, K. R., Henry, M., Ng, V., Hopewell, P. C., Ramsay, A., Cunningham, J., Urbanczik, R. & Perkins, M. Fluorescence versus conventional sputum smear microscopy for tuberculosis: a systematic review. The Lancet Infectious Diseases 6, 570-581 (2006).

9. Nicol, M. P. & Zar, H. J. New specimens and laboratory diagnostics for childhood pulmonary TB: Progress and prospects. Paediatric Respiratory Reviews 12, 16-21 (2011).

10. Organization, W. H. Fluorescent light-emitting diode (LED) microscopy for diagnosis of tuberculosis. 1-12 (2011).

11. Hendry, C., Dionne, K., Hedgepeth, A., Carroll, K. & Parrish, N. Evaluation of a Rapid Fluorescent Staining Method for Detection of Mycobacteria in Clinical Specimens. Journal of Clinical Microbiology 47, 1206-1208 (2009).

12. Patin, S., Alamo, L., Cimino, M., Casart, Y., Bartoli, F., Garca, M. J. & Salazar, L. Autofluorescence of Mycobacteria as a Tool for Detection of *Mycobacterium tuberculosis*. Journal of Clinical Microbiology 46, 3296-3302 (2008).

13. Holani, A. G., Ganvir, S. M., Shah, N. N., Bansode, S. C., Shende, V. ishali, Jawade, R. & Bijjargi, S. C. Demonstration of *Mycobacterium Tuberculosis* in Sputum and Saliva Smears of Tuberculosis Patients Using Ziehl Neelsen and Flurochrome Staining- A Comparative Study. Journal of Clinical and Diagnostic Research 8, 42-45 (2014).

14. Cohen, G. M. Access to diagnostics in support of HIV / AIDS and tuberculosis treatment in developing countries. AIDS 21, S81-S87 (2007).

15. Singh, V. TB in developing countries: Diagnosis and treatment. Paediatric Respiratory Reviews 7, S132-S135 (2006).

16. Khan, P. Y., Glynn, J. R., Fielding, K. L., Mzembe, T., Mulawa, D., Chiumya, R. & Fine, P. E. M. Risk factors for *Mycobacterium tuberculosis* infection in 2 - 4 year olds in a rural HIV- prevalent setting. International Journal of Tuberculosis and Lung Disease 20, 342-349 (2016).

17. Fisher, M., Dolby, T., Surtie, S., Omar, G., Hapeela, N., Basu, D., Dewalt, A., Kelso, D., Nicol, M. & Mcfall, S. Improved method for collection of sputum for tuberculosis testing to ensure adequate sample volumes for molecular diagnostic testing. Journal of Microbiological Methods journal 135, 35-40 (2017).

18. Shenai, S., Amisano, D., Ronacher, K., Kriel, M., Banada, P. P., Song, T., Lee, M., Joh, J. S., Winter, J., Thayer, R., Via, L. E., Kim, S., Walzl, G. & Alland, D. Exploring Alternative Biomaterials for Diagnosis of Pulmonary Tuberculosis in HIV-Negative Patients by Use of the GeneXpert MTB/RIF Assay. Journal of Clinical Microbiology 51, 4161-4166 (2013).

19. Wood, R. C., Luabeya, A. K., Weigel, K. M., Wilbur, A. K., Jones-engel, L., Hatherill, M. & Cangelosi, G. A. Detection of *Mycobacterium tuberculosis* DNA on the oral mucosa of tuberculosis patients. Scientific Reports 5, 1-5 (2015).

20. Medical Wire. Dryswab - leading in specimen collection Dryswab^{TM} - Better specimens for better science. 1-8

21. Ha, K., Chung, Y. & Ryoo, S. Adherence and Biofilm Formation of Staphylococcus Epidermidis and *Mycobacterium Tuberculosis* on Various Spinal Implants. Spine 30, 38-43 (2004).

22. Mullis, S. N. & Falkinham, J. O. Adherence and biofilm formation of Mycobacterium avium, Mycobacterium intracellulare and Mycobacterium abscessus to household plumbing materials. Journal of Applied Microbiology 115, 908-914 (2013).

23. Pe, R., Celdra, A., Garc, C. & Esteban, J. Bacterial Adherence to Different Meshes Used in Abdominal Surgery. Surgical Infections 15, 90-93 (2014).

24. Zhang, Y., Chai, C., Song, X., Hin, S. & Leong, K. W. Fibronectin immobilized by covalent conjugation or physical adsorption shows different bioactivity on aminated-PET. Materials Science and Engineering: C 27, 213-219 (2007).

25. Chen, W. & Mccarthy, T. J. Chemical Surface Modification of Poly(ethylene terephthalate). Macromolecules 31, 3648-3655 (1998).

26. Dinadayala, P., Kaur, D., Berg, S., Amin, A. G., Vissa, V. D., Chatterjee, D., Brennan, P. J. & Crick, D. C. Genetic Basis for the Synthesis of the Immunomodulatory Mannose Caps of Lipoarabinomannan in *Mycobacterium tuberculosis*. Journal of Biological Chemistry 28, 20027-20035 (2006).

Chapter 2

Historical and theoretical background

2.1 Tuberculosis: A general overview

Tuberculosis (TB), is an infamous infectious disease which has been afflicting human existence for millennia. While this malicious disease can be present in individuals as an extrapulmonary disease, it is most commonly found as the more lethal pulmonary type[1].

Presently the disease is no less of a burden, with the World Health Organisation (WHO) estimating it as the cause of death for 10.4 million persons, which excludes the deaths of a further 0.4 million persons who had also suffered from the human immunodeficiency virus (HIV), in 2015. This placed TB among the top 10 global causes of fatality in 2015. Accordingly, the WHO estimate that between 27.4-41.1% of the world population were already infected with the latent form of *Mycobacterium tuberculosis* (*Mtb*) by that year, having a lifetime risk of 5-15% of developing the active disease[2].

As recorded in 2015, there were six countries which together made up about 60% of the estimated 10.4 million incident cases of TB in the world. These countries in increasing order were South Africa: (4%), Pakistan (5%), Nigeria (6%), China (9%), Indonesia (10%) and India (27%)[3]. It is also no coincidence that these countries have some of the highest global famine figures[4], since there is a strong correlation between malnutrition and the severity as well as the frequency of TB infections[5,6].

In addition, these five countries, as well as several others with high TB incidences are strongly affected by poverty[3,7]. This too is a well-documented relationship pertaining to the associated trademarks of poverty such as poor living and working conditions, inadequate nutrient supply, overcrowding and finally a lack of basic health care services[8-10].

2.1.1 Infection and spread of the disease

TB is transmitted as an airborne pathogen. It is introduced into the airspace when a patient with active pulmonary TB aerosolises the bacilli by means of forceful expulsion of air from the lungs.

It follows that several respiratory activities, such as speaking, singing and breathing, are able to contribute to the spread of the disease, while coughing is still assumed to be the prevalent means of *Mtb* aerosolisation[11]. This is due to a cough entailing high shear inside of the intrathoracic airways. This occurs since these airways collapse as part of the cough action, while high velocity air is forced through the narrowing path. Accordingly, it is these high shear forces which are able to overcome the viscosity of mucus, leading to its dislodgement and expulsion as an aerosol[12].

Once an individual has been exposed to *Mtb*, the immune system can react in one of four ways[13,14]. In the first instance, the immune system can fail to recognise and register an infection. This may occur in cases of undernutrition, where the immune system is under stress and cannot act as an effective defence mechanism[9]. If, however the immune response is potent and the bacilli are of low virulence, then the body may become infected, but eventually clear the infection. Otherwise a latent infection may be developed, where the bacilli are still present but contained. Finally, a person can develop progressive TB.

2.1.2 Paediatric tuberculosis

Amongst the estimated 10.4 million new TB cases in 2015, roughly 10% (1.0 million) were paediatric cases[3]. It therefore follows that TB is amongst the top ten contributors to paediatric death figures[15]. TB resulted in the death of 210 000 children in 2015, of which the patients in 40 000 cases had HIV positive status[16].

These figures are likely an underestimate of the true paediatric TB burden, since many children develop paucibacillary disease. In this case a sputum smear test returns a negative result[17]. This is due their sputum not containing a bacillary population size greater than 10^4 colony-forming units units per milliletre (CFU/mL), which is threshold of detection with acid-fast smears[18-20]. It is also often found that the children who contract TB stem from disadvantaged communities. Therefore, these children suffer from poor access to health care and consequently limited diagnostic techniques are available[16].

The TB infection in children is different to that in adults. This is due to differences in their immunological and patho-physical responses to the disease. In turn, this makes them more susceptible to developing active TB after exposure to the bacterium[21,22]. That, amongst other factors, contribute to the difficulties surrounding the diagnosis, treatment and prevention of TB in children[6].

Since children often develop paucibacillary disease and also lack the ability to invoke a cough with enough force to aerosolise the *Mtb* pathogen[23-24], they are generally less infectious and, therefore, considered less of a health risk[1,6,14,25]. Nonetheless, diseased children along with children who have already recovered from the primary disease, embody the source of future infections, since they still have the potential to transmit the disease[26].

It is because of the lower risk of infectivity that paediatric TB has historically not enjoyed the same priority of focus from National TB Control Programmes as adult TB[25]. In accordance, recent efforts by the WHO include the 'End TB Strategy' which aims to essentially eradicate the disease by 2035, with paediatric TB treatment being a key component to reaching this target[3,16,27].

Accurate diagnosis of TB in children is a daunting task, and as such constrains predictions of global paediatric TB cases. Owing to this, it was not until the 2012 Global Tuberculosis Report, that the WHO had reported on the global burden of TB in children for the first time[28,29].

Children and infants often show nonspecific symptoms which subsides upon antibiotic treatment. In children, specimens are difficult to collect and the subsequent cultures as well as smears of *Mtb* are often negative[30-32]. In a developed country such as the United States, cases where infants and children who had moderate to severe pulmonary TB as radiographically diagnosed, were asymptotic, with respect to commonly used diagnostic procedures[30]. In these cases, the children were only suspected to have TB by contact tracing of an adult infected with the disease.

In developing countries, however, the difficulty of diagnoses of paediatric TB is hampered even more by economic factors. In these cases, combinations of clinical features are investigated, in order to presumptively diagnose paediatric TB. These include the tuberculin skin test, physical examination, contact history and chest radiography[32].

The impact of this is that in resource poor countries, who lack proper heath systems with up-to-date facilities such as radiographic instruments and well-equipped laboratories, a large number of paediatric cases go undiagnosed[18]. Accordingly, the true magnitude of the paediatric TB endemic and the mortality which arises from it, is greatly underappreciated.

2.2 Diagnosis of tuberculosis

Up to this point, it can be concluded that TB is a serious health concern, which is easily transmitted and especially difficult to detect. The slow development and absence of specific symptoms means patients often don't know they are ill, leading to subsequent spreading of the disease[33-34]. It is due to this that the

pathogen is so long lived and effective, since the best method to eradicate it, is by promptly identifying and treating it[3,36].

To further complicate this, the countries most affected by the disease suffer from significant resource constraints[37]. This means that diagnosis is primarily restricted to insensitive and outdated techniques, with limited diagnostic utility such as the popular low cost acid-fast stained sputum smear microscopy technique[38]. The result of which is a large number of undiagnosed or misdiagnosed patients.

Fortunately, this issue is being addressed, with several new techniques being developed which offer rapid, accurate and convenient diagnosis of TB[39]. To some extent, this has been achieved with the advent of Xpert MTB/RIF, a nucleic acid amplification tests platform[40].

Xpert MTB/RIF combines sample preparation, amplification and the simultaneous detection of the *Mtb* complex as well as the mutations which show resistance to a key treatment drug (rifampicin), all in less than two hours[41]. While it holds several other admirable advantages, it still requires relatively expensive equipment, with the prerequisite of needing a continuous source of energy and frequent equipment calibration[40]. None the less, the gap which exists in resource limited countries, between the detection methods required for accurate/rapid diagnosis, and the methods available is starting to shrink.

Enhancements have been made to the Xpert MTB/RIF equipment, with specific regards to its portability, energy dependence and sensitivity[40]. It is also very likely that such enhancements will continue to be made, until a product is achieved which falls within the parameters set for use in high incidence/ low income settings.

However, advances in diagnostic techniques have not been limited to only Xpert MTB/RIF. Microscopy has also evolved, seeing the replacement of the Ziehl-Neelsen stains with fluorescent dyes in conjunction with fluorescent light-emitting diode (LED) microscopes[42,43]. Automation of these techniques have also been established. All of this leads to increased sensitivity, as well as lowering the burden of the strenuous activity on microscopists[41]. There are also new techniques which are entering the market, many showing promising sensitivity and specificity.

Three prominent new candidates are Truenat MTB, EasyNAT Diagnostic Kit for *Mycobacterium tuberculosis* Complex and The VereMTB assay. All of these technologies focus on making detection methods resource independent and miniaturising it for easy portability, and succeed in doing so[44-48]. There are however significant amounts of testing and data acquisition which need to be done in order to assess their potential for TB control[41].

Amongst all of the mentioned techniques and several other (though not all), there exists a common denominator, namely sputum as the sample. This is a logical sample to collect for detection, since sputum

is the secretion produced in the lungs during pulmonary infection. Accordingly, it typically contains high counts of the bacteria.

Sputum, however, has several drawbacks, amongst which the prime contributors are its collection, safety to healthcare personnel and variation in its composition, consistency and volume[35,49,50]. In addition, most of a sputum sample is superfluous, with the main interest being either the bacteria itself or the bacterial deoxyribonucleic acid (DNA).

It follows that a means of sample collection which is able to capture and concentrate *Mtb* bacilli from a sample of bodily fluid, albeit sputum, would benefit the detection of TB. If in addition, such a platform could consist of an easy to handle and store device, sample collection would gain reproducibility, uniformity in composition and create a safer environment for collection and analysis.

2.3 *Mycobacterium tuberculosis*

The bacteria of the *Mtb* complex are responsible for TB in humans, with the *Mtb* species being the primary cause[51]. *Mtb* is an immotile, aerobic, non-encapsulated bacillus which does not form spores[14,52].

The cell wall of these bacilli is unique with regards to its high lipid content, which comprises 60% of the cell wall[53]. These lipids are primarily mycolic acids (long-chain α-alkyl β-hydroxy fatty acids), and provides the organism with a waxy, low permeability envelope[53-55]. It is due to this waxy outer layer that the bacteria have a greater resistance against antibiotics, and are also resistant to Gram staining[54,56]. This waxy layer then also grants the bacteria their hydrophobic character, as well as their tendency to aggregate[57,58].

2.3.1 The role of lipoarabinomannan in *Mtb*/host interactions

The tenacious and intimate relation which exists between *Mtb* and its host infers evolution of the bacteria, to the extent where it has developed mechanisms which prevent eradication by the immune system[59]. Consequently, the pathogen has adapted to such an extent that it is able to replicate within phagocytic cells, particularly the cell responsible for the eradication of microbes, namely the macrophages[59]. Therefore, contraction of TB is thought to depend strongly on nonopsonic invasion as well as colonisation of macrophages, following the primary infection brought on after the bacteria is inhaled[60].

The entry of the mycobacterial cell is likely mediated by various receptors present on the surface of the phagocytic cell, the receptors include C-type lectin, scavenger and complement receptors[61]. These

receptors are able to recognise exclusive ligands expressed on the *Mtb* cell surface and accordingly facilitate nonopsonic internalisation of mycobacteria in macrophages[60,62,63].

Among the variety of C-type lectin receptors which are involved with mycobacterial uptake, are the mannose receptor and the dendritic cell-specific intercellular adhesion molecule 3 grabbing nonintegrin[61,64,65]. The importance of these receptors is their ability to recognise mannosylated molecules like mannose-capped lipoarabinomannan (ManLAM) and phosphatidylinositol mannosides (PIMs) present in the pathogen's cell wall[66].

The mannose receptors, specifically, are able to detect the presence of mannose, fructose and N-acetylglucosamine fractions on the surfaces of pathogens and bind to them[61]. This is possible due to the eight carbohydrate recognising domains present in this extracellular transmembrane protein, where each domain possesses over C-type lectin properties[60,67,68].

In addition, a pronounced component of the mycobacterial cell envelope is lipoarabinomannan (LAM), which accounts for up to 0.5% of the bacterial cell weight[69]. This high molecular weight phosphatidylinositol-anchored lipoglycan, consists of a mannan core with oligoarabinosyl-containing side-chains with in turn relate to a diverse selection of biological activities[70-73]. Furthermore, all mycobacterium species poses other variations in LAM structures, which can be classed into three architectures. One of these classes is the ManLAM architecture, which is ubiquitous with the virulent strains of mycobacterium Erdman and H37Rv and the avirulent strains H37Ra and bacillus of Calmette-Guérin (BCG)[74,75]. It is classified as such due to the prevalence of α 1 $\rightarrow$ 2 mannose capped non- reducing arabinan termini (Figure 2.1), situated at the cell surface[73,76].

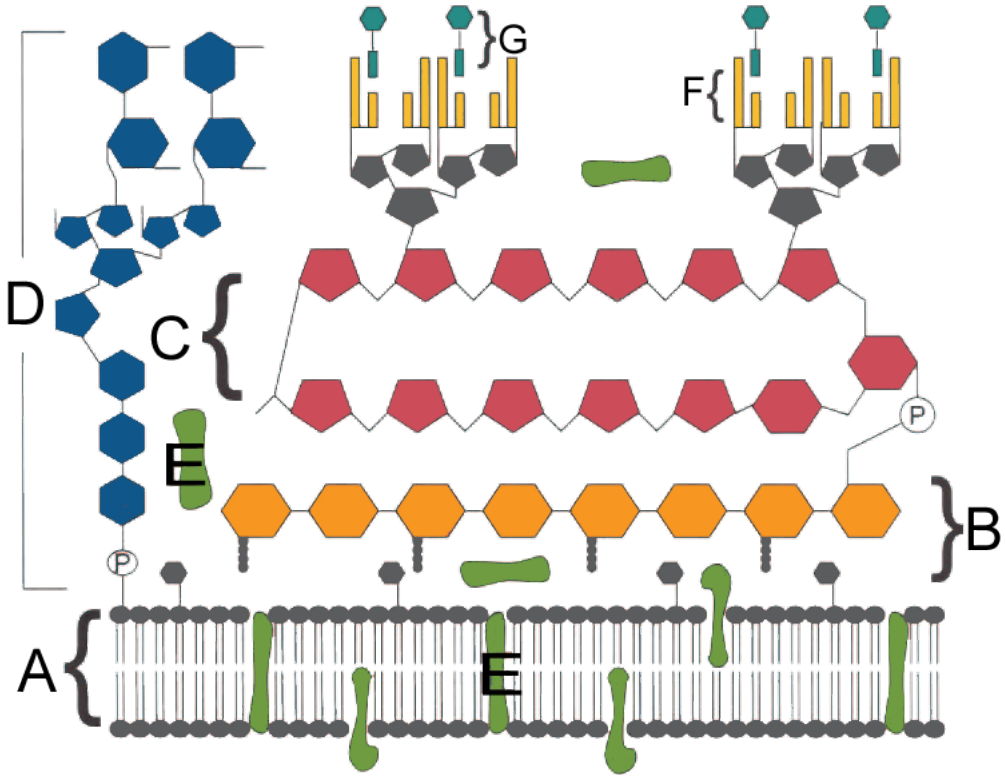

Figure 2.1: Schematic representation of the cell envelope of Mtb. The components include the (A) plasma membrane, (B) peptidoglycans, (C) arabinogalactan, (D) mannose-capped lipoarabinomannan, (E) plasma membrane- and cell envelope-associated proteins, (F) mycolic acids and (G) glycolipid surface molecules associated with the mycolic acids[76].

2.4 Concanavalin A

Concanavalin A (Con A) belongs to a family of carbohydrate-binding proteins called lectins[77]. Its name is derived from its source of extraction namely Canavalia ensiformis (jack bean) and has the reputation of being the most popular lectin for the characterisation as well as purification of sugar-containing molecules and cells[78]. Con A has an affinity for anomers of D-mannose and D-glucose, being able to bind to them with reasonable affinity[79,80]. When these molecules are accordingly present on a cell surface, Con A is able to bind to it with high avidity. This is the case since the protein is a tetramer with four identical subunits, each able to bind the carbohydrate targets[81].

Since the slow growing mycobacteria, which include *Mtb*, Mycobacterium leprae, Mycobacterium bovis, Mycobacterium avium, and Mycobacterium kansasii[2,5,7-12], poses α $1 \rightarrow 2$ mannose residue capped non-reducing arabinan termini of LAM, they are able to react with Con A[73]. It has in accordance been found that styrene maleic anhydride nanofibres, which had been surface functionalised with Con A, showed affinity

for BCG. Nanofibre mats consisting of these fibres were able to act as capture platform for the bacteria[52].

In addition, there are 13 primary amines per Con A monomer (12 lysene residues and one N-terminus) avaliable to facilitate its immobilisation onto a substrate, by the aid of bioconjugate molecules[52,82-84]. This then suggests than one can make use of this protein to impart a carbohydrate affinity to an otherwise unaffiliated polymeric material, giving it adhesion like properties for specific molecules and cells.

2.5 *Mtb* detection by oral swab

The diagnosis of pulmonary TB is still strongly dependent on the collection of sputum from patients[85]. This relates to several diagnostic obstacles and limitations, which originate from the difficulties of acquiring sputum as well as its varying composition and viscosity[35,86]. There is also the added danger of exposing testing personnel to *Mtb* when they handle samples and are exposed to an environment where patients have to produce sputum by means of coughing[49].

As such, studies have been conducted to find safer and easier ways to handle alternative biomaterials, so as to aid in the diagnosis of pulmonary TB. However, sputum remains to be the optimal sample type[38,86-94]. Nevertheless, a recent study has found that oral mucosa contains *Mtb* DNA, allowing for pulmonary TB diagnosis from buccal swabs[35]. The basic principle behind this inspired research into adhesion based buccal swabs, which are able to capture and concentrate the *Mtb* pathogen.

2.5.1 Adhesion based buccal swabs

Based on the transmission route of *Mtb*, which could imply migration from the lungs and gastrointestinal tract into the oral cavities, there is a rationale behind speculating that some of the bacilli might accumulate on the oral epithelium[35]. This was confirmed by the detection of *Mtb* DNA, by a polymerase chain reaction test, in oral swabs taken from humans and primates[35,95-97].

Mtb being bacterial cells, have evolved attachment mechanisms which allows them to adhere to one another, objects in their environments as well as foreign objects[98,99]. As examples of this, Mycobacterium leprae cells have shown interaction with nasal and alveolar epithelial cells[100] and Mycobacterium avium cells in turn have been found to interact with bronchial epithelium cells[101].

Of parallel importance is the ability of mycobacteria to adhere to foreign objects. In a number of studies done on the adherence and biofilm formation of nontuberculous mycobacteria on material surfaces as well as polymer ”material”, it was found that the bacilli had a noticeable (although highly variable) affinity for the

materials[102]. This variance was ascribed to a number of factors. A few of these were the bacterial species, surface roughness, surface energy and the composition of the substrate[102-106].

These phenomenon imply that TB sample acquisition can be improved by means of a buccal swab. One method of doing this is by making use of adhesion based interactions with the bacilli. In such a case, the swab matrix is able to bind to the mannose-containing phospholipids on the bacterial cell surface, thereby entrapping them[107-108]. This concept is supported by a study which had been conducted to find the force with which Con A binds to the glycopolymers on the surface of a single Lactobacillus plantarum cell[109]. This study also expressed the occurrence of rapid non-specific interactions between the bacteria and a hydrophobic surface.

It follows then, that a swab consisting of a hydrophobic polymer matrix, which has Con A covalently attached to its surface, could entrap *Mtb* bacilli by means of adherence. Such swabs could then act not only as capturing platforms for the bacteria, but also as a medium for the concentration of them in paucibacillary cases.

2.5.1.1 Safety

Nosocomial transmission of *Mtb* from either patients or samples to laboratory and heath care personnel is a serious issue[110-112]. A prominent contributor to these issues is the means of sample collection used. When sputum is collected from patients by means of a sputum cup, the patients necessarily need to cough in order to produce sputum. This means that several safety precautions need to be put in place to try and avoid the spread of the disease during the execution of this procedure.

In developed countries with few patients, these requirements are easily met. In developing countries, however, the precautions in place are rudimentary, which leads to an increase in the risk of transmission. The situation becomes even more constrained during TB screening events, where large numbers of possible TB patients come together at health care centres, and are asked to produce sputum samples. The reality is that such settings do not always meet the necessary requirements.

It follows that if the necessary sanitation prerequisites cannot be met, the risk of transmission is increased[37]. Since buccal swabs are used to swab the inside of the cheeks only, it does not result in the aerosolisation of the bacterium and, therefore, reduces the risk of transmission[35].

Sputum collection cups act as the transport medium from the point of exposure to the place of analysis, and therefore require proper sterilisation by healthcare workers[49,112]. In addition, the ability to automate *Mtb* detection from the swabs offers laboratory personnel further detachment from the infectious specimen[113].

2.5.1.2 Sample preservation

Due to the prevalent use of sputum as samples for the detection of pulmonary TB, there are typically microorganisms other than mycobacteria present in the collected specimen[37,85]. Specimens should also be refrigerated if they are going to be exposed to conditions which promote the growth of contaminating organisms[114]. Failure to do so could lead to an overgrowth proliferation of the non-mycobacterial contaminants[37]. Prolonged storage of samples at room temperature has been found to result in the reduced recovery of the *Mtb* as well as heightened contamination rates[115,116].

The above leads to significant issues with regards to the logistics surrounding the storage and transportation of the samples, as well as the associated costs[116,117]. When using swabs, the impact on these logistical and cost issues are lessened, since their containers take up less volume and weigh drastically less than sputum sample cups[118].

2.5.1.3 Training patients, including children, to produce sputum correctly

In order to obtain rapid and accurate test results from any of the TB diagnostic methods, high quality specimens are a prerequisite, and rapid transport to a laboratory or refrigeration is vital[49]. This is of particular importance for molecular detection methods, where the volume of collected sputum directly impacts upon the test sensitivity[49,119].

Health care workers must be properly trained to coach patients on providing proper sputum samples. This involves techniques for producing a cough, which necessarily implies aerosol production by the patient, and therefore must be conducted in a manner which does not hamper the safety of the health care worker[37]. It is also not uncommon for children up to the age of 12 years to have difficulty producing sputum. In such cases, the typical route to follow is a gastric aspirate in order to collect the necessary specimen[114].

These are only some of the reasons why other viable methods of sample collection have been investigated. Buccal swabs are one such alternative and avoid many of the prior mentioned obstacles. The collection procedure entails swabbing of the inside of the patient's cheeks approximately ten times, collecting both oral epithelium cells and saliva[114].

This not only means that less time needs to be spent in the presence of TB patients, but in addition the chance of producing a less-ideal specimen is reduced. According to Wood et al. buccal swabs vary from sputum samples in that they have smaller, but more constant sample volumes, and their composition is more uniform and less viscous. They suggest that this could lead to the implementation of more affordable point-of-care diagnostic techniques. These are currently under development. This may in turn result in more

accurate diagnosis in paediatric cases, without the need to follow the procedures for inducing sputum or gastric aspiration[35].

2.6 Poly(ethylene terephthalate)

Poly(ethylene terephthalate) (PET) is a low-cost thermoplastic with admirable mechanical properties, which includes a high tensile strength and modulus, together with a high crystalline melting temperature (270 °C)[120-122]. While predominantly chemically inert, there exist several methods of chemically modifying materials comprised of PET[121]. The ability to do this, as well as with its moderate biocompatibility has made PET particularly appealing to the medical research field[123-126].

The ability to modify the polyester originates from the fact that in its simplest form, the polymer consists of repetitive ester moieties (Figure 2.2). Most interconversion reactions of esters are effective at changing its molecular composition. When difunctional molecules are used for these type of reactions, one can introduce reactive functional groups onto a material surface. This allows for further modification of the substrate via the latter mentioned groups.

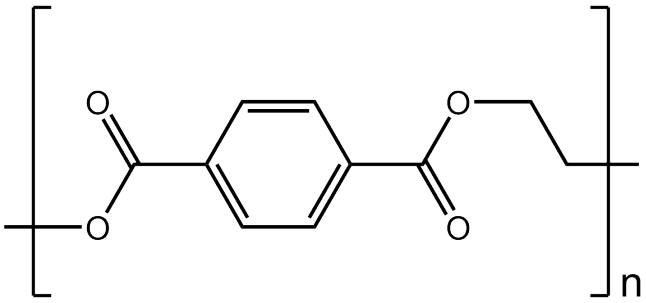

Figure 2.2: Monomer unit of poly(ethylene terephthalate).

PET is generally produced on an industrial scale as a commercial plastic in various forms. One of these is staple microfibre, commonly used in the textile industry, but also for sample collection swabs[118]. As such, the final textile form of PET, which is needed for this study is readily available. In addition, these fibres are produced to comply with certain standards, and as such makes for a universal-type product. This means that the chemical reaction parameters used to surface modify these fibres, should be applicable across the board for various PET based swabs.

The various properties of PET make it an ideal polymer to use as a scaffold for entities, which have an affinity for *Mtb*. By taking advantage of this, buccal swabs can be created from PET microfibres that have been surface functionalised with Con A. These swabs can then act as favourable adhesion surfaces for

Mtb bacilli. There is also the added advantage that surface modification of these fibres influences their water affinity properties. This allows for tailoring of the final fibrous composites moisture management. This permits the environment for *Mtb* adhesion to be tailored. Conclusively, swabs composed of such a material, will potentially promote the capture and concentration of *Mtb* bacilli when an oral mucosa sample of a patient is taken.

2.7 References

1. Grosset, J. H. & Chaisson, R. E., editors. Handbook of Tuberculosis. Gewerbestrasse: Springer International Publishing. 2017.
2. Vynnycky, E. & Fine, P. E. M. Lifetime Risks, Incubation Period, and Serial Interval of Tuberculosis. American Journal of Epidemiology 152, 247263 (2000).
3. World Heath Organization. Global Tuberculosis Report. 2016.
4. 2016 Hunger Report the Nourishing Effect : Ending Hunger, Improving Heath, Reducing Inequality. 2016.
5. Jones, K. D. J. & Berkley, J. A. Severe acute malnutrition and infection. Paediatrics and International Child Health 34, S1-S29 (2014).
6. Starke, J. R. & Donald, P. R., editors. Handbook of child and adolescent tuberculosis. New York: Oxford University Press. 2016.
7. The World Factbook Central Intelligence Agency. Available at: https://www.cia.gov/library/publications/the-world-factbook/geos/pl.html. (Accessed: 30th October 2017)
8. World Health Organization. What is the relationship between TB and poverty. 1-5 (2002).
9. Badmus, O., Camorlinga, S., Embs, I. & Simpson, O. Poverty and the Emergence of Tuberculosis: An Agent Based Modelling Approach. Biomedical and Health Informatics 561-564 (2016).
10. Caminero, J. A. An ecological analysis of incidence of tuberculosis and per capita gross domestic product. European Respiratory Journal 32, 1413-1415 (2008).
11. Turner, R. D. & Bothamley, G. H. Cough and the Transmission of Tuberculosis. The Journal of Infectious Diseases 211, 1367-1372 (2017).
12. Leith, D. E., Butler, J. P., Sneddon, S. L. & Brain, J. D. Handbook of Physiology: The Respiratory System, Mechanics of Breathing. 1986.

13. Sáenz, B., Hernandez-pando, R., Fragoso, G., Bottasso, O. & Cárdenas, G. The dual face of central nervous system tuberculosis: A new Janus Bifrons? Tuberculosis 93, 130-135 (2013).

14. Dorothee, H., Caws, M., Ben, M. & Jeremy, F. Tuberculosis in Adults and Children. New York: Springer. 2015.

15. Swaminathan, S. & Rekha, B. Pediatric Tuberculosis: Global Overview and Challenges. Clinical Infectious Diseases 50, S184-S194 (2010).

16. World Heath Organization. Ending tuberculosis in children. (2016).

17. Newton, S., Brent, A., Anderson, S. & Whittaker, E. Paediatric Tuberculosis. The Lancet Infectious Diseases 8, 498-510 (2010).

18. Nicol, M. P. & Zar, H. J. New specimens and laboratory diagnostics for childhood pulmonary TB: Progress and prospects. Paediatric Respiratory Reviews 12, 16-21 (2011).

19. Graham, S. M. Research into tuberculosis diagnosis in children. The Lancet Infectious Diseases 10, 581-582 (2010).

20. Hesseling, A. C., Schaaf, H. S., Gie, R. P., Starke, J. R. & Beyers, N. A critical review of diagnostic approaches used in the diagnosis of childhood tuberculosis. The International Journal of Tuberculosis and Lung Disease 6, 1038-45 (2002).

21. Sandgren, A., Cuevas, L. E., Dara, M., Gie, R. P., Grzemska, M., Hawkridge, A., Hesseling, A. C., Kampmann, B., Lienhardt, C., Manissero, D., Wingfield, C. & Graham, S. M. Childhood tuberculosis: progress requires an advocacy strategy now. 40, 294-297 (2012).

22. Pai, M., Minion, J., Steingart, K. & Ramsay, A. New and improved tuberculosis diagnostics: evidence, policy, practice, and impact. Current Opinion in Pulmonary Medicine 3, 271-284 (2010).

23. Marais, B. J., Gie, R. P., Schaaf, H. S., Beyers, N., Donald, P. R. & Starke, J. R. Childhood Pulmonary Tuberculosis Old Wisdom and New Challenges. American Journal of Respiratory and Critical Care Medicine 173, 1078-1090 (2006).

24. Peeling, R. W. & Mabey, D. Point-of-care tests for diagnosing infections in the developing world. Clinical Microbiology and Infection 16, 1062-169 (2010).

25. Pang, Y., Zhao, A., Cohen, C., Kang, W., Lu, J. & Wang, G. Current status of new tuberculosis vaccine in children. Human Vaccines & Immunotherapeutics 12, 960-970 (2016).

26. Nelson, L. J. & Wells, C. D. Global epidemiology of childhood tuberculosis. International Journal of Tuberculosis and Lung Disease 8, 636-647 (2004).

27. World Heath Organization. End TB Strategy. 1-26 (2014).

28. Dodd, P. J., Gardiner, E., Coghlan, R. & Seddon, J. A. Burden of childhood tuberculosis in 22 high-burden countries: a mathematical modelling study. The Lancet 2, 453-459 (2012).

29. World Heath Organization. Global tuberculosis report. 2012.

30. Schlossberg, D., editor. Tuberculosis and nontuberculous mycobacterial infections. Washington: ASM Press. 2011.

31. Eamranond, P. & Jaramillo, E. Tuberculosis in children: reassessing the need for improved diagnosis in global control strategies. International Journal of Tuberculosis and Lung Disease 5, 594-603 (2001).

32. Oberhelman, R. A., Soto-castellares, G., Gilman, R. H., Caviedes, L., Castillo, M. E., Kolevic, L., Pino, T. Del, Saito, M., Salazar-lindo, E., Negron, E., Montenegro, S., Laguna-torres, V. A., Moore, D. A. J. & Evans, C. A. Diagnostic approaches for paediatric tuberculosis by use of diff erent specimen types , culture methods , and PCR : a prospective case-control study. The Lancet Infectious Diseases 10, 612-620 (2010).

33. Storla, D. G., Yimer, S. & Bjune, G. A. A systematic review of delay in the diagnosis and treatment of tuberculosis. BMC Public Health 8, 1-9 (2008).

34. Virenfeldt, J., Rudolf, F., Camara, C., Furtado, A., Gomes, V., Aaby, P., Petersen, E. & Wejse, C. Treatment delay affects clinical severity of tuberculosis: a longitudinal cohort study. BMJ Open 4, 1-8 (2014).

35. Wood, R. C., Luabeya, A. K., Weigel, K. M., Wilbur, A. K., Jones-engel, L., Hatherill, M. & Cangelosi, G. A. Detection of *Mycobacterium tuberculosis* DNA on the oral mucosa of tuberculosis patients. Scientific Reports 5, 1-5 (2015).

36. Andrews, R. H., Devadatta, S., Fox, W., Radhakrishna, S., Ramakrishnan, C. V & Velu, S. Prevalence of Tuberculosis among Close Family Contacts of Tuberculous Patients in South India , and Influence of Segregation of the Patient on the Early Attack Rate. Bulletin of the World Health Organization 24, 463-510 (1960).

37. Parsons, L. M., Gutierrez, C., Lee, E., Paramasivan, C. N., Abimiku, A., Spector, S., Roscigno, G. & Nkengasong, J. Laboratory Diagnosis of Tuberculosis in Resource-Poor Countries: Challenges and Opportunities. Clinical Microbiology Reviews 24, 314-350 (2011).

38. Green, C., Huggett, J. F., Talbot, E., Mwaba, P., Reither, K. & Zumla, A. I. Rapid diagnosis of tuberculosis through the detection of mycobacterial DNA in urine by nucleic acid amplifi cation methods. The Lancet Infectious Diseases 9, 505-511 (2009).

39. Pai, M., Kalantri, S. & Dheda, K. New tools and emerging technologies for the diagnosis of tuberculosis: Part II . Active tuberculosis and drug resistance. Expert Review of Molecular Diagnostics 4, 423-432 (2006).

40. Gómez, A. V., González-martín, J. & García-basteiro, A. L. Xpert MTB/RIF: Usefulness for the diagnosis of tuberculosisand resistance to rifampicin. Medicina Clinica 149, 399-405 (2017).

41. Mcnerney, R., Cunningham, J., Hepple, P. & Zumla, A. New tuberculosis diagnostics and rollout. International Journal of Infectious Diseases 32, 81-86 (2015).

42. World Heath Organization. Fluorescent light-emitting diode (LED) microscopy for diagnosis of tuberculosis. 1-12 (2011).

43. Lewis, J. J., Chihota, V. N., Meulen, M. Van Der, Fourie, P. B., Fielding, K. L., Grant, A. D., Dorman, S. E. & Churchyard, G. J. "Proof-Of-Concept" Evaluation of an Automated Sputum Smear Microscopy System for Tuberculosis Diagnosis. Plos One 7, 1-6 (2012).

44. Mhimbira, F. A., Bholla, M., Sasamalo, M., Mukurasi, W., Hella, J. J. & Jugheli, L. Detection of *Mycobacterium tuberculosis* by EasyNAT Diagnostic Kit in Sputum Samples from Tanzania. Journal of Clinical Microbiology 53, 1342-1344 (2015).

45. Nikam, C., Jagannath, M., Narayanan, M. M. & Ramanabhiraman, V. Rapid Diagnosis of *Mycobacterium tuberculosis* with Truenat MTB : A Near-Care Approach. Plos One 8, 1-7 (2013).

46. Fang, R., Li, X., Hu, L., You, Q., Li, J., Wu, J., Xu, P., Zhong, H., Luo, Y., Mei, J. & Gao, Q. Cross-Priming Amplification for Rapid Detection of *Mycobacterium tuberculosis* in Sputum Specimens. Journal of Clinical Microbiology 47, 845-847 (2009).

47. Ou, X., Song, Y., Zhao, B., Li, Q., Xia, H., Zhou, Y., Pang, Y., Wang, S., Zhang, Z., Cheng, S., Liu, C. & Zhao, Y. A multicenter study of Cross-Priming Ampli fi cation for tuberculosis diagnosis at peripheral level in China. Tuberculosis 94, 428-433 (2014).

48. Veredus Laboratories. Rapid Detection, Differentiation and Identification of MDR-TB. 1-2 (2017).

49. Fisher, M., Dolby, T., Surtie, S., Omar, G., Hapeela, N., Basu, D., Dewalt, A., Kelso, D., Nicol, M. & Mcfall, S. Improved method for collection of sputum for tuberculosis testing to ensure adequate sample volumes for molecular diagnostic testing. Journal of Microbiological Methods journal 135, 35-40 (2017).

50. Rom, Wi. N., editor. Environmental and Occupational Medicine. Philadelphia: Wolter Kluwer. 2007.

51. De Jong, B. C., Antonio, M. & Gagneux, S. Mycobacterium africanum Review of an Important Cause of Human Tuberculosis in West Africa. PLOS Neglected Tropical Diseases 4, 1-9 (2010).

52. Cronje, L. PhD Thesis: Surface modification of styrene maleic anhydride nanofibers for efficient capture of *Mycobacterium tuberculosis*. Stellenbosch. 2012.

53. Kolattukudy, P. E., Fernandes, N. D., Azad, A. K., Fitzmaurice, A. M. & Sirakova, T. D. Biochemistry and molecular genetics of cell-wall lipid biosynthesis in mycobacteria. Molecular Microbiology 24, 263-270 (1997).

54. Czyk, J. P. Å. & Kremer, L. The Molecular Genetics of Mycolic Acid Biosynthesis. Microbiology Spectrum 4, 1-20 (2014).

55. Barry, C. E., Lee, R. E., Mdluli, K., Sampson, A. E., Schroeder, B. G., Slayden, R. A. & Ying, Y. Mycolic acids: structure, biosynthesis and physiological functions. Progress in Lipid Research 37, (1998).

56. Vilchèze, C. & Kremer, L. Acid-Fast Positive and Acid-Fast Negative *Mycobacterium tuberculosis*: The Koch Paradox. Microbiology Spectrum 5, 1-14 (2017).

57. Jarher, V. & Nikaido, H. Mycobacterial cell wall: Structure and role in natural resistance to antibiotics. FEMS Microbiology Letters 123, 11-18 (1994).

58. Ojha, A., Anand, M., Bhatt, A., Kremer, L., Jacobs, W. R. & Hatfull, G. F. GroEL1: A Dedicated Chaperone Involved in Mycolic Acid Biosynthesis during Biofilm Formation in Mycobacteria. Cell 123, 861-873 (2005).

59. Stanley, S. A. & Cox, J. S. HostPathogen Interactions During *Mycobacterium tuberculosis* infections. Current Topics in Microbiology and Immunology 374, 211-241 (2013).

60. Villeneuve, C., Gilleron, M., Maridonneau-parini, I., Daffé, M., Astarie-dequeker, C., Etienne, G., Montrozier, H., Bordier, C., Laval, F. & Daffe, *M. Mycobacteria* use their surface- exposed glycolipids to infect human macrophages through a receptor-dependent process. Journal of Lipid Research 46, 475-483 (2005).

61. Pieters, J. & Mckinney, J. D., editors. Current Topics in Microbiology and Immunology: Pathogenesis of *Mycobacterium tuberculosis* and its Interaction with the Host Organism. New York: Springer. 2013.

62. Bermudez, L. E. & Sangari, F. J. Cellular and molecular mechanisms of internalization of mycobacteria by host cells. Microbes and Infection 3, 37-42 (2001).

63. Ernst, J. D. Macrophage Receptors for *Mycobacterium tuberculosis*. Infection and Immunity 66, 1277-1281 (1998).

64. Schfer, G., Wilkinson, R. J. & Brown, G. D. Non-Opsonic Recognition of *Mycobacterium tuberculosis* by Phagocytes. Journal of Innate Immunity 1, 231-243 (2009).

65. Ehlers, S. DC-SIGN and mannosylated surface structures of *Mycobacterium tuberculosis*: a deceptive liaison. European Journal of Cell Biology 89, 95-101 (2010).

66. Torrelles, J. B., Azad, A. K., Schlesinger, L. S. & Alerts, E. Fine Discrimination in the Recognition of Individual Species of Phosphatidyl-myo-Inositol Mannosides from *Mycobacterium tuberculosis* by C-Type Lectin Pattern Recognition Receptors. The Journal of Immunology 177, 1805-1816 (2017).

67. Stahl, P., Schlesinger, P. H., Sigardson, E., Rodman, J. S. & Leet, Y. C. Receptor- Mediated Pinocytosis of Mannose Glycoconjugates by Macrophages: Characterization and Evidence for Receptor Recycling. Cell 19, 207-215 (1980).

68. Feinberg, H., Park-snyder, S., Kolatkar, A. R., Heise, C. T., Taylor, M. E. & Weis, W. I. Structure of a C-type Carbohydrate Recognition Domain from the Macrophage Mannose Receptor. The Journal of Biological Chemistry 275, 21539-21548 (2000).

69. Hunter, S. W., Gaylord, H. & Brennans, P. J. Structure and Antigenicity of the Phosphorylated Lipopolysaccharide Antigens from the Leprosy and Tubercle Bacilli. The Journal of Biological Chemistry 6, 12345-12351 (1986).

70. Chatterjee, D. & Khoo, K. Mycobacterial lipoarabinomannan: an extraordinary lipoheteroglycan with profound physiological effects. Glycobiology 8, 113-120 (1998).

71. Chatterjee, D., Bozic, C. M., Mcneils, M. & Brennan, P. J. Structural Features of the Arabinan Component of the Lipoarabinomannan of *Mycobacterium tuberculosis*. The Journal of Biological Chemistry 266, 9652-9660 (1991).

72. Hunter, S. W. & Brennan, P. J. Evidence for the Presence of a Phosphatidylinositol Anchor on the Lipoarabinomannan and Lipomannan of *Mycobacterium tuberculosis*. The Journal of Biological Chemistry 265, 9272-9279 (1990).

73. Dinadayala, P., Kaur, D., Berg, S., Amin, A. G., Vissa, V. D., Chatterjee, D., Brennan, P. J. & Crick, D. C. Genetic Basis for the Synthesis of the Immunomodulatory Mannose Caps of Lipoarabinomannan in *Mycobacterium tuberculosis*. Journal of Biological Chemistry 28, 20027-20035 (2006).

74. Chatterjee, D., Lowell, K., Mcneil, M. R. & Brennans, J. Lipoarabinomannan of *Mycobacterium tuberculosis*. The Journal of Biological Chemistry 267, 6234-6239 (1992).

75. Brewan, J., May, R. I., June, I. & Bernard, C. Structure and antigenicity of lipoarabinomannan from Mycobacterium bovis BCG. Journal of General Microbiology 139, 2649-2658 (1993).

76. Karakousis, P. C., Bishai, W. R. & Dorman, S. E. Microreview *Mycobacterium tuberculosis* cell envelope lipids and the host immune response. Cellular Microbiology (2004) 6, 105-116 (2004).

77. Brooks, S. A., Schumacher, U. & Dwek, M., editors. Metastasis Research Protocols. Humana Press. 2012.

78. Hirabayashi Jun & Walker, J. M., editors. Lectins Methods and Protocols. Humana Press. 2014.

79. Agrawal, B. B. B. L. & Goldstein, I. J. Specific Binding of Concanavalin A to Cross-Linked Dextran Gels. Biochemical Journal 96, 23-25 (1965).

80. Goldstein, I. J., Hollerman, C. E. & Smith, E. E. Protein-Carbohydrate Interaction. II. Inhibition Studies on the Interaction of Concanavalin A with Polysaccharides. Biochemistry 4, 867-883 (1965).

81. Scott, J. K., Loganathant, D., Easley, R. B., Gong, X. & Goldsteint, I. J. A family of concanavalin A-binding peptides from a hexapeptide epitope library. Biochemistry 89, 5398-5402 (1992).

82. Harmanson, G. T.Audet, J., editor. Bioconjugate Techniques. London: Elsevier. 2013.

83. Locke, A. K., Cummins, B. M., Abraham, A. A. & Coteí, G. L. PEGylation of concanavalin a to improve its stability for an in vivo glucose sensing assay. Analytical Chemistry 86, 9091-9097 (2014).

84. Kim, J. J. & Park, K. Glucose-Binding Property of Pegylated Concanavalin A. Pharmaceutical Research 18, 794-799 (2001).

85. Lawn, S. D., Mwaba, P., Bates, M., Piatek, A., Alexander, H., Marais, B. J., Cuevas, L. E., Mchugh, T. D., Zijenah, L., Kapata, N., Abubakar, I., Mcnerney, R. & Hoelscher, M. Tuberculosis 2013: 1 Advances in tuberculosis diagnostics: the Xpert MTB/RIF assay and future prospects for a point-of-care test. The Lancet Infectious Diseases 13, 349-361 (2013).

86. Shenai, S., Amisano, D., Ronacher, K., Kriel, M., Banada, P. P., Song, T., Lee, M., Joh, J. S., Winter, J., Thayer, R., Via, L. E., Kim, S., Walzl, G. & Alland, D. Exploring Alternative Biomaterials for Diagnosis of Pulmonary Tuberculosis in HIV-Negative Patients by Use of the GeneXpert MTB/RIF Assay. Journal of Clinical Microbiology 51, 4161-4166 (2013).

87. Pfaffe, T., Cooper-white, J., Beyerlein, P., Kostner, K. & Punyadeera, C. Diagnostic Potential of Saliva: Current State and Future Applications. Clinical Chemistry 57, 675-687 (2011).

88. Chiappin, S., Antonelli, G., Gatti, R. & Palo, E. F. De. Saliva specimen: A new laboratory tool for diagnostic and basic investigation. Clinica Chimica Acta 383, 30-40 (2007).

89. Lawrence, H. P. Salivary Markers of Systemic Disease: Noninvasive Diagnosis of Disease and Monitoring of General Health. Journal of the Canadian Dental Association 68, 170-174 (2002).

90. Education, T. S. Detection of *Mycobacterium Tuberculosis* DNA from peripheral blood in patients with HIV-seronegative and new cases of smear-positive pulmonary tuberculosis by polymerase chain reaction. Respiratory Medicine 97, 676-681 (2003).

91. Condos, R., Mcclune, A., Rom, N. & Neil, W. Peripheral-blood-based PCR assay pulmonary tuberculosis to identify patients with active. The Lancet 347, 1082-1085 (1996).

92. Rebollo, J., San, R., Garrido, J., Folgueira, D., Palenque, E., D, C., Lumbreras, C. & Aguado, M. Blood and urine samples as useful sources for the direct detection of tuberculosis by polymerase chain reaction. Diagnostic Microbiology and Infectious Disease 56, 141-146 (2006).

93. Peter, J. G., Theron, G., Muchinga, T. E., Govender, U. & Dheda, K. The Diagnostic Accuracy of Urine-Based Xpert MTB/RIF in HIV-Infected Hospitalized Patients Who Are Smear- Negative or Sputum Scarce. Plos One 7, 1-8 (2012).

94. Ahmed, N., Mohanty, A. K., Mukhopadhyay, U., Batish, V. K. & Grover, S. PCR-Based Rapid Detection of *Mycobacterium tuberculosis* in Blood from Immunocompetent Patients with Pulmonary Tuberculosis. Journal of Clinical Microbiology 36, 3094-3095 (1998).

95. Wilbur, A., Engel, G., Rompis, A., Putra, I. A., Lee, B. Y.-H., Aggimarangsee, N., Chalise, M., Shaw, E., Oh, G., Schillaci, M. & Jones-Engel, L. From the mouths of monkeys: Detection of *Mycobacterium tuberculosis* complex DNA from buccal swabs of synanthropic macaques. American Journal of Primatology 74, 676-686 (2013).

96. Engel, G. A., Wilbur, A. K., Westmark, A., Horn, D., Johnson, J. & Jones-engel, L. Naturally acquired *Mycobacterium tuberculosis* complex in laboratory pig-tailed macaques. Emerging Microbes and Infections 1, 1-5 (2012).

97. Wilbur, A. K., Salter, L., Hurtado, A. M., Hill, K. R. & Stone, A. C. Vitamin D receptor gene polymorphisms and susceptibility *M. tuberculosis* in Native Paraguayans. Tuberculosis 329-337 (2007).

98. Pollard, T., Earnshaw, W., Lippincott-Schwartz, J. & Johnson, G. Cell Biology. California: Elsevier. 2017.

99. Peterson, J. W.Baron, S., editor. Medical Microbiology. Galveston: University of Texas Medical Branch. 1996.

100. Silva, C. A. M., Danelishvili, L., Mcnamara, M., Berredo-pinho, M., Bildfell, R., Biet, F., Rodrigues, L. S., Oliveira, A. V, Bermudez, L. E. & Pessolani, C. V. Interaction of Mycobacterium leprae with Human Airway Epithelial Cells: Adherence, Entry, Survival, and Identification of Potential Adhesins by Surface Proteome Analysis. Infection and Immunity 81, 2645-2659 (2013).

101. Yamazaki, Y., Danelishvili, L., Wu, M., Hidaka, E., Katsuyama, T., Stang, B., Petrofsky, M., Bildfell, R. & Bermudez, L. E. The ability to form biofilm influences Mycobacterium avium invasion and translocation of bronchial epithelial cells. Cellular Microbiology 8, 806-814 (2006).

102. Ha, K., Chung, Y. & Ryoo, S. Adherence and Biofilm Formation of Staphylococcus Epidermidis and *Mycobacterium Tuberculosis* on Various Spinal Implants. Spine 30, 38-43 (2004).

103. Mullis, S. N. & Falkinham, J. O. Adherence and biofilm formation of Mycobacterium avium, Mycobacterium intracellulare and Mycobacterium abscessus to household plumbing materials. Journal of Applied Microbiology 115, 908-914 (2013).

104. Pe, R., Celdra, A., Garc, C. & Esteban, J. Bacterial Adherence to Different Meshes Used in Abdominal Surgery. Surgical Infections 15, 90-93 (2014).

105. Geier, H., Mostowy, S., Cangelosi, G. A., Behr, M. A. & Ford, T. E. Autoinducer-2 Triggers the Oxidative Stress Response in Mycobacterium avium, Leading to Biofilm Formation. Applied and Environmental Microbiology 74, 1798-1804 (2008).

106. Freeman, R., Geier, H., Weigel, K. M., Do, J., Ford, T. E. & Cangelosi, G. A. Roles for Cell Wall Glycopeptidolipid in Surface Adherence and Planktonic Dispersal of Mycobacterium avium. Applied and Environmental Microbiology 72, 7554-7558 (2006).

107. Velayati, A. A. & Farnia, P. Atlas of *Mycobacterium tuberculosis*. Elsevier. 2017.

108. Andre, G., Deghorain, M., Bron, P. A., Swam, I. I. Van, Kleerebezem, M., Hols, P. & Dufr, Y. F. Fluorescence and Atomic Force Microscopy Imaging of Wall Teichoic Acids in Lactobacillus plantarum. ACS Chemical Biology 6, 366-376 (2011).

109. Beaussart, A., El-kirat-chatel, S., Herman, P., Alsteens, D., Mahillon, J., Hols, P. & Dufre, Y. F. Single-Cell Force Spectroscopy of Probiotic Bacteria. Biophysical Journal 104, 1886-1892 (2013).

110. Ito, Y., Nagao, M., Iinuma, Y., Matsumura, Y., Yamamoto, M., Takakura, S., Rn, J. I., Rn, H. Y., Rn, A. H., Hirai, T., Niimi, A., Ichiyama, S. & Mishima, M. Risk factors for nosocomial tuberculosis transmission among health care workers. American Journal of Infection Control 44, 596-598 (2015).

111. Zaza, S., Blumberg, H. M., Beck-sague, C., Haas, W. H., Woodley, C. L., Pineda, M., Parrish, C., Crawford, J. T., Mcgowan, J. E. & Jarvis, W. R. Nosocomial Transmission of *Mycobacterium tuberculosis*: Role of Health Care Workers in Outbreak Propagation. The Journal of Infectious Diseases 172, 1542-1549 (1995).

112. Banada, P. P., Sivasubramani, S. K., Blakemore, R., Boehme, C., Perkins, M. D., Fennelly, K. & Alland, D. Containment of Bioaerosol Infection Risk by the Xpert MTB / RIF Assay and Its Applicability to Point-of-Care Settings. Journal of Clinical Microbiology 48, 3551-3557 (2010).

113. Jones, G., Matthews, R., Cunningham, R. & Jenks, P. Comparison of Automated Processing of Flocked Swabs with Manual Processing of Fiber Swabs for Detection of Nasal Carriage of Staphylococcus aureus. Journal of Clinical Microbiology 49, 2717-2718 (2011).

114. Jorgensen, J. H., Carroll, K. C. & Funke, G.Pfaller, M. A., Landry, M. L., Richter, S. S. & Warnock, D. W., editors. Manual of Clinical Microbiology. Washington: ASM Press. 2015.

115. Paramasivan, C. N., Narayana, A. S., Prabhakar, R., Rajagopal, M. S., Somasundaram, P. R. & Tripathy, S. P. Effect of storage of sputum at room temperatureon smear and culture results. Tubercle 64, 119-124 (1983).

116. Lumb, R., Ardian, M., Waramori, G., Syahrial, H., Tjitra, E., Maguire, G. P., Anstey, N. M., Kelly, P. M., Science, V. & Ministry, D. An alternative method for sputum storage and transport for *Mycobacterium tuberculosis* drug resistance surveys. International Journal of Tuberculosis and Lung Disease 10, 172-177 (2006).

117. Tagliani, E., Alagna, R., Tafaj, S., Hafizi, H. & Cirillo, D. M. Evaluation of *Mycobacterium tuberculosis* viability in OMNIgene-SPUTUM reagent upon multi-day transport at ambient temperature. BMC Infectious Diseases 17, 1-5 (2017).

118. Medical Wire. Dryswab - leading in specimen collection Dryswab TM - Better specimens for better science. 1-8

119. Reed, J. L., Basu, D., Butzler, M. A. & Mcfall, S. M. XtracTB Assay, a *Mycobacterium tuberculosis* molecular screening test with sensitivity approaching culture. Scientific Reports 7, 1-12 (2017).

120. Yang, P., Zhang, X., Xie, J., Chen, J. & Yang, W. Micro/Nanoscale Well and Channel Fabrication on Organic Polymer Substrates via a Combination of Photochemical and Alkaline Hydrolysis Etchings. Biomacromolecules 7, 2770-2775 (2006).

121. Drobota, M., Persin, Z., Zemljic, L. F., Mohan, T., Stana-kleinschek, K., Doliska, A., Bracic, M., Ribitsch, V., Harabagiu, V. & Coseri, S. Chemical modification and characterization of poly(ethylene terephthalate) surfaces for collagen immobilization. Central European Journal of Chemistry 11, 1786-1798 (2013).

122. Irena, G., Jolanta, B., Karolina, Z. & Pet, E. Applied Surface Science Chemical modification of poly(ethylene terephthalate) and immobilization of the selected enzymes on the modified film. Applied Surface Science 255, 8293-8298 (2009).

123. Liu, Y., Lu, H., Zhong, W., Song, P., Kong, J., Yang, P., Girault, H. H. & Liu, B. Multilayer-Assembled Microchip for Enzyme Immobilization as Reactor Toward Low-Level Protein Identification. Analytical Chemistry 78, 6426-6433 (2006).

124. Fu, J., Ji, J., Fan, D. & Shen, J. Construction of antibacterial multilayer films containing nanosilver via layer-by-layer assembly of heparin and chitosan-silver ions complex. Journal of Biomedical Materials Research Part A 79, 665-674 (2006).

125. Fu, J., , J. J., Yuan, W. & Shen, J. Construction of anti-adhesive and antibacterial multilayer films via layer-by-layer assembly of heparin and chitosan. Biomaterials 26, 6684-6692 (2005).

126. Jiang, X., Chai, C., Zhang, Y. & Zhuo, R. Surface-immobilization of adhesion peptides on substrate for ex vivo expansion of cryopreserved umbilical cord blood CD34 cells. Biomaterials 27, 2723-2732 (2006).

Chapter 3

Surface functionalisation and characterisation of PET microfibres

3.1 Introduction

Poly(ethylene terephthalate) (PET) is a commercially available thermoplastic, sought after by several industries, as a result of its physical and optical properties. Similar to other polyesters, its produced by the reaction of dicarboxylic acids and diols. In the case of PET, the dicarboxylic acid is terephthalic acid and the diol is ethylene glycol. It follows that the consequential recurrent ester entity, or more accurately electrophilic carbonyl carbon moiety, makes PET material a prospective polymer in several regards other than just the mere commonplace uses. The molecular structure of PET is inert to a broad spectrum of chemical reactions, but the carbonyl groups do make it prone to nucleophilic attack. This is a property which can be utilised to promote subsequent chemical modifications to these materials, while maintaining a predominantly unreactive base polymer.

Surface functionalisation is one such modification of PET. This implies that the bulk chemical composition of the original material remains unchanged, while the chemical properties at the surface of the material can be markedly different[1]. The surface functionalisation of these polymers can be achieved by any one of several methods such as the controlled breaking of ester bonds by means of amination[2-8], enzymatic treatment[9], plasma treatment[10], hydrolysis[11] and several other techniques[12-14], or by surface grafting polymerisation[15-23]. Surface functionalisation does, however, not necessarily imply the formation of chemical bonds between the material surface and the surface-active agent to be introduced. It is also possible to physically immobilise the surface-active agent onto the polymer surface. This approach does not offer the

durability chemical immobilisation does. As such, forming a covalent bond between the surface-active agent and the polymer surface prevents leaching from the matrix, making this the preferred approach[24,25].

PET modification is not limited to only surface modifications. The thermoplastic property permits bulk functionalisation of the polymer in the molten state as well. The advantages of surface functionalisation nevertheless often outweigh this option, primarily since it is a more practical approach at achieving a tailored PET material. The physical properties of PET materials make them desirable, and while surface modification leaves the physical properties largely unchanged, modification in the bulk will necessarily influence the aforementioned properties. This obviously also means that the extent of surface modification before the physical properties are negatively affected, is limited. This is because surface modification is largely achieved through chain scission reactions. Modification in the bulk is limited to the point of material failure, while surface modification is limited as a function of sample depth. If the requirement of the modification is only for the part of the polymer in contact with the environment to be modified, then modification of the bulk of the material is superfluous. Together with this, fewer amount of chemicals are used during the surface functionalisation process[26]. Finally, surface reaction conditions are generally much milder and easier to control than bulk reactions in the melt, since PET has a melting point in excess of 250 $^{\circ}$C.

In order to chemically immobilise surface-active agents onto the polymer surface, there must be reactive groups present on both the material and the compound of interest[24]. Within the scope of this study, a nucleophilic fibre surface was created, by the introduction of hydroxyl and primary amine groups. This was achieved by reacting the material with glycol and diamine molecules respectively. Consecutively, the surface-active agent to be immobilised was Concanavalin A (Con A), a protein with 13 reactive primary amine substituent per molecule[27,28].

In what follows, we report the selective surface degradation and characterisation of PET microfibres. The general procedure entailed that the surface of the PET microfibres were solvent annealed preceding treatment with difunctional nucleophilic molecules. The virgin PET microfibres were characterised using total reflectance Fourier transform infrared (ATR-FTIR) spectroscopy and scanning electron microscopy (SEM). The treated fibres were characterised by selective dye staining, energy dispersive X-ray spectroscopy (EDX) and SEM.

3.2 Selective surface degradation of PET

The chemically inert nature of PET means that materials comprised of the polymer are not easily chemically modified. To introduce of functional groups onto the surface of such materials, therefore, requires cleavage

of the polyester polymer chains. Due to the electrophilicity of the carbonyl group, this can be achieved by exposing the polymer to a source of nucleophiles. Both primary amines and alcohols can be used for this purpose. Primary amines being the more nucleophilic of the two, and producing less reactive amides compared to esters as product, were preferentially used throughout this study[29]. Treating PET with either of the two nucleophiles, results in a nucleophilic substitution reaction at polyester carbonyl carbon, leading to the remainder of the PET chain being dislodged as a leaving group. As such polyester chain scission occurs leading to the selective degradation of the material.

To create functional groups on a microfibrous PET surface, diamines and diols were used as the nucleophilic molecules. One end of the molecule could then cleave the polymer chain, while the other remains available for subsequent reactions. For the purposes of this study, ethylene glycol and ethylenediamine were used. This lead to the presence of primary amine and hydroxyl functional groups on the fibre surfaces (Scheme 3.1) Once these functional groups are introduced, all subsequent reactions occur only at the functional groups, leaving the bulk of the fibre unaffected.

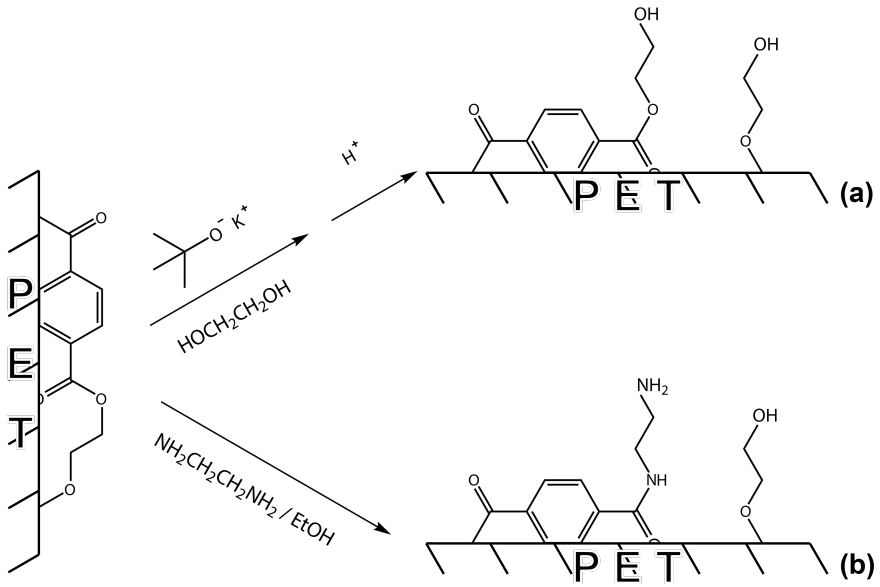

Scheme 3.1: PET surface degradation reaction by means of (a) glycolysis with ethylene glycol or (b) amination with ethylenediamine.

3.2.1 Material limitations

In addition to the substrate chemistry, several material properties also need to be accounted for, due to the fibrous form of PET used. This is the case since all modification reactions intended would be biphasic, in which the solid fibre phase would necessarily occupy a large volume. This necessitates that the chemical

reactions be conducted in a manner which ensures an equivalent experimental environment throughout the study.

3.2.1.1 Surface morphology

Microfibres are produced by means of air drawing molten PET upon extrusion, followed by cold drawing the fibres down to a desired fibre diameter. This has a pronounced effect on the morphology of the polymer chains, resulting in their alignment parallel to the direction of drawing. This phenomenon can be observed from the presence of several striations parallel to the fibre length; when viewing a SEM micrograph of a sectioned fibre (Figure 3.1 a and b).

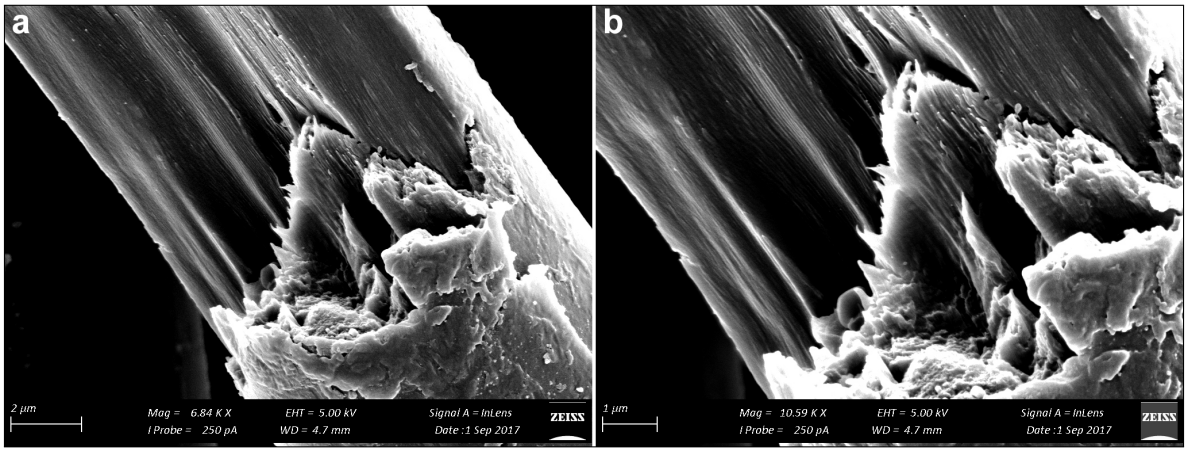

Figure 3.1: (a) SEM micrographs of a sectioned PET fibre. (b) Enlargement of (a).

This aligned morphology and particularly the parallel orientation of the polymer chains to the fibre surface, acts as an inhibitor for degradation reactions. Consequently, this limits the maximum density of functional groups achievable on the fibre surface. The occurrence can be explained by using Figure 3.2. The density of functional groups increases when chains have a less parallel, but rather a more perpendicular orientation with respect to the plane of the surface. This results in more chain segments being available for cleavage[30].

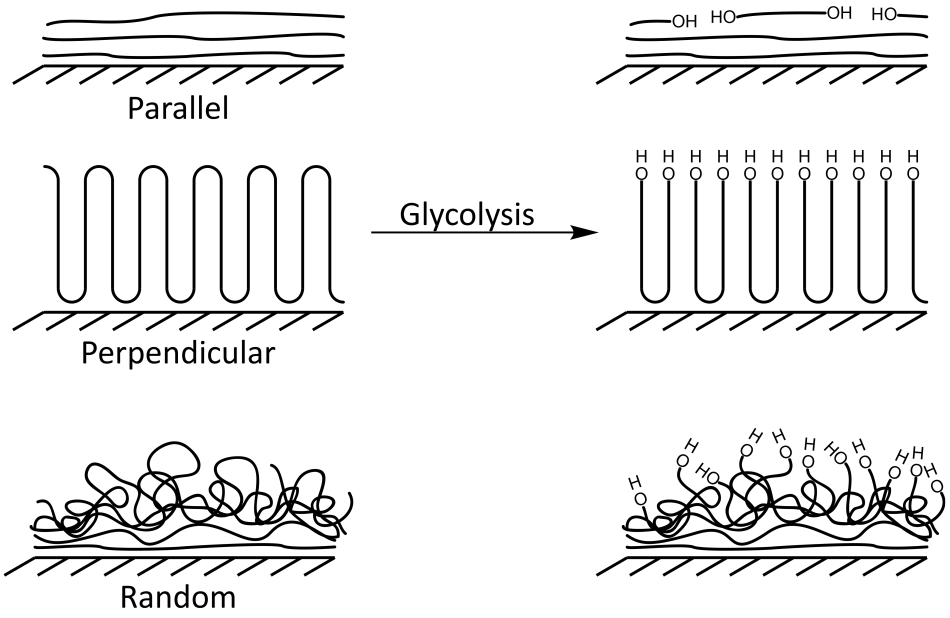

Figure 3.2: Conformations of polymer chains at the surface of a PET fibre[30].

To remedy this, the polymer fibres were annealed in tetrahydrofuran (THF). This promotes relaxation and accordingly reorientation of the polymer chains at the surface of the fibres, facilitating randomisation. This random orientation makes more chain segments susceptible to nucleophilic attack and hence leads to greater surface functional group densities.[30]

3.2.1.2 Extent of surface modification reaction

Since polymer chains are cleaved in order to yield functional groups, degradation of the substrate will necessarily occur. It follows that reaction conditions need to be optimised to find a balance between the concentration of functional surface groups and the integrity of the material as a whole. This becomes especially pronounced as the surface area to volume ratio increases, as is the case of microfibres.

In addition, the yield of functional groups which can be achieved may vary with sample depth. This relates to surface morphology, where the morphology of the polymer chains can vary as a function of depth. This together with the issues highlighted in Section 3.2.1.1 can be solved by limiting the reagent concentration, exposure time and reaction temperature.

3.2.1.3 Fibre logistics

When working with high modulus fibres of sufficient length to entangle, several logistical issues prohibit reproducible reaction conditions. Accordingly, these issues and their overall solution is discussed below.

When modifying loose fibres in solution, the fibres combine to form tightly knotted clusters. These clusters can become dense enough to prevent sufficient penetration of solvents, and also prohibit stirring and later washing.

Another problem relates to the volume occupied by the fibres and the interstitial spaces which exists between them. Since the fibres have a large surface to volume ratio and are unbound, they necessarily occupy a large volume. This limits reaction parameters to small sample size/large solvent volumes. In addition, the spaces in between the fibres trap air inside, resulting in the presence of air pockets and the exclusion of solvents.

It follows from the above-mentioned this that not all fibre segments can be equivalently treated while the substrate is in its loose fibre form. To overcome these issues, the fibres were carded and loosely secured onto a glass tripod (Figure 3.3). This could then be suspended in the reaction mixture, contained in a Schlenk tube. The entrapment of air was circumvented by using low viscosity solvent systems.

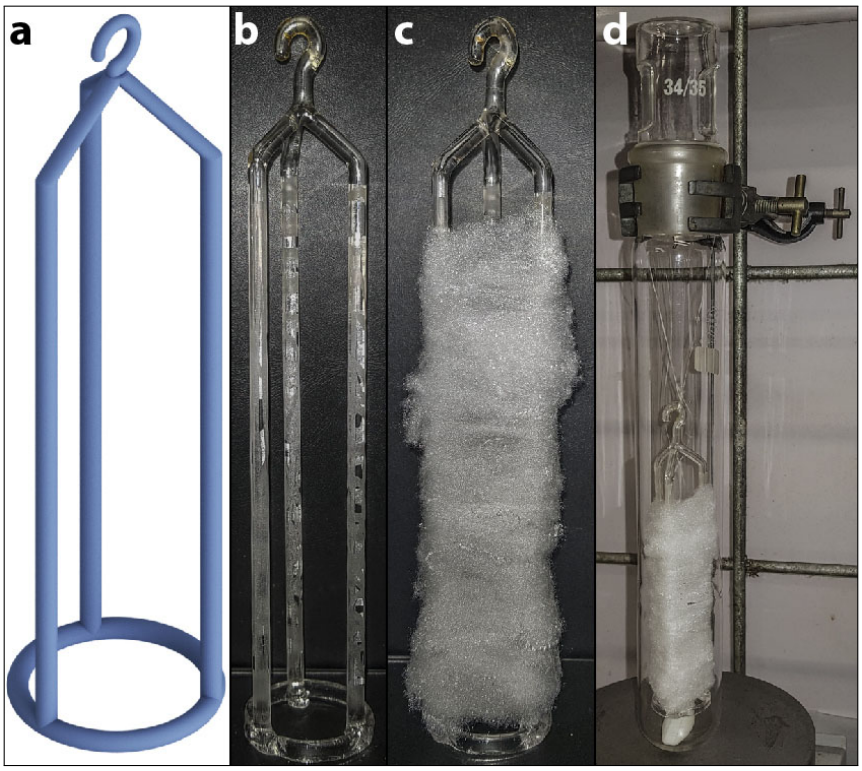

Figure 3.3: (a) Three-dimensional model of the glass tripod used to secure PET microfibres during functionalisation and activation reactions. (b) Picture of actual device used, (c) fibres secured onto the tripod and (d) the secured fibres inside the Schlenk tube reaction vessel.

3.3 Experimental

3.3.1 Materials

PET microfibres were donated by Propet SA (Pty) Ltd. The fibres had an average diameter of 10 µm, density of 1.38 g/cm^3 and were composed of 40% virgin and 60% recycled food grade PET. The production process included air drawing of the fibres from molten state, upon extrusion from a spinneret, hereafter they were drawn down to a desired diameter by means of counter rotating rollers.

The following chemicals were utilised in this part of the project: ethylene glycol (Merck, 99%), ethylenediamine (Sigma-Aldrich, 99%), tetrahydrofuran (Merck), ethanol (Merck, 99%), hexane (Merck, 99%), hydrochloric acid 32% (Merck), potassium tert-butoxide (Sigma-Aldrich, ≥98%).

3.3.2 Characterisation techniques

3.3.2.1 Attenuated total reflectance Fourier transform infrared (ATR-FTIR) spectroscopy

All Infrared spectra were collected with a Nicolet^{TM} iS^{TM} 10 FT-IR from Thermo-Fischer. The instrument had been equipped with Smart iTR^{TM}, attenuated total reflectance (ATR) sampling accessory configured with a diamond ATR crystal. The crystal had an incident angle of 42 °, refractive index of 2.4 and enabled a penetration depth of 2.03 µm.

Spectra were produced from 64 individual scans, with a spectral resolution of 4 cm^{-1} recorded in the range of 4000 cm^{-1} to 650 cm^{-1}. Thermo-Fischer Scientific Inc. Omnic 8.1 software was used for data acquisition and processing, which included baseline correction. Samples were analysed in the solid state, requiring no preparation.

3.3.2.2 Scanning electron microscopy (SEM)

SEM micrographs were collected with the aid of a Zeiss MERLIN Scanning Electron Microscope. For every sample analysed, the fibres were secured onto an 8 x 10 mm square of double sided carbon tape and mounted on SEM specimen stubs. Subsequently the fibres were coated with gold sputter under vacuum with an Edwards S15OA Sputter Coater. This coating was applied in order to make the sample surfaces electrically conductive. Micrographs were attained with Zeiss SmartSEM software.

3.3.2.3 Energy dispersive X-ray spectrometer (EDX)

EDX analysis was performed with the use of a ZEISS EVO MA15VP SEM instrument. This analysis allowed for the semi-quantitative detection of nitrogen moieties on the surface of PET fibres. A boron hydride standard was selected as a reference standard for nitrogen. Sample preparation was similar to that of SEM, where the only difference was a carbon coating of the samples, rather than a gold coating. The carbon coating was produced by means of carbon rod evaporation under vacuum, enabled by a Quorum Q150T E Turbo-Pumped Sputter Coater/ Carbon Coater.

3.3.2.4 Ninhydrin test

A ninhydrin test was performed on the PET-NH_2 microfibres to confirm the presence of primary amine groups. Since the test returned a positive result, it could not subsequently be used to confirm the presence of immobilised protein on the fibre surface.

The test was performed by placing a 0.5 mg fibre sample in a test tube, to which 100 µL of ninhydrin in ethanol (500 mg ninhydrin in 10 mL 95% absolute ethanol), 100 µL phenol in ethanol (40 mg phenol in 10 mL 95% absolute ethanol) and 50 µL KCN in pyridine (2 mL 0.001M KCN solution in distilled water, diluted to 100 mL with distilled pyridine) was added. Thereafter, a glass marble was placed over the opening of the tube and the mixture heated to 80 °C for 5 minutes. A colour change from colourless to Ruhemann's purple confirmed the presence of primary amine groups. The colour change was compared to the control fibre study which consisted of virgin PET, and did not indicate any colour change.

3.3.3 Experimental Procedures

3.3.3.1 Annealing PET fibres

PET micro-fibres (about 1 g) were carded and mounted on a glass tripod. The tripod was then submerged in THF contained in a Schlenk tube. These fibres were then allowed to anneal for three days at 30 °C under constant stirring. Thereafter, the fibres were washed with ethanol followed by hexane to remove the majority of THF from the fibres. The mounted fibres were placed in a vacuum oven at 50 °C and allowed to dry for two hours under vacuum.

3.3.3.2 Surface glycolysis of PET fibres (PET-OH)

Annealed and mounted PET micro-fibres (0.75 g) were submerged in a nitrogen purged 0.60 M potassium tert-butoxide in ethylene glycol solution. After 4 hours of reacting at 30 °C under constant magnetic stirring, the fibres were washed with ethylene glycol, water (two aliquots), 0.1 M HCl (two aliquots), water (two aliquots), ethanol and hexane. Thereafter, the fibres were allowed to dry for 16 hours in a vacuum oven at 50 °C under vacuum. This procedure for the introduction of hydroxyl groups onto a PET surface, is based on a method described in the work of Chen et al[30].

The reaction which takes place is a base catalysed transesterification of PET with ethylene glycol (Scheme 3.2). A nucleophilic substitution takes place at one of the PET carbonyl carbons at the surface of the fibre.

This then leads to the formation of a tetrahedral intermediate, succeeded by the expulsion of the PET chain, which acts as a leaving group. Upon acidification, a PET surface enriched with hydroxyl groups is produced.

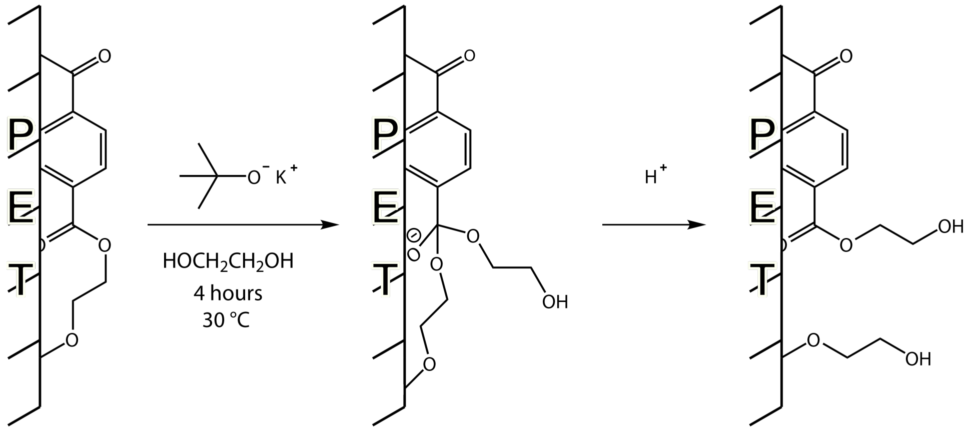

Scheme 3.2: Base catalysed glycolysis of PET.

3.3.3.3 Surface amination of PET fibres (PET-NH_2)

Annealed and mounted PET micro-fibres (1.00 g) were submerged in an ethylenediamine in ethanol solution (ethylenediamine/ethanol=1:3) and allowed to react for 3 hours at 30 °C under constant stirring. The fibres were sequentially rinsed with ethanol (3 aliquots) and hexane, before being placing in a vacuum oven at 50 °C for 16 hours under vacuum. The amine introduction procedure is based on a method by Zhang et al[6].

The reaction proceeds in a similar fashion to the glycolysis reaction, where one nucleophilic end of ethylenediamine can partake in a nucleophilic substitution reaction with a carbonyl carbon. This then also leads to a tetrahedral intermediate formation (Scheme 3.3). In this case, however, the PET alkoxide is a much better leaving group than the amine. As such, the reaction progresses rapidly, with the formation of both amine and hydroxyl groups on the surface.

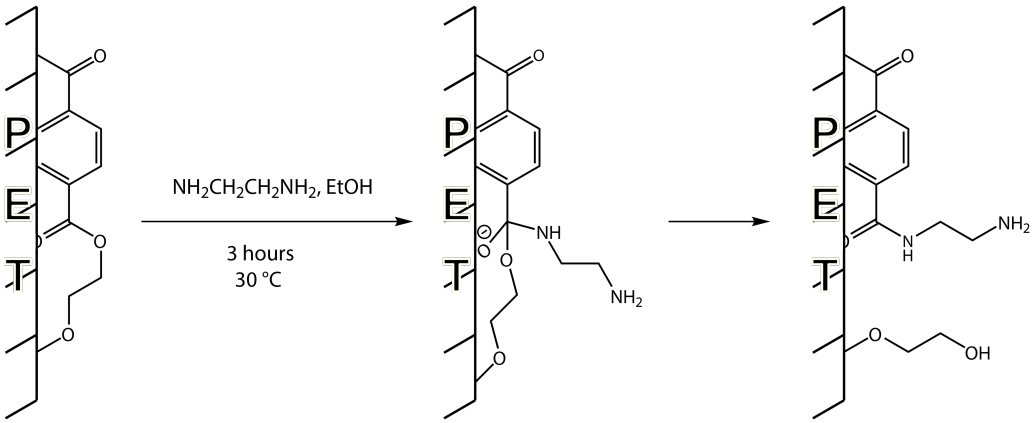

Scheme 3.3: Amination of PET.

3.3.3.4 Reactive dye staining of PET-OH

Glycolised PET fibres (0.5 g) and virgin PET fibres (0.5 g) where dispersed in separate vials of deionised water (20 mL), before being transferred to dye solution filled stainless steel dye cylinders. The dye solutions consisted of NaCl (8.0 g), Corafix Red GD-B reactive dye (0.04 g) and deionised water (60 mL).

The dye tubes where then sealed, shaken and placed in a Roaches Pyrotech 2000 series dye apparatus. The dye profile consisted of heating the dye bath to 40 °C, letting it equilibrate for 10 minutes, followed by heating to 60 °C (3 °C/min) and allowing the reaction to proceed for 30 minutes. At this point, Na_2CO_3 (2.0 g) dissolved in deionised water (20 mL), was injected into the cylinders and the procedure continued at 60 °C for 60 minutes. Upon completion, the fibres where washed with deionised water (10 aliquots), acetone (5 aliquots), ethanol and hexane, before allowing them to dry in a vacuum oven at 50 °C for 2 hours under vacuum.

Comparable samples where produced by first securing 0.1 g of virgin, dye exposed virgin and dyed hydrolysed PET fibres to double sided tape, covering the fibres with Sellotape and placing 15 tonnes of pressure on the samples for 5 minutes. Thereafter the various fibre mats where compared to one another in a lightbox under CIE Standard Illuminant D65. The reference used was a grey scale for assessing change in colour ISO 105 A02.

3.3.3.5 Acid dye staining of PET-NH_2

Aminated PET fibres (0.5 g) and virgin PET fibres (0.5 g) where dispersed in separate vials of deionised water (20 mL), before being transferred to dye solution filled stainless steel dye cylinders. The dye solutions

consisted of Corafix Blue 2R Leavaset acid dye (0.045 g), deionised water (78 mL) and 10% acetic acid (2 mL).

The dye tubes where then sealed, shaken and placed in a Roaches Pyrotech 2000 series dye apparatus. The dye profile consisted of heating the dye bath to 40 °C, letting it equilibrate for 10 minutes, followed by heating to 100 °C (2.5 °C/min) and allowing the reaction to proceed for 30 minutes. Thereafter the dyebath was cooled to 60 °C (5 °C/min) and the fibres removed. Upon completion, the fibres where washed with deionised water (10 aliquots), acetone (5 aliquots), ethanol and hexane, before allowing them to dry in a vacuum oven at 50 °C for 2 hours under vacuum.

Sample comparison was done in the same fashion as the reactive dye stained PET-OH fibres.

3.4 Results and discussion

This section is dedicated to the discussion of the synthesis and characterisation of functionalised PET precursor substrates. These include a hydroxyl rich (PET-OH) fibre surface attained by glycolysis, as well as a hydroxyl and amine rich (PET-NH_2) fibre surface attained by amination of the PET microfibres. The aminated substrate was preferentially chosen for subsequent activation and immobilisation reactions.

3.4.1 Poly(ethylene terephthalate) (PET) fibres

Commercially available crimped PET staple fibres (3 cm in length with a 10 µm diameter) were used as the base polymer throughout this study. Since these fibres are produced from 40% virgin PET and 60% recycled food grade PET, the exact composition and molecular weight of the polymer could not be verified. The limited solubility of the polymer in organic solvents meant that analysis of the fibres before and after its modifications were limited to surface analysis techniques.

3.4.1.1 Attenuated total reflectance Fourier transform infrared (ATR-FTIR) spectroscopy

To verify that the base polymer was PET, an FTIR spectrum of the fibres was compared against that of pristine PET. Figure 3.4 shows that the IR spectrum for (a) microfibres comprised of 40% virgin PET and 60% recycled PET closely match that of (b) pristine PET. The characteristic absorption bands of PET are summarised in Table 3.1 and are marked as broken lines on Figure 3.4.

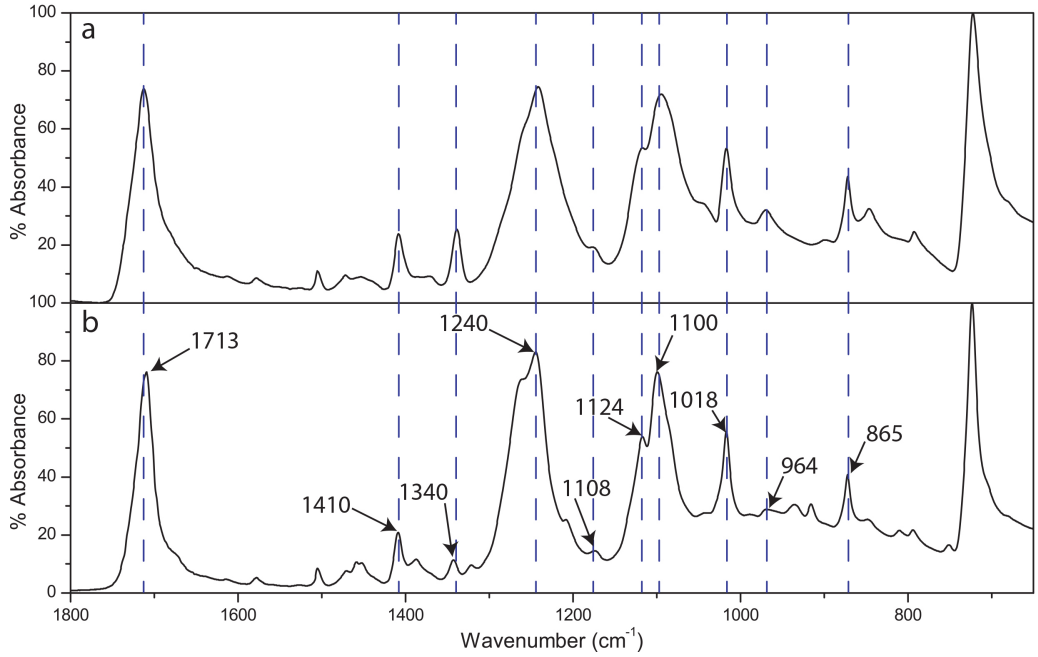

Figure 3.4: FTIR spectra of (a) microfibres comprised of 40% virgin PET and 60% recycled PET (b) pristine PET.

Table 3.1: FTIR spectral absorption bands of PET[31].

Absorption bands of PET	Attribution
1713 cm^{-1}	(C=O) Stretching vibrations
1410, 1018, and 865 cm^{-1}	Aromatic ring vibration
1340 and 1180 cm^{-1}	(-CH_2) Bending vibration
1240 and 964 cm^{-1}	(C-O) Stretching vibration in amorphous region
1124 and 1100 cm^{-1}	(C-O) Stretching vibration in crystalline region

The IR spectra of (a) and (b) are predominantly in agreement with respect to the characteristic absorption bands of PET. This suggests that the fibres selected for this study consists of PET and will be suitable to conduct this study with.

3.4.2 Glycolysis of PET (PET-OH)

Glycolised PET (PET-OH) (Figure 3.5) is the product obtained from a transesterification reaction of PET with a glycol. It is generally synthesised by reacting the polyester substrate with an excess of ethylene glycol, in a basic environment[30]. When this reaction occurs, a PET surface rich in hydroxyl groups is produced. The presence of hydroxyl groups were confirmed by a reactive dye staining test (Figure 3.6).

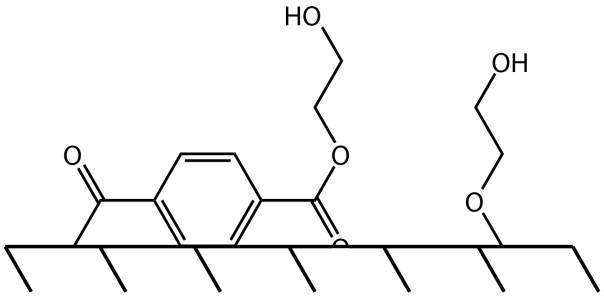

Figure 3.5: PET surface glycolysis product (PET-OH).

3.4.2.1 Reactive dye stain test

Reactive dyes are polyfunctional molecules, which possess over several groups able to react with hydroxide groups on a substrates surface[32]. When the glycolised PET fibres were treated with such a reactive dye, namely Corafix Red GD-B, a colour change from white to pink could be observed (Figure 3.6).

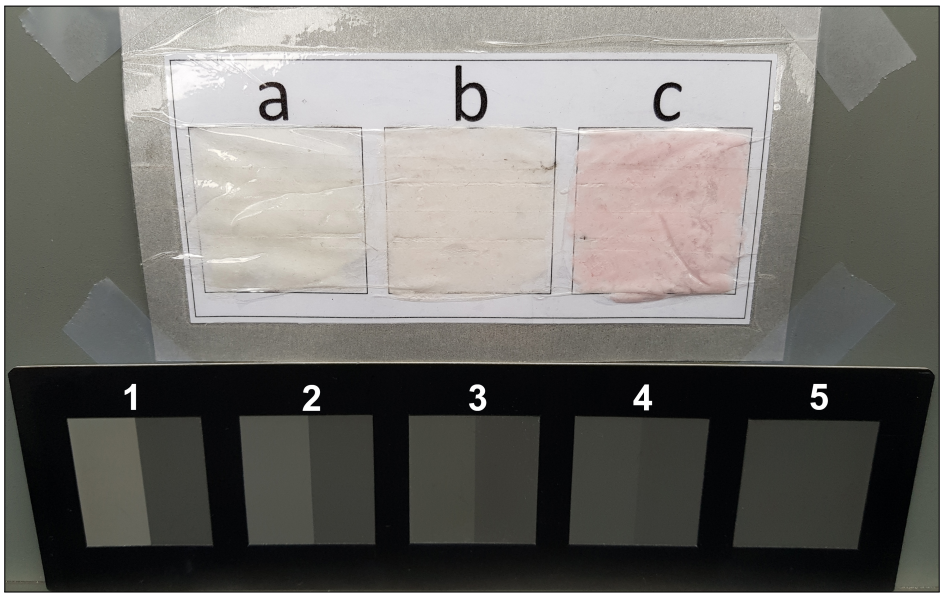

Figure 3.6: Grey scale assessment of the colour change observed for (a) un-dyed virgin PET microfibres, (b) reactive dye treated virgin PET fibres and (c) reactive dye treated PET-OH fibres.

Visual comparison, by the aid of a grey scale for assessing colour change, revealed that virgin PET (b) had dyed one shade darker than the original colour of the fibres (a). This corresponded to a scale value of 4 (Figure 3.6). PET-OH fibres (c) treated with the dye had dyed four shades darker than (a), corresponding to a scale value of 1.

The overall change in colour when comparing samples (b) and (c) to one another was three shades. This indicated that the glycolysis reaction had been successful in producing reactive groups on the fibre surface. With respect to the chemical reagents used, the consulted literature and the reactivity of the dye, these functional groups were presumed to be hydroxyl groups[35].

3.4.2.2 Scanning electron Microscopy (SEM)

SEM was used to analyse the fibre surface after glycolysis to determine whether any topographical changes had occurred (Figure 3.7). From the micrographs, no changes due to degradation, could be observed between the virgin and the gycolised fibres. This suggest that the reaction conditions were mild enough to prevent damage to the surface of the fibres, yet potent enough to change the chemistry of it. The latter is observable from the reactive dye stain test (Section 3.4.2.1).

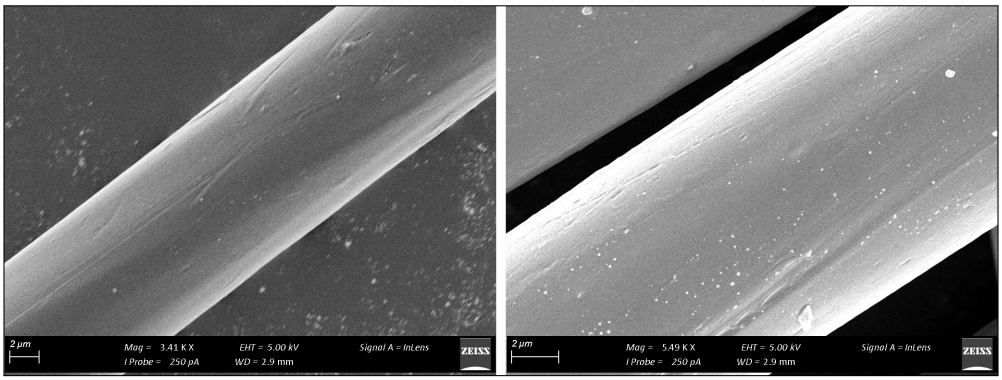

Figure 3.7: SEM micrographs of (a) Virgin PET and (b) PET-OH fibres.

3.4.3 Amination of PET (PET-NH_2)

Aminated PET (PET-NH_2) (Figure 3.8) is the substrate obtained from the nucleophilic substitution reaction at the carbonyl carbon of PET with a diamine, to form an amide. The product of this reaction is a fibre surface functionalised with primary amine as well as hydroxyl groups.

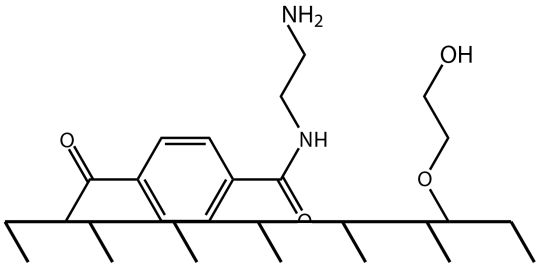

Figure 3.8: PET surface amination product (PET-NH_2).

During the amination of PET, the concentration of surface amine and hydroxyl groups are strongly influenced by the sequence in which ester cleavage reactions take place. This can be explained with reference to Scheme 3.4, with cleavage sites indicated as broken lines.

If position 1 is considered to be the initial site of cleavage, one hydroxyl and one primary amine group would be generated on the surface. If in addition, cleavage is limited to only primary events, then a surface with an equal distribution of hydroxyl and amine groups will be produced. When this is not the case and sequential cleavage occurs in close proximity to position 1, then an unequal distribution of hydroxyl and amine groups will be produced. In such cases, the relative concentration of functional groups depends on the rates at which the different nucleophile substitution reactions take place. The reaction which then follows the primary cleavage can occur at:

2a → yielding two amine groups.
2b → yielding two hydroxyl groups.
or 2c → which will yield one amine and one hydroxyl group.

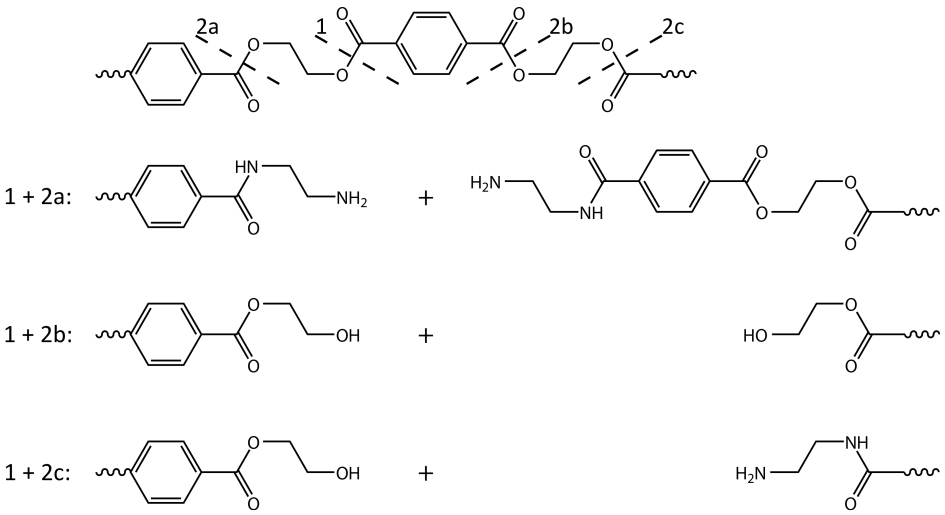

Scheme 3.4: Sequential ester cleavage events and their corresponding products[30].

The amide derivatives which do form, however, are more stable than the corresponding esters. In addition, the functional amine groups introduced onto the surface, are also more nucleophilic than the hydroxyl groups generated in both this and the glycolysis reaction. These two factors, make surface amination the preferred method of surface preparation.

This type of modification is typically done by exposing a PET surface to ethylenediamine, which has been diluted in ethanol, to a preferred concentration[6]. The extent of dilution moderates the reaction rate of the diamine, allowing for a controlled homogeneous surface modification.

The presence of primary amine groups were confirmed by a ninhydrin test, acid dye staining test and EDX analysis.

3.4.3.1 Ninhydrin test

Ninhydrin reactions are widely used for the analysis and characterisation of compounds which poses primary or secondary amine groups[33]. Once the ninhydrin reacts with these groups, a purple dye known as Ruhemann's purple is formed. Accordingly, the presence of amine groups can be observed by a colour change of the ninhydrin solution[34].

This test is anomalous amongst chromogenic reactions, since ninhydrin's reaction with primary amines at a pH of 5.5 generates the same chromophore, irrespective of the molecular architecture of the amine. As a result of this, ninhydrin assays are applicable to either soluble or insoluble solid samples[35,36].

The application of this assay to PET-NH_2 fibres resulted in the formation of Ruhemann's purple,thereby confirming the presence of primary amines on the fibre surface. The drawback of the assay is, however, its limitation to provide only qualitative analysis. This is due to the fact that the amount of the chromophore produced, is not always stoichiometric. Accordingly, variations are observed depending on the nature of the sample analysed, irrespective of the primary amine concentration[35].

3.4.3.2 Acid dye stain test

Acid dye staining is a dye process, which involves not only ionic interaction between cationic groups on the fibre surface (protonated amines) and anionic dye molecules in solution, but also hydrophobic affiliation[32]. To favour the ionic interaction, the functional groups on the fibre were protonated, by conducting the reaction in the presence of acetic acid. When the aminated PET fibres were treated with such an acid dye, namely Corafix Blue 2R Leavaset acid dye, a colour change from white to blue could be observed (Figure 3.9).

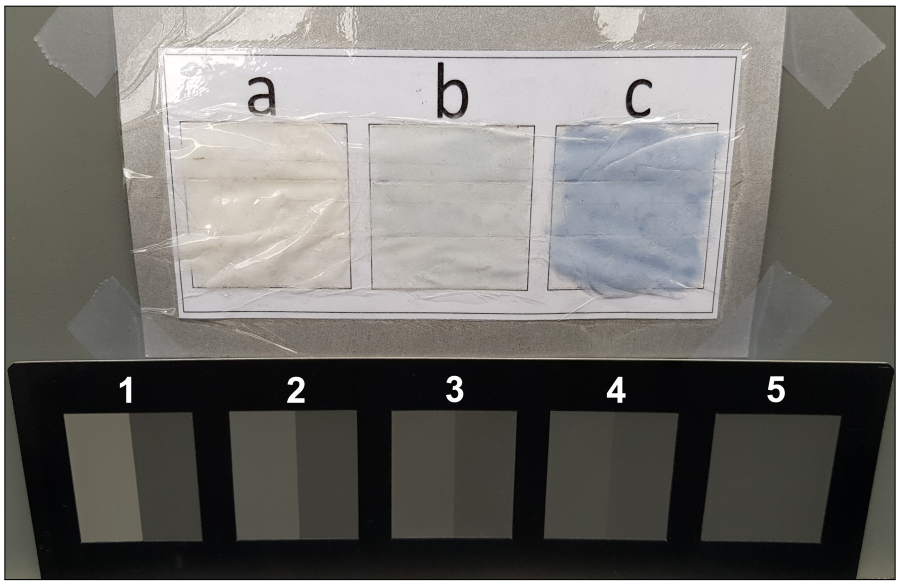

Figure 3.9: Grey scale assessment of the colour change observed for (a) un-dyed PET microfibres, (b) Leavaset Blue 2R dye treated PET fibres and (c) dye treated PET-NH_2 fibres.

The various dye treated fibres were compared to one another by aid of a grey scale for assessing colour change. From Figure 3.9 it can be seen that the virgin PET (b) had dyed one shade darker than the original colour of the fibres (a). This corresponded to a scale value of 4. PET-OH fibres (c) treated with the dye had dyed four shades darker than (a), corresponding to a scale value of 1.

The net colour change observed when comparing samples (b) and (c) to one another was three shades. This was an indication that the amination reaction had been successful in producing reactive groups on the fibre surface, capable of reacting with the acid dye. With respect to the chemical reagents used and the consulted literature, primary amine groups were presumed to be present on the fibre surface[6].

3.4.3.3 Energy dispersive X-ray spectroscopy (EDX)

EDX is a surface analysis technique commonly used for localised elemental analysis. Since PET is comprised of only carbon, oxygen and hydrogen, this technique is useful for detecting the presence of foreign elements, such as nitrogen introduced into the PET matrix. Accordingly, EDX could be used to approach a quantitative assessment of the extent of PET fibre amination, by detecting the amount of nitrogen analogues introduced.

Figure 3.10 represents the data collected from such an analysis. It shows that a source of nitrogen had been present in the virgin PET fibres. This is likely an additive used during the production of the fibres, or a

contaminant from the recycled sources of PET. The figure also shows that upon aminating the fibres, the detected nitrogen content increased from the 0.28 weight percent observed from the virgin PET fibres to 0.67 weight percent.

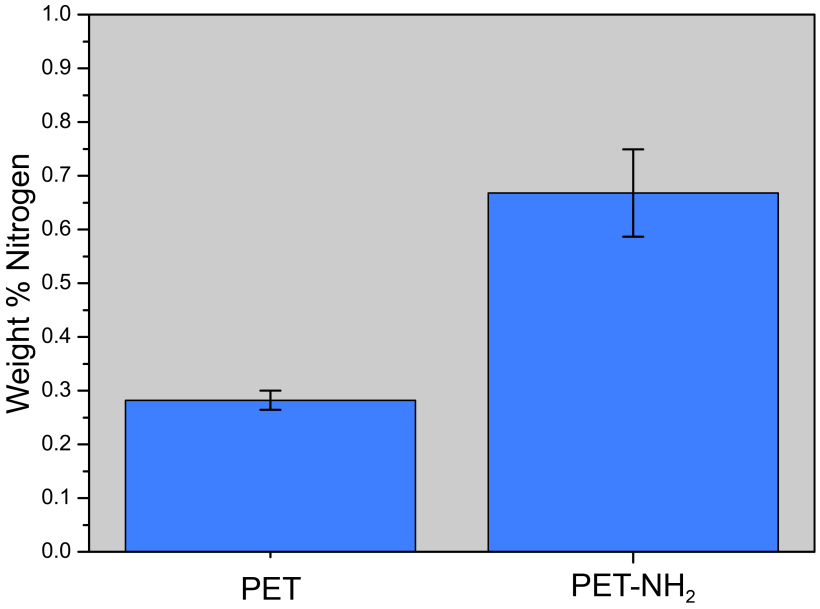

Figure 3.10: Average weight % nitrogen present in a virgin PET sample and an aminated PET sample (PET-NH_2). Error bars correspond to standard deviation.

The data from this study suggests that amination lead to a 2.4 fold increase in the nitrogen content on the surface of the fibres. It is also apparent that there is a greater standard deviation associated with the aminated fibres. The latter can be attributed to two factors. The first of which is, rapidly degradation of the fibres during the analysis. This entailed that the fibres either melted away as the scanning beam passed over them, or blew apart. As a result, it was not only the surface of the samples being analysed. This resulted in elemental detection within the bulk of the sample, rather than the modified outer layer. The variation was, therefore, less prominent in the virgin PET sample, as its surface and core are homologous. The second contributing factor was the distribution of the fibres on the detection surface. The regularity of the virgin fibres and the fact that they had been crimped together, meant that they were able to pack together uniformly on the detection surface. The aminated fibres, having been carded before treatment, could no longer pack together closely. This meant that they could not cover the detection surface uniformly, leading to several voids between the fibre strands. Since the EDX instrument reports the elemental content per area scanned, non-uniform detection areas are prone to produce data sets with large standard deviations.

The analysis can be concluded to have been semi-quantitative, yet useful for confirming an increase in nitrogen containing moieties upon amination of PET fibres.

3.4.3.4 Scanning electron Microscopy (SEM)

After amination, the surface of the fibres were analysed by SEM and compared to virgin material (Figure 3.11). From these micrographs, it can be seen that the topography of the fibres had markedly changes, once they had been aminated. The presence of fissures perpendicular to the length of the fibres are clear, as well as fibre breakage. These results are in agreement with the handle of the fibres, since they were found to become noticeably weak upon amination. This suggest that the reaction conditions had been sufficient to induce polymer chain scission and accordingly produce a functionalised fibre surface.

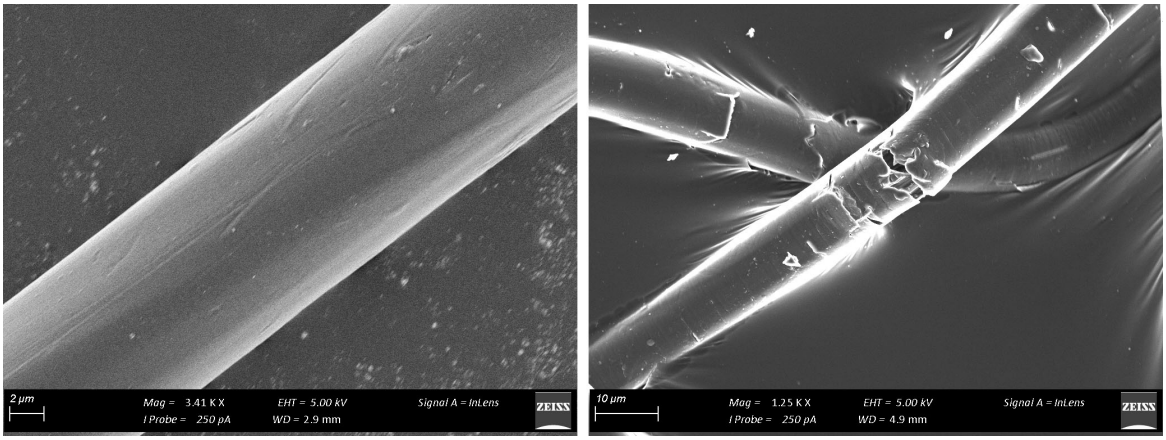

Figure 3.11: SEM micrographs of (a) Virgin PET and (b) PET-NH_2 fibres.

3.5 Conclusion

It was found that PET fibres treated with ethylene glycol displayed an increased reactivity towards reactive dyes. This suggests that the reaction had been successful in producing hydroxyl groups on the fibre surface. It was also found that primary amine groups could be introduced onto a PET fibre surface, by treating it with ethylene diamine. This was confirmed by an Acid dye stain test, a ninhydrin test and EDX.

These substrates were synthesised as precursors for subsequent activation protein immobilisation. Between them, the aminated PET surface was selected to further the study with, due to its increased reactivity.

3.6 References

1. Stepanova, M. & Dew, S., editors. Nanofabrication Techniques and Principles. NewYork: Springer. 2012.

2. Bhat, V. T., James, N. R. & Jayakrishnan, A. A photochemical method for immobilization of azidated dextran onto aminated poly(ethylene terephthalate) surfaces. Polymer international 57, 171-180 (2008).

3. Ohe, T., Yoshimura, Y., Abe, I., Ikeda, M. & Shibutani, Y. Chemical Introduction of Sugars onto PET Fabrics Using Diamine and Cyanuric Chloride. Textile Research Journal 77, 131-137 (2007).

4. Bech, L., Meylheuc, T., Lepoittevin, B. & Roger, P. Chemical Surface Modification of Poly(ethylene terephthalate) Fibers by Aminolysis and Grafting of Carbohydrates. Journal of Polymer Science 45, 2172-2183 (2007).

5. Feng, Q., Chai, C., Jiang, X., Leong, K. W. & Mao, H. Expansion of engrafting human hematopoietic stem/progenitor cells in three-dimensional scaffolds with surface-immobilized fibronectin. Journal of Biomedical Materials Research Part A 76, 781-791 (2006).

6. Zhang, Y., Chai, C., Song, X., Hin, S. & Leong, K. W. Fibronectin immobilized by covalent conjugation or physical adsorption shows different bioactivity on aminated-PET. Materials Science and Engineering: C 27, 213-219 (2007).

7. Rusu, E., Drobota, M. & Barboiu, V. Structural investigations of amines treated polyester thin films by FTIR-ATR spectroscopy. Journal of Optoelectronics and Advanced Materials 10, 377-381 (2008).

8. Li, X., Ji, J., Pu, M., Wang, X. & Shen, J. Surface tailoring of poly(ethylene terephthalate) via ligand-tethered comb-like PEG to enhance endothelialization. Journal of Materials Science: Materials in Medicine 19, 291-299 (2008).

9. Brueckner, T., Eberl, A., Heumann, S., Rabe, M. & Guebitz, G. M. Enzymatic and Chemical Hydrolysis of Poly(ethylene terephthalate) Fabrics. Journal of Polymer Science: Part A 46, 6435-6443 (2008).

10. Chen, K. S., Ku, Y. A., Lin, H. R., Yan, T. R., Sheu, D. C. & Chen, T. M. Surface grafting polymerization of N-Vinyl-2-pyrrolidone onto a poly(ethylene terephthalate) nonwoven by plasma pretreatment and its antibacterial activities. Journal of Applied Polymer Science 100, 803-809 (2006).

11. Zhang, W., Yi, X., Sun, X. & Zhang, Y. Surface modification of non-woven poly(ethylene terephthalate) fibrous scaffold for improving cell attachment in animal cell culture. Journal of Chemical Technology and Biotechnology 83, 904-911 (2007).

12. Zohdy, M. H. Cationization and gamma irradiation effects on the dyeability of polyester fabric towards disperse dyes. Radiation Physics and Chemistry 73, 101-110 (2005).

13. Fávaro, S. L., Rubira, A. F., Muniz, E. C. & Radovanovic, E. Surface modification of HDPE, PP, and PET films with $KMnO_4$/HCl solutions. Polymer Degradation and Stability 92, 1219-1226 (2007).

14. Kim, E., Kong, J., An, S. & Kim, H. Surface modification of polymers and improvement of the adhesion between evaporated copper metal film and a polymer. I. Chemical modification of PET. Journal of Adhesion Science and Technology 14, 1119-1130 (2012).

15. Pavon-Djavid, G., Gamble, L. J., Ciobanu, M., Gueguen, V., Castner, D. G. & Migonney, V. Bioactive poly(ethylene terephthalate) fibers and fabrics: Grafting, chemical characterization, and biological assessment. Biomacromolecules 8, 3317-3325 (2007).

16. Jou, C., Yuan, L., Lin, S., Hwang, M., Chou, W., Yu, D. & Yang, M. Biocompatibility and Antibacterial Activity of Chitosan and Hyaluronic Acid Immobilized Polyester Fibers. Journal of Applied Polymer Science 104, 220-225 (2007).

17. Jou, C., Lin, S., Yun, L., Hwang, M., Yu, D., Chou, W., Lee, J.-S. & Yang, M. Biofunctional properties of polyester fibers grafted with chitosan and collagen. Polymers for Advanced Technologies 18, 235-239 (2007).

18. Curti, P. S., Moura, M. R. D., Veiga, W., Radovanovic, E., Rubira, A. F. & Muniz, E. C. Characterization of PNIPAAm photografted on PET and PS surfaces. Applied Surface Science 245, 223-233 (2005).

19. Singh, N., Bridges, A. W., García, A. J. & Lyon, A. Covalent Tethering of Functional Microgel Films onto Poly(ethylene terephthalate) Surfaces. Biomacromolecules 8, 3271-3275 (2007).

20. Ciobanu, M., Siove, A., Gueguen, V., Gamble, L. J., Castner, D. G. & Migonney, V. Radical graft polymerization of styrene sulfonate on poly(ethylene terepthalate) films for ACL applications: 'Grafting from' and chemical characterization. Biomacromolecules 7, 755-760 (2006).

21. Zhu, A. P., Zhao, F. & Fang, N. Regulation of vascular smooth muscle cells on poly(ethylene terephthalate) film by O-carboxymethylchitosan surface immobilization. Journal of Biomedical Materials Research - Part A 86, 467-476 (2008).

22. Chen, J. & Chiang, Y. Surface modification of non-woven fabric by DC pulsed plasma treatment and graft polymerization with acrylic acid. Journal of Membrane Science 270, 212-220 (2006).

23. Laskarakis, A., Logothetidis, S., Kassavetis, S. & Papaioannou, E. Surface modification of poly(ethylene terephthalate) polymeric films for flexible electronics applications. Thin Solid Films 516, 1443-1448 (2008).

24. Yoo, H. S., Kim, T. G. & Park, T. G. Surface-functionalized electrospun nanofibers for tissue engineering and drug delivery. Advanced Drug Delivery Reviews 61, 1033-1042 (2009).

25. Agarwal, S., Wendorff, J. H. & Greiner, A. Use of electrospinning technique for biomedical applications. Polymer 49, 5603-5621 (2008).

26. Yao, C., Li, X., Neoh, K. G., Shi, Z. & Kang, E. T. Surface modification and antibacterial activity of electrospun polyurethane fibrous membranes with quaternary ammonium moieties. Journal of Membrane Science 320, 259-267 (2008).

27. Locke, A. K., Cummins, B. M., Abraham, A. A. & Coteí, G. L. PEGylation of concanavalin a to improve its stability for an in vivo glucose sensing assay. Analytical Chemistry 86, 9091-9097 (2014).

28. Kim, J. J. & Park, K. Glucose-Binding Property of Pegylated Concanavalin A. Pharmaceutical Research 18, 794-799 (2001).

29. Clayden, J., Greeves, N. & Warren, S. Organic Chemistry Organic Chemistry. Oxford: Oxford University Press. 2012.

30. Chen, W. & Mccarthy, T. J. Chemical Surface Modification of Poly(ethylene terephthalate). Macromolecules 31, 3648-3655 (1998).

31. Drobota, M., Persin, Z., Zemljic, L. F., Mohan, T., Stana-kleinschek, K., Doliska, A., Bracic, M., Ribitsch, V., Harabagiu, V. & Coseri, S. Chemical modification and characterization of poly(ethylene terephthalate) surfaces for collagen immobilization. Central European Journal of Chemistry 11, 1786-1798 (2013).

32. Broadbent, A. D. Basic Principles of Textile Coloration. Yorkshire: Society of Dyers and Colourists. 2001.

33. Lamothe, P. J. & Mccormickl, P. G. Role of Hydrindantin in the Determination of Amino Acids Using Ninhydrin. Analytical Chemistry 45, 1906-1911 (1973).

34. Boas, U. & Mirsharghi, S. Color Test for Selective Detection of Secondary Amines on Resin and in Solution. Organic letters 16, 5918-5921 (2014).

35. Friedman, M. Applications of the Ninhydrin Reaction for Analysis of Amino Acids, Peptides, and Proteins to Agricultural and Biomedical Sciences. Agricultural and Food Chemistry 52, 385-406 (2004).

36. Kaiser, E., Colescott, R. L., Bossinger, C. D. & Cook, P. I. Color test for detection of free terminal amino groups in the solid-phase synthesis of peptides. Analytical Biochemistry 34, 595-598 (1970).

Chapter 4

Aminated PET microfibre activation for Concanavalin A immobilisation

4.1 Introduction

Functional groups on the surface of a materials are advantageous, since they can act as anchoring sites for covalent immobilisation of various surface-active agents, such as biomolecules[1,2]. When the functional groups on such a material surface and those of surface-active agent are unable to react with one another, a linker molecule can act as a mediator or activating agent[3]. When this surface-active agent is a biomolecule such as Concanavalin A (Con A), the linker molecule which attaches it to the surface is referred to a bioconjugate molecule.

Since Con A has 13 primary amine groups per molecule, available for its immobilisation, a bioconjugate molecule was needed to activate the nucleophilic fibre surface for its covalent attachment[4,5]. The bioconjugates used for this purpose were glutaraldehyde (GA) and N,N'- Disuccinimidyl carbonate (DSC).

GA is a popular bis-aldehyde homobifunctional cross-linker[3], and is the most common bifunctional reagent used for protein immobilisation[3,6]. When using GA as a homobifunctional bioconjugate, an amine containing surface can very simply be activated for coupling with an amine-containing ligand. It is for this reason that this activation method is widely used[7-12]. Correspondingly, this molecule was predominantly used in this study on an aminated poly(ethylene terephthalate) (PET) surface, due to its cost and the facile reaction conditions used for attachment.

DSC in turn is a homobifunctional compound which is a highly reactive electrophile. As such it rapidly

hydrolyses in aqueous environments. This leads to the formation of two N-hydroxysuccinimide (NHS) molecules and one molecule of carbon dioxide. Activation of a substrate is consequently performed in anhydrous solvents, were it can effectively be used to activate hydroxyl and amine groups to succinimidyl carbonate and succinimidyl carbamate groups respectively[3].

In what follows we report the surface activation of aminated PET microfibres, followed by the immobilisation of Con A and its detection. The general procedure entailed that the aminated PET surfaces were treated with the respective activating agents, whereafter covalent attachment of Con A to the fibre surface. The protein functionalised PET microfibres were characterised using attenuated total reflectance Fourier transform infrared (ATR-FTIR) spectroscopy, confocal fluorescence microscopy (CFM), scanning electron microscopy (SEM), correlative light-electron microscopy (CLEM) and a horseradish peroxidase (HRP) assay.

The surface chemical structures of the functionalised PET microfibres prepared in this study are presented in Figure 4.1. In addition to the fibre functionalisation with Con A, cross-linked protein aggregate (CLPA) functionalised substrates were also synthesised.

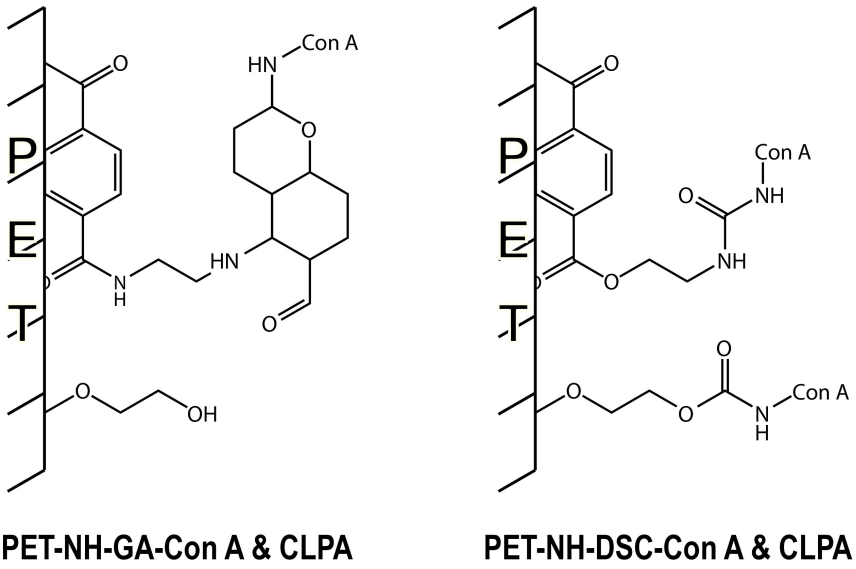

Figure 4.1: Chemical surface structures of Con A functionalised PET fibres prepared in this study.

4.2 Experimental

4.2.1 Materials

The following chemicals were utilised in this part of the project: ethylene glycol (Merck, 99%), ethylenediamine (Sigma-Aldrich, 99%), glutaraldehyde (Sigma-Aldrich, 50 wt.% in H_2O), N,N'-disuccinimidyl carbonate (Sigma-Aldrich, 95%), Concanavalin A from Canavalia ensiformis type IV, lyophilized powder (Sigma-Aldrich), Concanavalin A from Canavalia ensiformis fluorescein isothiocyanate (FITC) conjugate, type IV, lyophilized powder (Sigma-Aldrich), 1,4-dioxane anhydrous (Sigma-Aldrich, 99.8%), tetrahydrofuran (Merck, 99%), ethanol (Merck, 99%), hexane (Merck, 99%), hydrochloric acid 32% (Merck), 2,2'-azino-bis(3-ethylbenzthiazoline-6-sulfonic acid) diammonium salt tablets (Sigma), hydrogen peroxide solution (Sigma-Aldrich, 37% ww in H_2O), Citric acid (Sigma-Aldrich, $\geq$99.5%) potassium phosphate monobasic (Sigma-Aldrich), Tris-HCl (Sigma-Aldrich), Tween 20 (Merck), Sodium chloride (Merck), potassium chloride (Merck), sodium phosphate dibasic (Merck), manganese(II) chloride beads 99.999% (Sigma-Aldrich), peroxidase from horseradish type VI-A (Sigma-Aldrich).

4.2.2 Characterisation techniques

4.2.2.1 Confocal fluorescence microscopy (CFM)

For the acquisition of CFM micrographs, the samples were analysed with a Carl Zeiss LSM 780 confocal microscope with super-resolution platforms. Zen software was utilised for the acquisition and processing of images. Samples were prepared by securing a portion of the fibre mass to a glass microscope slide with Sellotape, then drawing the fibres along the length of the slide before securing the other end. Thereafter, a glass coverslip was placed over the fibres and sellotaped firmly in place. The magnification most often used was 40 $\times$ while the laser used differed with respect to the study conducted.

4.2.2.2 Correlative light-electron microscopy (CLEM)

CLEM is the powerful analytic tool, which combines the strengths of light and electron microscopy. In this study, the combination of CFM and SEM was used. This made it possible to correlate chemical changes made to a fibre surface with morphological attributes.

The same instrumentation was utilised as in the SEM and CFM studies. The main difference being that

exactly the same area had to be scanned by a SEM as was initially analysed by CFM. This meant that sample preparation had to be done in such a way that the fibres could not move in-between the two analyses. The single fibres were picked out with tweezers, elongated and secured on an 8 × 10 mm square of double sided carbon tape, which was concurrently secured onto a glass microscope slide. Thereafter, the fibres were pressed into the adhesive matrix with a sterile polytetrafluoroethylene film.

Preparation for the SEM analysis succeeded CFM and included carbon coating of the fibres by means of carbon rod evaporation under vacuum.

Correlation of the CFM and SEM images was mediated by a combination of Zen and Zeiss image processing software. The final adjustments to align and manipulate the layering of the CFM images onto the SEM images was performed on Photoshop CC 2015, using the Puppet warp tool.

4.2.2.3 Horseradish peroxidase assay (HRP)

The enzymatic assay of HRP with 2,2'-azino-bis(3-ethylbenzthiazoline-6-sulfonic acid) (ABTS) as a substrate was used to determine whether immobilised Con A had retained its biological activity.

To execute the assay the following procedure was followed[13]:

10mg of of each of the various PET microfibre derivatives, were placed in separate glass vials and incubated for one hour in a 1× phosphate buffered saline (PBS) (8 g NaCl, 0.2 g KCl, 1.44 g Na_2HPO_4 and 0.24 g KH_2PO_4; pH 7.4) solution of HRP (4 mg/mL) on a laboratory orbital shaker. Hereafter the fibres were washed thrice at 10min intervals with a PBS-Tween solution (1× PBS, 0.01% Tween 20).

A substrate solution was prepared by dissolving ABTS (10 mg) in 20 mL of citrate buffer (0.1 M, pH 5.0) to which 37 % H_2O_2 (10 µL) was added.

Substrate solution was then added to each of the fibrous substrates, and the colour change observed.

4.2.3 Experimental Procedures

4.2.3.1 GA activation of PET-NH_2 fibres (PET-NH-GA)

The aminated fibres were activated with GA by following a procedure similar to that used by Betancor et al[9]. The mounted fibres were wetted with 1× PBS (8 g NaCl, 0.2 g KCl, 1.44 g Na_2HPO_4 and 0.24 g KH_2PO_4 in 1l of deionised water, pH 7.0), succeeded by submersion in 20% (v/v) GA in 1× PBS pH 7.0. After allowing

the reaction to proceed for 15 hours at 30 °C under constant stirring, the fibres were washed four times with coupling buffer. This coupling buffer consisted of 1× PBS pH 7.4 containing $MnCl_2$ (0.013 mg/mL) and $CaCl_2$ (0.011 mg/mL). The fibres were now ready for subsequent protein immobilisation reactions.

The presumed reactive intermediate is formed as a result of a 1,4 Michael-type addition reaction to the double bond of dimeric GA. This then leaves the hemiacetal ring available for subsequent reaction with primary amines (Scheme 4.1).

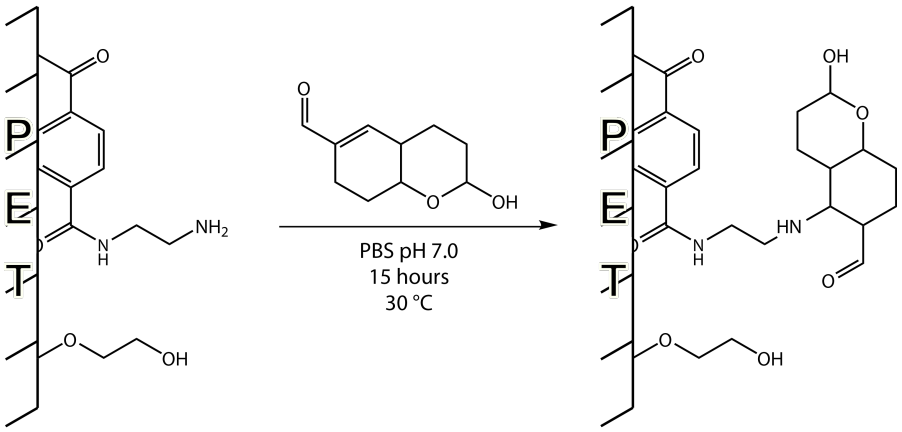

Scheme 4.1: Dimeric GA activation of primary amine groups.

4.2.3.2 Con A immobilisation onto GA activated PET fibres (PET-NH-GA-Con A)

The wet, activated fibres were cut loose from the tripod and wrung dry. The fibres were then divided into fractions of approximately 10 mg each. These fractions were placed in glass vials containing coupling buffer (3 mL) and Con A (4 mg/mL)[15,16]. The vials were then capped and incubated for 1 hour at 37 °C on an orbital shaker, before reducing the temperature to 4 °C and allowing the reaction to proceed for an additional 3 hours. Upon completion, the contents of the vials were left un-agitated in a refrigerator at 4 °C for 16 hours. For the preparation of the CLPA-fibre, a GA solution was added to the reaction mixture 90 minutes into the 4 °C incubation (final GA concentration was 0.5% w/v)[17].

Upon completion of the immobilisation reaction (Scheme 4.2), the fibres were incubated in PBS containing 0.1 M Tris-HCl (pH 7.8). This allowed tris(hydroxymethyl)aminomethane molecules to quench any unreacted GA groups[17]. Thereafter, the fibres were washed three times with PBS- Tween buffer (PBS, 0.01 wt% Tween 20), to remove the unreacted Con A adsorbed onto the fibre surface[18]. This was performed by aid of a vortex shaker, entailing 2 minutes of vortexing per wash. This was again followed by washing the fibres three times with PBS so as to remove the Tween. The fibres were then squeezed dry between two spatulas

and allowed to dry for 24 hours in a vacuum oven at 50 °C under vacuum. The dried fibres were then placed in vials and stored in a refrigerator at 4 °C until used.

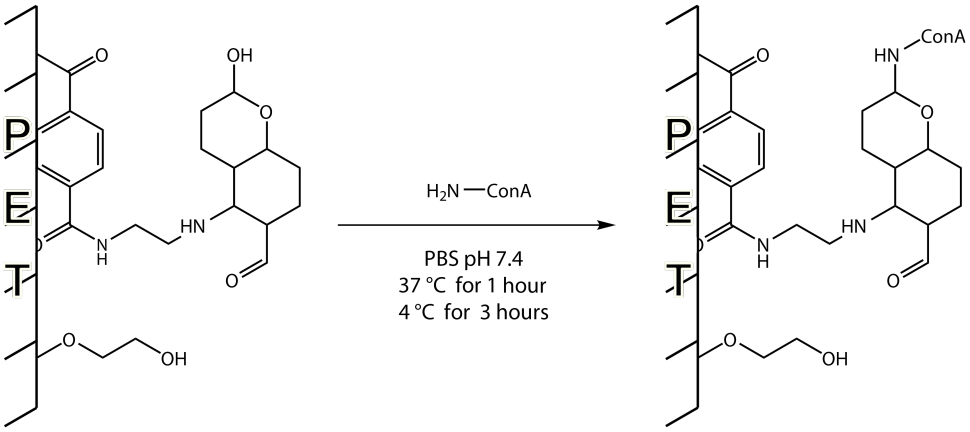

Scheme 4.2: Immobilisation of Con A onto a GA activated PET surface.

4.2.3.3 DSC activated PET-NH_2 (PET-NH-DSC)

The aminated fibres were activated with succinimidyl carbonate groups following a literature procedure[3]. This entailed the aminated fibres being submerged in 0.2 M DSC and 0.5 M diisopropylethylamine (DIEA) in anhydrous 1,4-dioxane, and allowed to react at 30 °C for 2 hours under constant stirring. The fibres were then washed with anhydrous 1,4-dioxane (3 aliquots) whereafter they were dried in a vacuum oven at 50 °C for 16 hours.

The nucleophilic hydroxyl and amine groups react with the carbonyl carbon of DSC, according to the same nucleophilic substitution reactions described earlier. In both cases the tetrahedral intermediate formation is succeeded by the expulsion of the N-hydroxysuccinimide (Scheme 4.3).

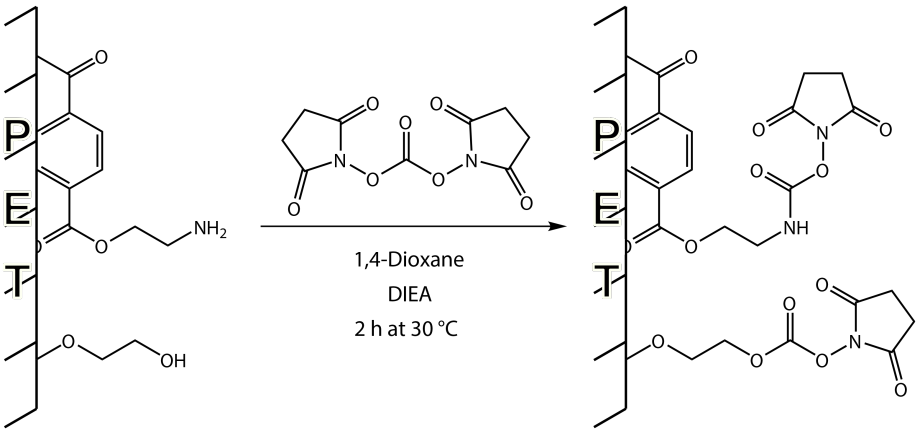

Scheme 4.3: DSC activation of primary amine and hydroxyl groups.

4.2.3.4 Con A immobilisation onto DSC activated PET fibres (PET-NH-DSC-Con A)

Upon activation, the succinimidyl carbonate groups on the surface were prone to hydrolysis, as such, wetting and preparing of the fractions for immobilisation was performed rapidly and with a cold coupling buffer. Other than this, the procedure for immobilising Con A onto the activated surface was identical to that employed for GA activated fibres (Scheme 4.4).

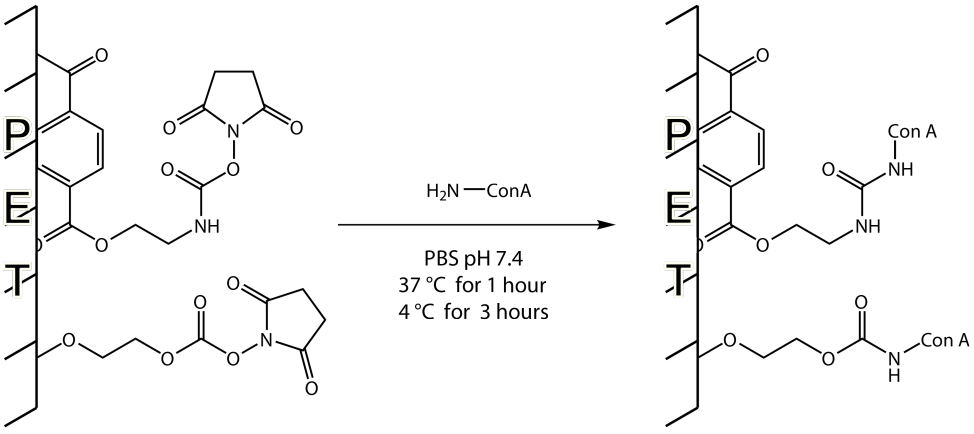

Scheme 4.4: Immobilisation of Con A onto a DSC activated PET surface.

4.3 Results and discussion

This section is dedicated to the discussion of the synthesis and characterisation of activated PET derivatives. These include Con A modified PET succeeding GA activation (PET-NH-GA-Con A) and Con A modified

PET succeeding DSC activation (PET-NH-DSC-Con A) as well as PET succeeding glycolysis (PET-OH). The aminated PET samples were preferentially chosen over glycolised PET for subsequent activation and Con A immobilisation. The Con A derivatised fibres were synthesised in order to study the possible affinity which these fibres may have for the *Mycobacterium tuberculosis* (*Mtb*) cell wall.

4.3.1 GA activation of PET-NH_2 (PET-NH-GA)

Upon amination of the PET fibres, the surface needs to be activated for protein immobilisation. This is due to the target functional groups on the protein being primary amines, and therefore similar to the functional groups on the fibre surface.

In order to couple the analogous groups, a bioconjugate molecule with at least two functional sites is required. One such a molecule is GA, which is an effective homobifunctional cross-linker, often used to activate an amine rich surfaces for protein immobilisation (Figure 4.2), as well as cross-linking of additional proteins[19].

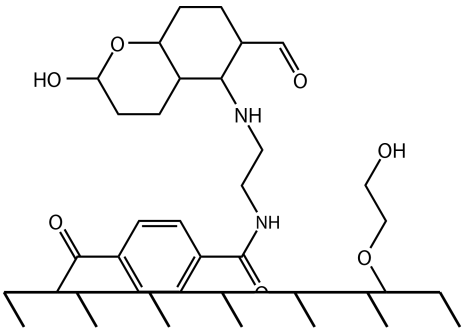

Figure 4.2: Surface activation of PET-NH_2 with glutaraldehyde (PET-NH-GA)

GA coupling is, however, not mechanistically as simple as its molecular structure suggests[20]. While this molecule is expected to react with amine containing molecules by initial Schiff base formation, the interaction is in actuality far more intricate. Amine containing molecules treated with GA but not with a reducing agent, show stabilities uncharacteristic of Schiff base formation[14]. This is the consequence of the molecule partaking in marked transformations in aqueous solution. The result of which is an array of no less than thirteen different reactive species (Scheme 4.5). It follows that GA/amine coupling could entail Michael-type addition of the amines to α, β-unsaturated sites in a GA macromolecule, Schiff base formation with a remaining aldehyde terminal, covalent attachment to a hemiacetal ring, cyclic quaternary pyridinium complexes formation or a combination of these options[3,20].

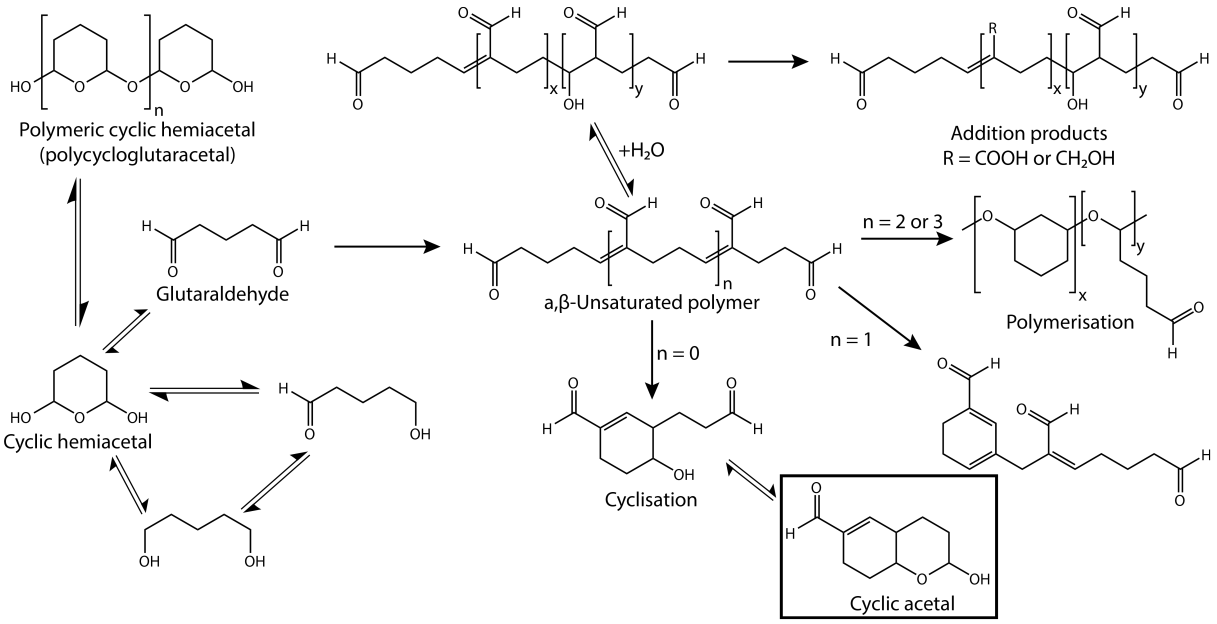

Scheme 4.5: Summary of the possible forms of glutaraldehyde in aqueous solution. Bordered is the bicyclic derivative used for amine coupling throughout this study[3,20].

The conformation of GA presumed to be responsible for the activation of amine rich surfaces, is the bicyclic derivative (Scheme 4.5)[14]. This form of GA is a potent amine coupling agent, and is accordingly suggested as the form which shows the best cross-linking activity as far as tissue fixation, protein conjugation or enzyme immobilisation is concerned[21]. To promote its formation in aqueous solution, reaction parameters can be modulated. These parameters include reacting the amine rich fibres with a high concentration of GA for a prolonged period of time, in an aqueous solution buffered to a pH of 7.0[14].

Coupling amines via the bicyclic form occurs by initial 1,4 Michael-type addition to the double bond, forming a stable secondary amine link. Introduction of a second amine containing component infers nucleophilic substitution at the anomeric carbon of the hemiacetal ring, again forming a stable secondary amine link (Scheme 4.6).

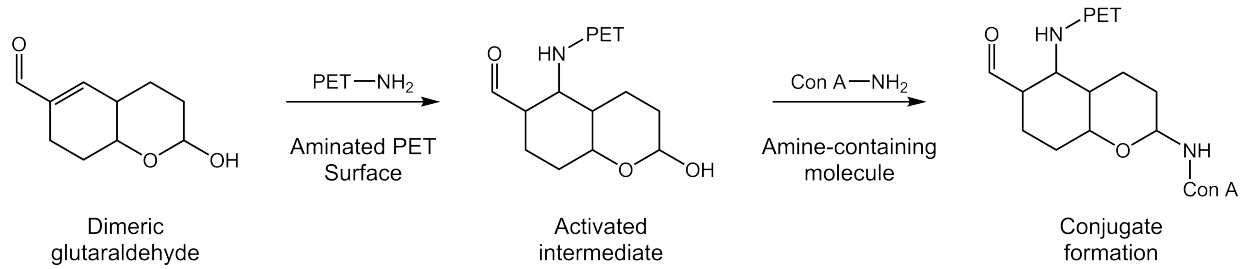

Scheme 4.6: Reaction of bicyclic GA with PET-NH_2 and α-amine on Con A.

4.3.1.1 CFM detection of GA

CFM is a useful technique for the observation of fluorescent signals stemming from exited fluorophores within a sample[22]. Fluorescence as a form of luminescence, occurs when a fluorophore absorbs a photon of a certain energy and then re-emits a photon, typically of a lower energy[22]. Auto-fluorescence then, is a term used to differentiate between the fluorescence observed due to fluorophores intrinsic to a material, and fluorescence observed due to the deliberate introduction of fluorescent markers[23]. While practically all molecular systems show fluorescence, it is often very weak. As such their fluorescence often goes undetected, or their excitation range falls so far in the ultraviolet region of the electromagnetic spectrum that they are rarely exited[24]. During a CFM analysis, the excitation prerequisites of some of these molecules can be met, and accordingly produce auto-fluorescence in a sample.

Typically, this auto-fluorescence is an unwanted source of fluorescence when doing fluorescence imaging, as it can result in bright backgrounds. This can lead to a dramatic reduction in the signal-to-noise ratio, limiting the detection of other fluorescent signals[25]. One instance where this phenomenon is observed, is when GA is used as a fixative. GA produces particularly high auto-fluorescent signals, making it a troublesome agent to use when CFM microscopy is performed[26].

While it is still not fully understood why GA has such high auto-fluorescent emissions, the anomaly is especially advantageous when attempting to detect its presence as a surface activating agent. This was done by utilising CFM to analyse the surface of virgin PET and PET-NH_2 fibres, then comparing their emission signals to that obtained from PET-NH-GA fibres (Figure 4.3).

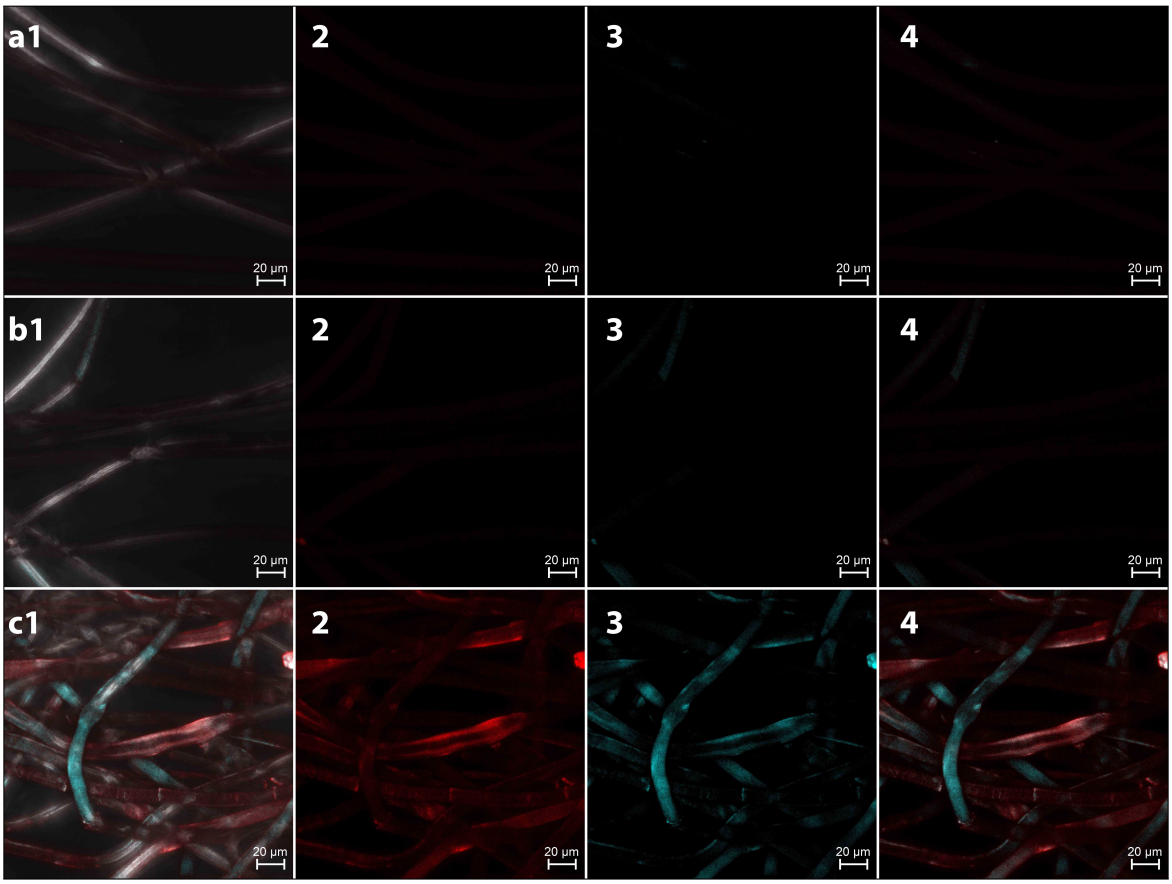

Figure 4.3: Maximum intensity projected z-stack (40 × magnified) CFM images of (row a) virgin PET, (row b) PET-NH_2 and (row c) PET-NH-GA. Columns 1-4 represent the fluorescent signals produced by (1) excitation by 405 & 561 nm laser and detected at 472-526 and 576-735 nm as well as by T PMT filter, (2) excitation by 561 nm laser and detection between 576-735 nm (3) excitation by 405 nm laser and detection between 472-526 nm and (4) overlay of (2 & 3).

Row (a) of Figure 4.3 indicates that PET itself auto-fluoresces in the detection ranges of 472-526 and 576-735 nm when exited with a 405 or 561 nm laser respectively. The intensities of the auto-fluorescent signals are seen to slightly increases when the fibres are aminated (row (b)). From row (c) it is clear that GA activation leads to the strongest intensification of the fluorescent signals, in both of the detection ranges. This indicates that a GA derived moiety was able to successfully react with primary amine groups present on the surface of the PET-NH_2 precursor substrate. As such, surface activation, mediated by GA, was confirmed not by the presence of fluorescent signals, but by the intensification of significant signals.

From column (1) row (c) of Figure 4.3, it can be seen that all of the PET-NH-GA fibres detected by the T PMT filter, produce emission signals. This is in contrast with the fluorescent signals observed for the other fibre types in column (1), which only show partial fluorescence per fibre, for some of the fibres. From this it can be concluded that the precursor substrate has homogeneously reacted with the GA moiety.

4.3.2 Con A immobilisation onto PET-NH-GA (PET-NH-GA-Con A and PET-NH-GA-CLPA)

Upon activation with GA, the PET surface is suited for protein immobilisation. The general procedure holds that the activated surface be introduced into a buffered solution of the amine-containing protein and allowed to react. It follows that one of the thirteen primary amine groups on the Con A molecule, can then partake in a nucleophilic substitution reaction to the hemiacetal ring of the activating group (Scheme 4.6 and Figure 4.4 (a)), forming PET-NH-GA-Con A.

A cross-linked protein aggregate derivative substrate (PET-NH-GA-CLPA) could be synthesised, sequential to the PET-NH-GA-Con A substrate. This entailed the addition of GA to the protein and fibre reaction mixture, after the immobilisation reaction had commenced. This leads to rapid cross-linking of the protein molecules to one another, but also to the already immobilised protein on the fibre surface (Figure 4.4 (b)). The product of this reaction, would be a fibre with a greater protein loading per surface area, than could be achieved with only initial immobilisation.

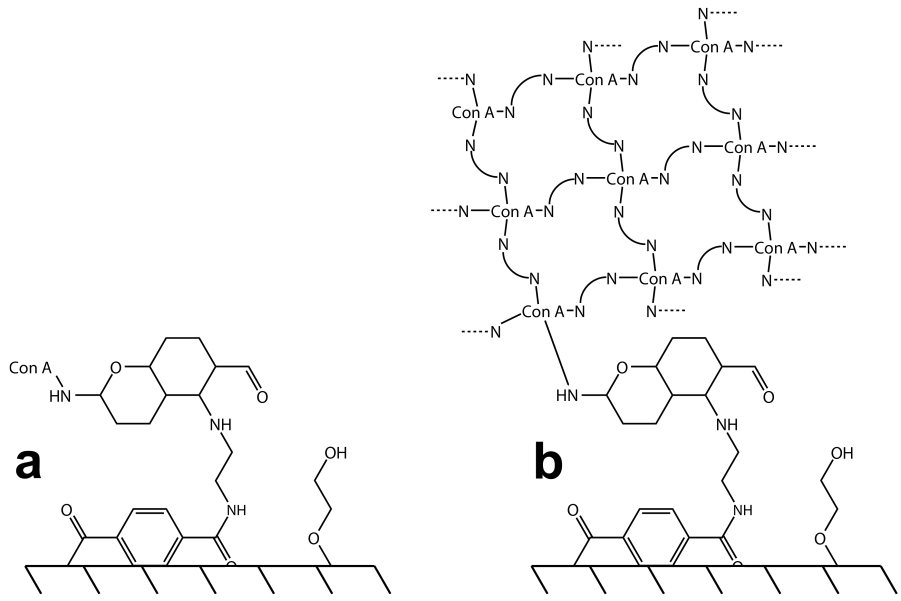

Figure 4.4: (a) Con A immobilised onto a GA activated surface (PET-NH-GA-Con A) and (b) CLPA derivative of PET-NH-GA-Con A (PET-NH-GA-CLPA).

4.3.2.1 ATR-FTIR spectroscopy detection of immobilised Con A

Immobilisation of Con A results in a solid deposition onto the fibre surface. This, unlike surface degradation and activation reactions, results in a layer-like coating which in turn can be detected by ATF-FTIR. Hence, the presence of immobilised Con A on the fibre surface, can be identified by the appearance of its amide

bands on the FTIR spectrum of PET (Figure 4.5). The assignments of the Con A reference peaks were aided by literature and is shown in Table 4.1[27].

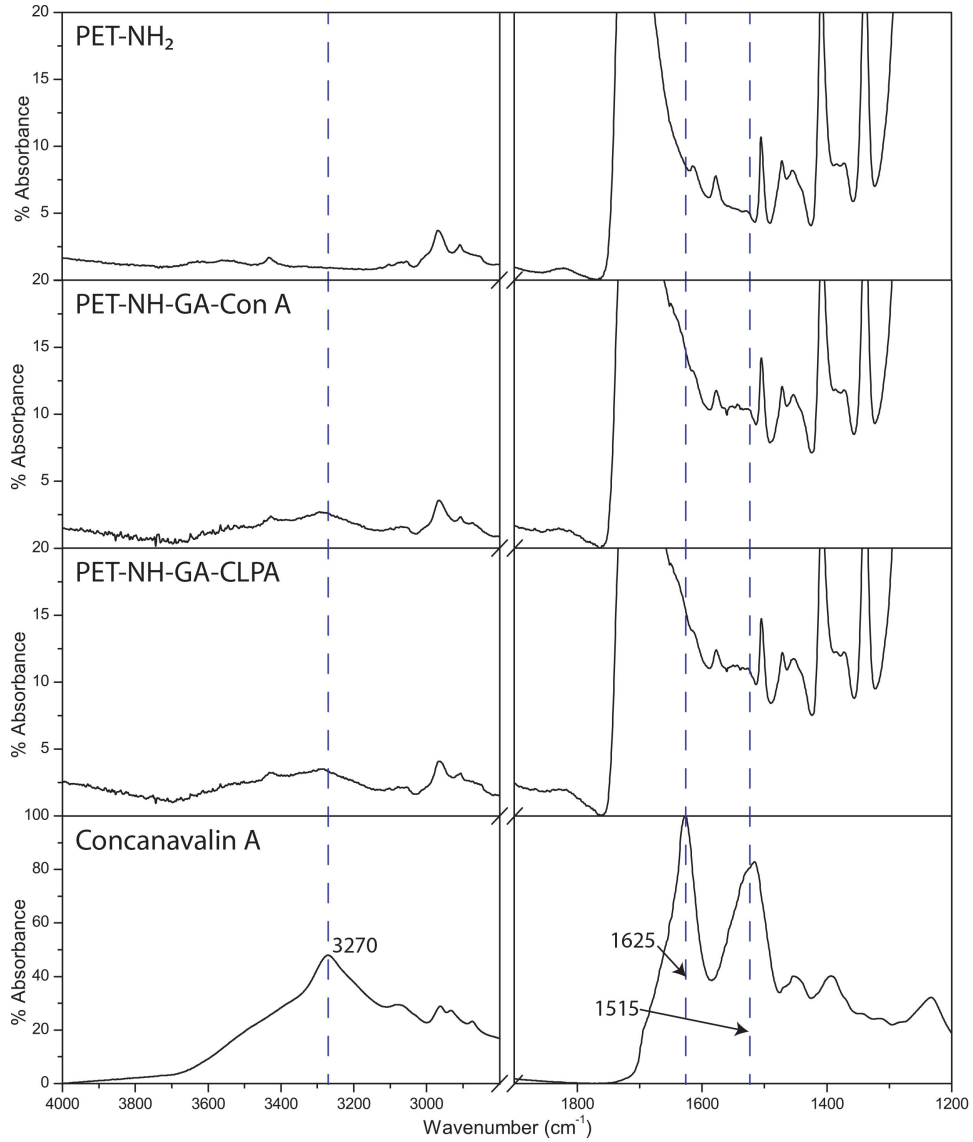

Figure 4.5: FTIR spectral correlation of Con A immobilisation by aid of GA activation.

Table 4.1: FTIR spectral absorption bands of Con A[27].

Absorption bands of Con A	Attribution
1515 cm^{-1}	Amide II band
1625 cm^{-1}	Amide I band - indicative of high percentage β-sheet secondary structures
3270 cm^{-1}	Amide A band

The presence of Con A is most apparent from its amide A band in the 3600-3100 cm^{-1} range, since PET

typically shows little to no absorption in the 4000-3000 cm^{-1} region. On the contrary, the amide I and amide II absorption peaks appear as shoulders on the (C=O) stretching vibrations of PET, often leading to their obscurance.

4.3.2.2 CFM detection of immobilised Con A

The detection of GA on the fibre surface by CFM, proposed that Con A immobilised due to the GA surface activation, would bring on a change in its fluorescent emission signals. Hence, PET-NH_2, PET-NH-GA-Con A and PET-NH-GA-CLPA fibres were analysed by CFM and compared to one another (Figure 4.6).

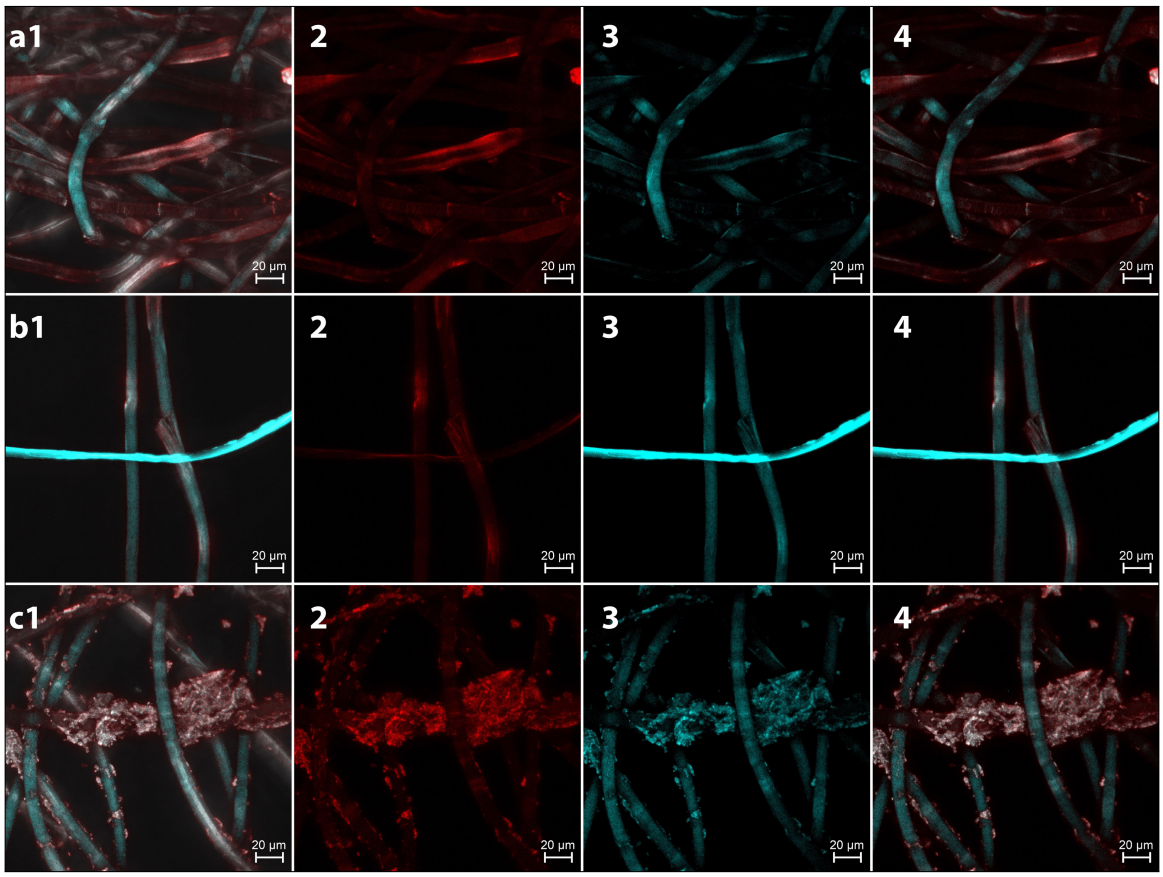

Figure 4.6: Maximum intensity projected z-stack (40 × magnified) CFM images of (row a) PET-NH-GA, (row b) PET-NH-Con A and (row c) PET-NH-GA-CLPA. Columns 1-4 represent the fluorescent signals produced by (1) excitation by 405 & 561 nm laser and detected at 472-526 and 576-735 nm as well as by T PMT filter, (2) excitation by 561 nm laser and detection between 576-735 nm (3) excitation by 405 nm laser and detection between 472-526 nm and (4) overlay of (2 & 3).

When comparing rows (a) and (b) of Figure 4.6, little can be seen to suggest the presence of immobilised Con A for the PET-NH-GA-Con A derivative. Row (b) does however show an increase in emission intensity

compared to row (a), but this is contradicted by row (c). The latter clearly shows the presence of Con A as aggregates, but the corresponding fluorescent intensity is comparable to that of row (a). The aggregates in row (c) are seen to be predominantly present as small clusters along the length of the fibres, but also as large clumps, which cover a portion of a fibre's surface entirely.

These CFM results do not prove that immobilisation of unistructural Con A had been achieved. The results do, however, show that protein aggregates had formed in the case of the PET-NH-GA-CLPA derivative.

A Con A-fluorescein isothiocyanate conjugate could be used to show that the protein was immobilised on the surface of the fibres. This is a fluorescent derivative of Con A (Con A-FITC), and is shown in Figure 4.7. It has approximate fluorescence excitation and emission maxima at 494 and 518 nm respectively[28]. As such, it would not excite, nor show a strong emission in the same range as PET, which is predominantly exited in the 405 nm range and emits in the 420-463 nm range. Accordingly, the fibres were exited with a 488 nm laser and their emissions detected in the range of 499-579 nm. These chosen excitation and emission ranges were selected to account for the auto-fluorescent contribution from GA.

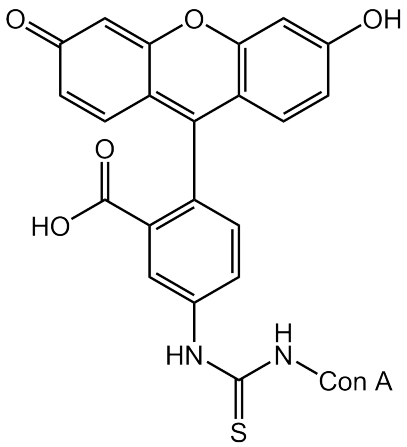

Figure 4.7: Con A-FITC molecular structure.

By synthesising PET-NH-GA-Con A-FITC and PET-NH-GA-CLPA-FITC, the presence of the protein on the fibre surface could be detected by CFM (Figure 4.8). The detection of non-specifically bound protein was assessed by analysing PET-NH_2 fibres treated with Con A-FITC as a control.

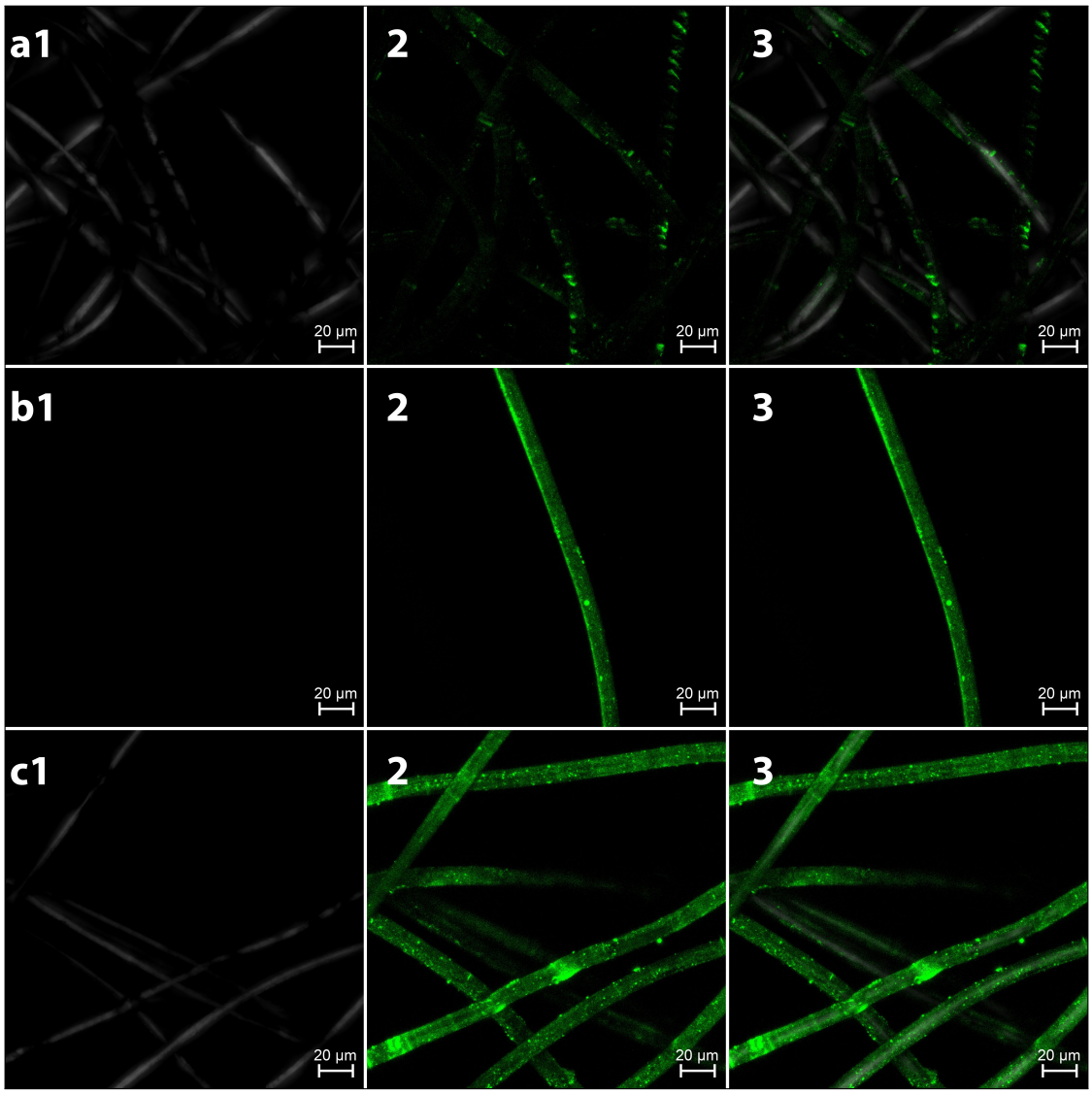

Figure 4.8: Maximum intensity projected z-stack (40 × magnified) CFM images of (row a) PET-NH_2 treated with Con A-FITC, (row b) PET-NH-GA-CON A-FITC and (row c) PET-NH-GA-CLPA-FITC. Columns 1-3 represent the fluorescent signals produced by (1) excitation by 488 nm laser and detection by T PMT filter, (2) excitation by 488 nm laser and detection between 499 and 579 nm (3) overlay of (1) & (2).

It must be noted that the FITC conjugate of Con A is structurally somewhat different than the pure Con A, due to its extent of fluorescein labelling (3-6 mol of FITC per mol of protein). Potential consequences of this are the blocking of the residual amine sites due to the physical bulk of the FITC molecule, and changed chemical properties. The latter relates to the reduced solubility in aqueous media, decreased reactivity with GA and accordingly lower degrees of cross-linking. When comparing rows (a) to (c) of Figure 4.8, it is clear that protein immobilisation principally occurs only when the PET surface has been activated. Row (c) also illustrates that the addition of GA after immobilisation results in protein aggregate formation. The

aggregates formed in this instance are smaller than that typically observed for GA mediated cross-linking (Figure 4.6 row c).

Row (a) (Figure 4.8), shows that the presence of fluorescent emission due to FITC is still present. The majority of this is present in fissures perpendicular to the fibre length. Simplistically, the protein-dye conjugate confined to the fissures are present due to the difficulty water has to penetrate these regions and can therefore not remove the unreacted Con A-FITC. This is in part hindered even further due to the hydrophobic nature of FITC, and the impartment of this characteristic to the conjugate.

Additional weak fluorescence along the length of the fibre is inexplicable at this stage. One possibility for this, is scattering of the light emitted from the crevasses along the length of the fibre. Another likely reason is hydrophobic affiliation with the fibre surface[29]. The latter may occur since the FITC molecule exhibits many similarities to some acid dyes, which are typically used to dye amine rich fibres. The staining ability of these dyes has also been illustrated with the acid dye stain test of the animated fibres. Nevertheless, the control fibres showed considerably lower fluorescent signals compared to the activated fibres. In addition, as previously mentioned, the presence of Con A on the control study fibres is most likely due to the presence of the residual dye molecules.

With reference to rows (b) and (c) it is apparent that Con A immobilisation had been successful, resulting in uniformly coated fibre surfaces. This correlates well with the results presented in Figure 4.3 row (c), which showed a homogeneous surface activation. From this it can be concluded that activating the surface of aminated PET fibres with GA is a suitable technique to mediate subsequent immobilisation of amine rich molecules.

4.3.2.3 SEM detection of immobilised Con A

Topographical changes to the fibre surface, due to protein immobilisation was assessed by SEM[30]. The smooth fibre surface makes it possible to detect small-scale protrusions which could result from binding Con A to the fibres (Figure 4.9). The study was performed by comparing the surfaces of PET-NH-GA-Con A and CLPA fibres to that of PET-NH-GA fibres, as well as PET-NH_2 fibres which had been incubated in a protein coupling solution.

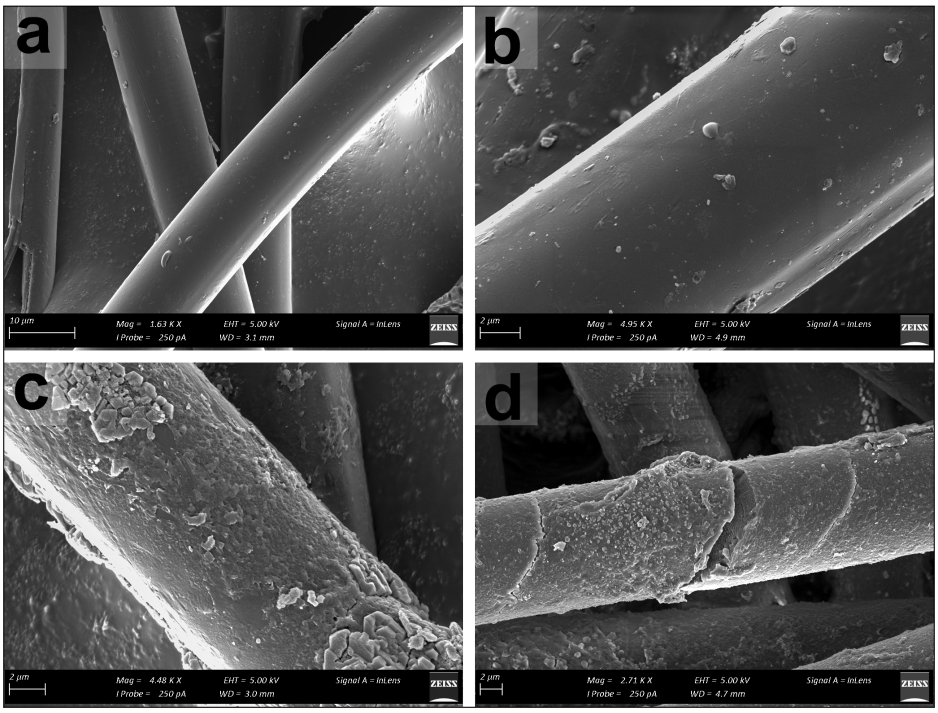

Figure 4.9: SEM micrographs of (a) PET-NH_2 treated with Con A (b) PET-NH-GA, (c) PET-NH-GA-Con A and (d) PET-NH-GA-CLPA fibres.

Micrographs (c) and (d) of Figure 4.9, shows that the fibre surface becomes irregular upon protein immobilisation, bearing distinct nodules along the length of the fibres. This change is surface topography is not observed for the GA activated fibres (micrograph (b)). It can also not be prescribed to non-specific binding of the protein, since micrograph (a) shows no nodulation of the fibres.

When comparing micrographs (c) and (d) (Figure 4.9), it can be seen that the PET-NH-GA-CLPA fibres have a greater loading of Con A per fibre length, as the protein forms a continuous layer on the surface. This layer of protein can be seen in a magnification of micrograph (d) in Figure 4.10. Figure 4.10, shows that the surface of the fibre is entirely covered with a Con A layer. Upon this, the tendency of the protein layer to fracture along with the fibre, rather than pealing away, indicates a chemical bond to the fibre surface. In addition, micrograph (c) of Figure 4.9 shows objects with regular fracture planes in the top left and bottom right hand corners. These can be prescribed crystals of the various salts used in the PBS solution, from which Con A was immobilised.

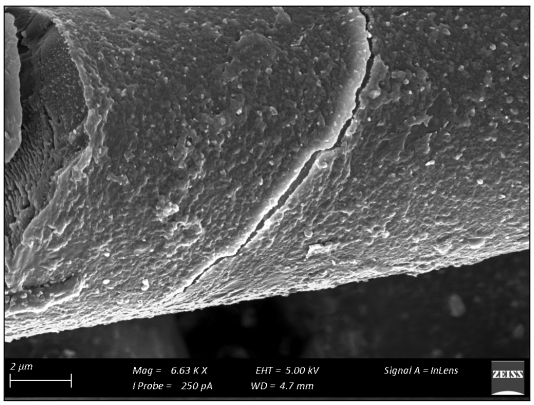

Figure 4.10: SEM micrograph of the area of interest in Figure 4.9 (d).

From these results, it could be concluded that immobilisation of Con A onto the GA activated PET-NH_2 fibres, leads to topographical changes to the fibre surface. The structure and distribution of the nodules observed from a SEM analysis, correlate well with the fluorescent signals observed for Con A from the CFM analyses. These indicated that Con A had homogeneously been immobilised onto the fibre surface, and that the CLPA derivatives generally have a surfaces covered in aggregates of the protein.

4.3.2.4 CLEM detection of immobilised Con A

Visual confirmation of Con A immobilisation onto the activated fibre surface has so far been obtained from SEM and CFM analysis. SEM analysis, while beneficial, is limited to the detection of topographical changes. This means that its use is limited to detecting Con A only at concentrations high enough to result in nodulation of the fibre surface. CFM in turn, provided conclusive evidence only when Con A was substituted for a Con A-FITC conjugate. Due to the cost of this conjugate and the limited sensitivity of SEM, the ability to optimise the immobilisation reaction through serial studies, is constrained. These limitations can potentially be alleviated by making use of a combination of SEM and CFM in an analysis method called CLEM.

CLEM is a not a new analytical technique, yet in has only recently been drawing attention. This is mainly due to the advent of green fluorescent protein and improvements in the fields of light and electron microscopy[31]. One of the benefits of this technique, is the synergistic relationship between light and electron microscopy[32]. This allows the fluorescent information from CFM to be combined with the ultrastructural information of SEM[33]. Hence, the rationale for making use of this technique was to correlate the GA induced fluorescent emissions of immobilised protein, as detected by CFM (Figure 4.6), with the nodular structures on the fibre surface, as detected by SEM (Figure 4.9). If sufficient information, to conclude Con A immobilisation, could

be collected from such a study, it could be used as an alternative to CFM detection by the aid of an Con A-FITC conjugate.

To assess the correlation between the CFM and SEM techniques, a PET-NH-GA-CLPA sample was analysed (Figures 4.11 and 4.12). This was done since the Con A aggregates could readily be observed in both the CFM and SEM analyses. Hereafter, the analysis was repeated on PET-NH-GA-Con A, PET-NH-GA and PET-NH_2 fibres. In addition, the CFM excitation and detection parameters were selected to draw a distinction between Con A cross-linked with GA and the PET fibres. The parameters entailed that the fibres were exited with a 405 nm laser, hereafter the emissions associated with the PET fibres were detected in the range of 410-463 nm, and those associated with the GA/Con A complex in the range of 472-508 nm.

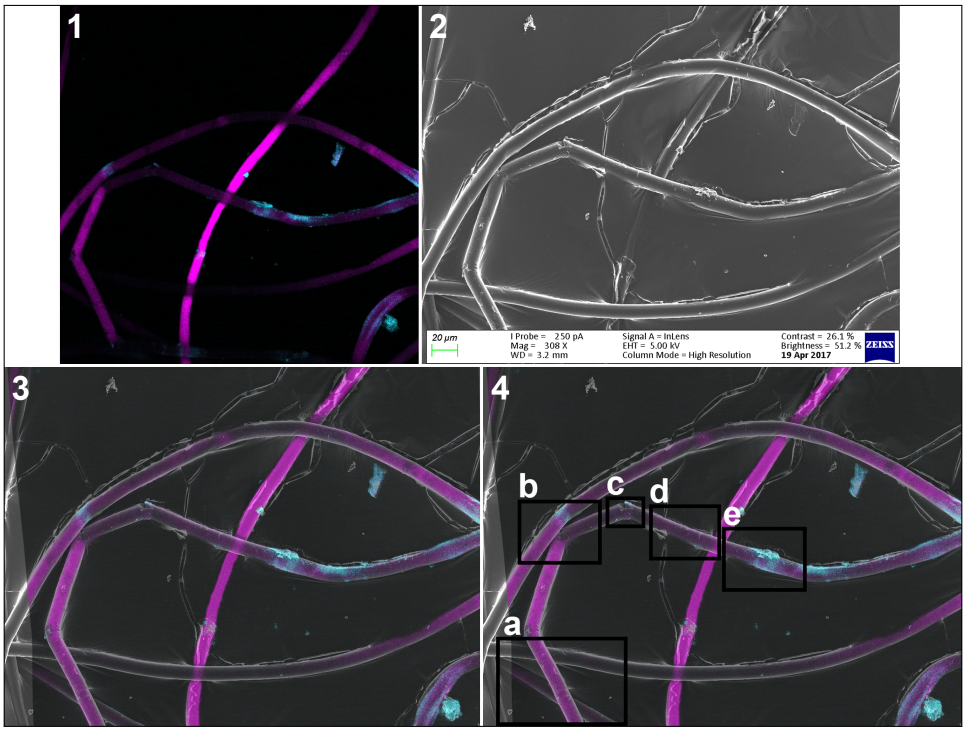

Figure 4.11: (1) Maximum intensity projected z-stack (40 × magnified) CFM images of PET-NH-GA-CLPA, (2) SEM micrograph of the CFM image area, (3) correlative image produced from overlaying (1) & (2) and (4) marked areas of interest on (3).

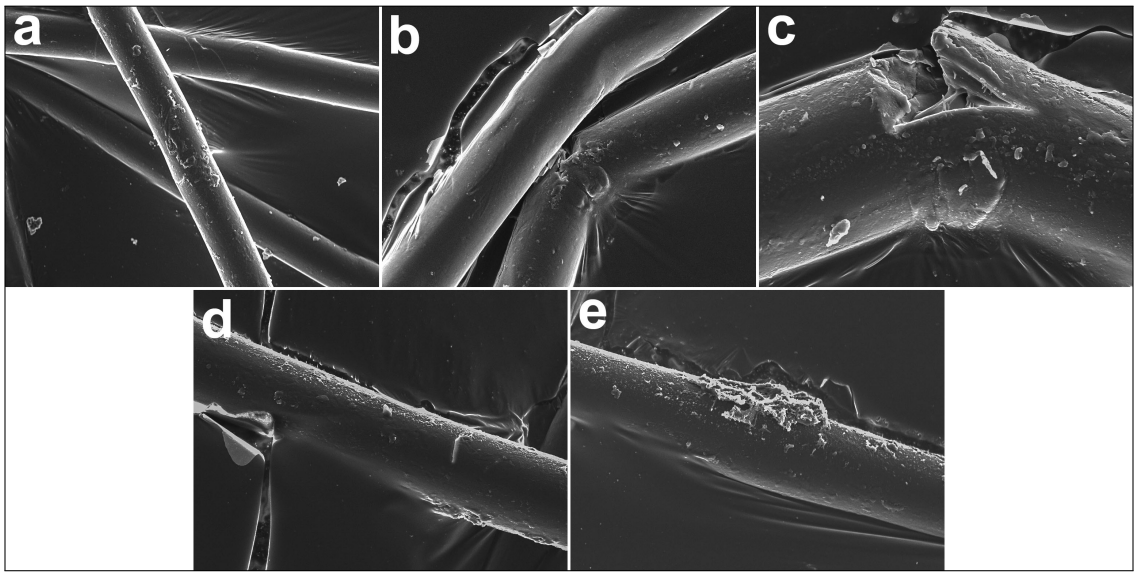

Figure 4.12: SEM micrographs of marked areas (a)-(e) on Figure 4.11.

Throughout this analysis, the auto-fluorescence emanating from GA/Con A complexes is denoted by turquoise and that of PET by magenta. Micrograph (1) of Figure 4.11, shows that the lumps present on the fibres, result from a GA/Con A complex. This is similar to the clusters observed in Figure 4.6 row (c). When micrograph (1) (Figure 4.11) is correlated with the same area imaged by SEM (micrograph (2) Figure 4.11), it can be seen that similar attributes align, as shown in the correlation image (micrograph (3) Figure 4.11). From the correlation image, GA/Con A complex associated signals could be selected for structural investigation (micrograph (4) Figure 4.11) by SEM as shown in Figure 4.12.

The marked areas in micrograph (4) (Figure 4.11), show that areas (b) to (e) all have prominent turquoise attributes, while area (a) does not. When comparing this to the micrographs of Figure 4.12, areas (b) to (e) as well as (a) show prominently nodulated fibre surfaces. It follows that these nodules are likely due to the presence of Con A, as discussed in Section 4.3.2.3 (SEM detection of immobilised Con A). This suggests that the auto-fluorescent emissions for this complex did not fall within the detection parameters chosen. Furthermore, it can be observed, in the cases where a turquoise attribute is present, that the corresponding SEM micrograph shows large nodules in a distribution matching that of the CFM image. The SEM micrographs, however, also show small nodules all over the surface, which could not be discerned from the PET auto-fluorescent signals in the CFM micrographs.

The results of the PET-NH-GA-CLPA analysis suggests that the technique could be used for the detection of cross-linked Con-A on a fibre surface. Its sensitivity, however, could not yet be concluded to be sufficient at detecting the presence of unistructural Con A. Therefore, the analysis was repeated with PET-NH-GA-Con A and PET-NH-GA fibres (Figures 4.13 to 4.16)

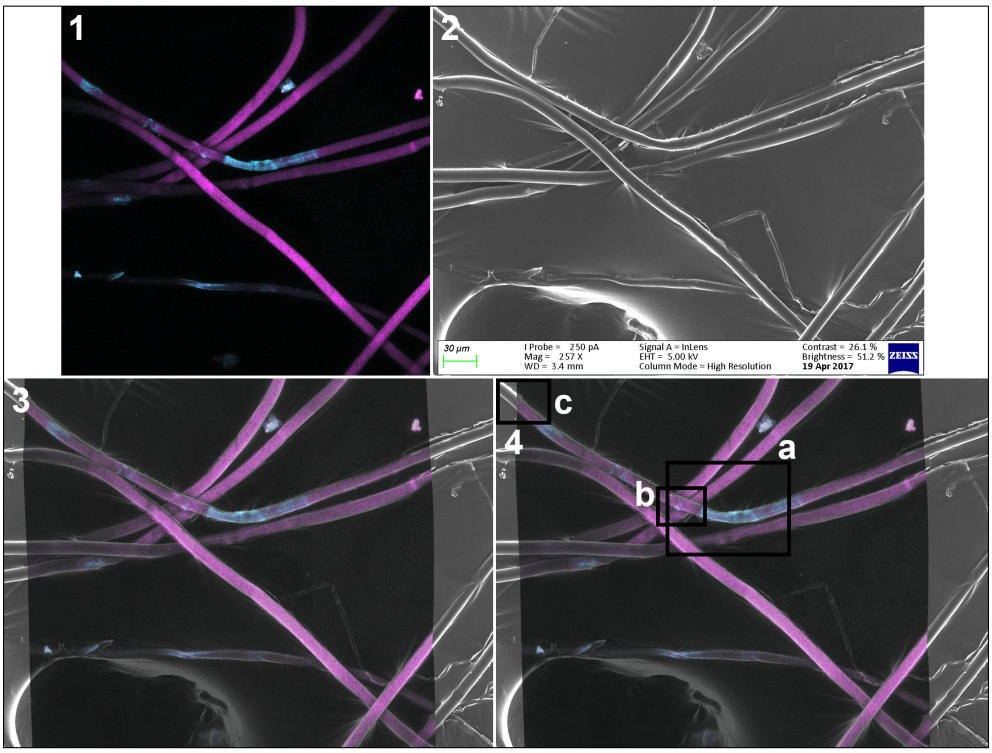

Figure 4.13: Maximum intensity projected z-stack (40 × magnified) CFM images of PET-NH-GA-Con A, (2) SEM micrograph of the CFM image area, (3) correlative image produced from overlaying (1) & (2) and (4) marked areas of interest on (3).

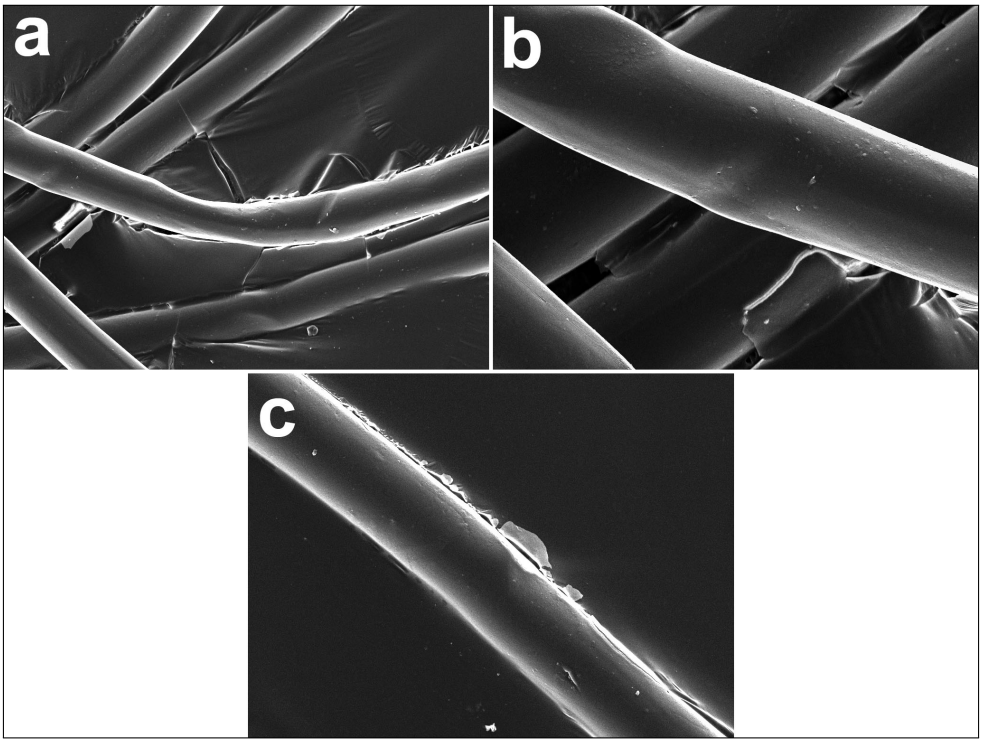

Figure 4.14: SEM micrographs of marked areas (a)-(d) on Figure 4.13.

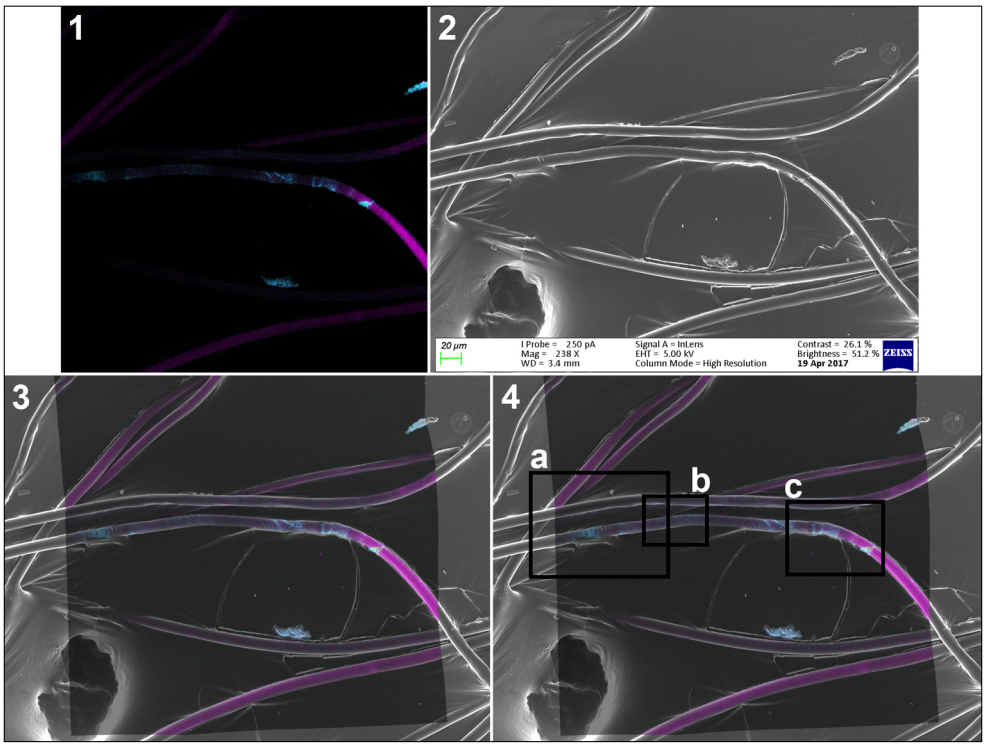

Figure 4.15: (1) Maximum intensity projected z-stack (40 × magnified) CFM images of PET-NH-GA, (2) SEM micrograph of the CFM image area, (3) correlative image produced from overlaying (1) & (2) and (4) marked areas of interest on (3).

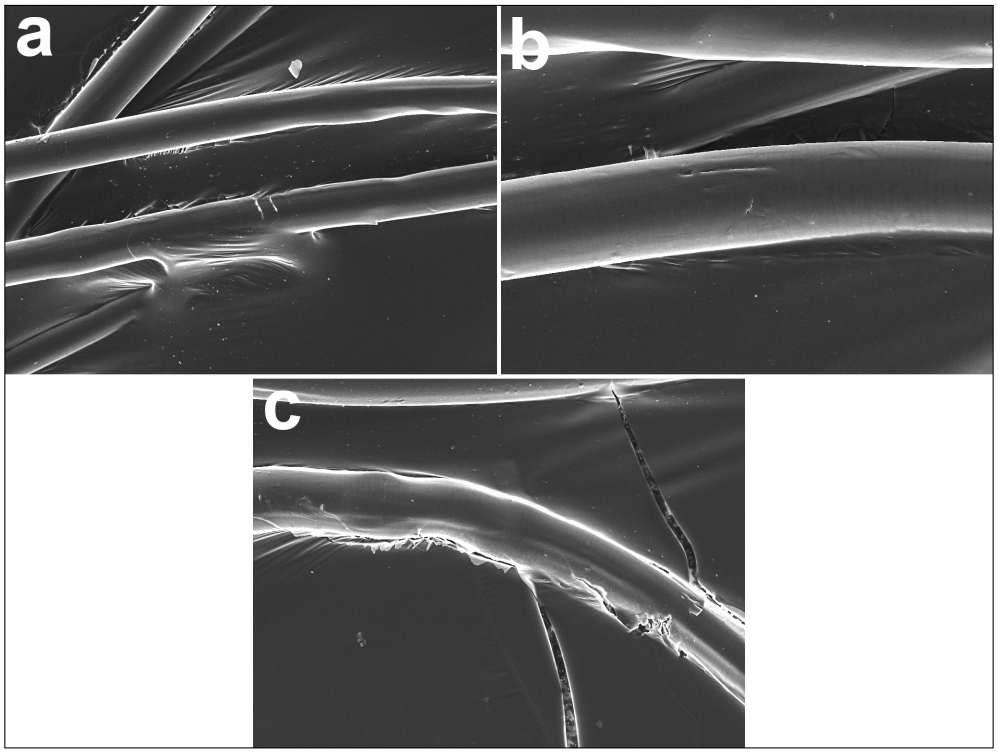

Figure 4.16: SEM micrographs of marked areas (a)-(c) on Figure 4.15.

The CFM micrograph of PET-NH-GA-Con A (micrograph (1) of Figure 4.13) suggests the presence of GA/Con-A complexes along the length of the fibres. These turquoise areas are dissimilar to those of PET-NH-GA-CLPA (micrograph (1) of Figure 4.11), due to the absence of clustering. However, when comparing micrograph (1) of Figure 4.13 to the CFM micrograph of PET-NH-GA (micrograph (1) of Figure 4.15), these turquoise areas are indistinguishable and hence require further resolving.

Comparing the SEM micrographs of PET-NH-GA-Con A and PET-NH-GA (micrographs (2) of Figures 4.13 and 4.15 respectively), there is also no market topographical features to discern the two types of fibres. By correlating the CFM and SEM images of the two types of fibres, areas of interest could again be selected for closer inspection by SEM (micrographs (4) of Figures 4.13 and 4.15 respectively).

SEM micrographs of areas (a) to (c) (Figure 4.14), show that the fibres are nodulated, in the case of the PET-NH-GA-Con A substrate. These nodules can be observed on the portion of the fibres which produced a turquoise signal, as well as the portions where only a magenta signal was apparent. In addition, no difference in the size nor amount of nodules could be observed between the turquoise and the magenta areas.

From the SEM micrographs of areas (a) to (c) (Figure 4.16), no nodules could be observed on the surface of the PET-NH-GA fibres. It was however observed that areas (a) to (c) showed signs of surface degradation. With areas (a) to (c) displaying fissure formation and (c) also showing notch formation. While these signs of degradation could possibly account for the GA/Con-A complex signals, the areas (b) to (d) of Figure 4.11 (micrograph 4) also showed signs of degradation but no turquoise attributes. Accordingly, this phenomenon will need to be studied further, in order to draw a conclusion.

A final CLEM analysis was conducted on PET-NH_2 fibres, which had been incubated in a protein coupling solution. This would aid in determining whether PET itself could produce emission signals indicative of the GA/Con-A complex (Figures 4.17 and 4.18). While this is predominantly true for the CFM micrograph of PET-NH_2 (micrograph (1) of Figure 4.17), a turquoise mass is present on the surface of a fibre. The CFM could again be correlated with the SEM micrograph (micrograph (2) of Figure 4.17) to generate the correlation image (micrograph (3) of Figure 4.17). The SEM micrographs of areas (a) and (b) of micrograph (4) (Figure 4.17) shows that this mass is not attached to the fibre surface (micrographs (a) and (b) of Figure 4.18). It can therefore be assumed that the observed mass is a contaminant, most likely from the PET-NH-GA-CLPA samples. Finally, the micrographs of Figure 4.18 show globular structures on the fibre surfaces. While their origin and composition are unknown, their appearance is not similar to that of the nodules associated with immobilised Con A.

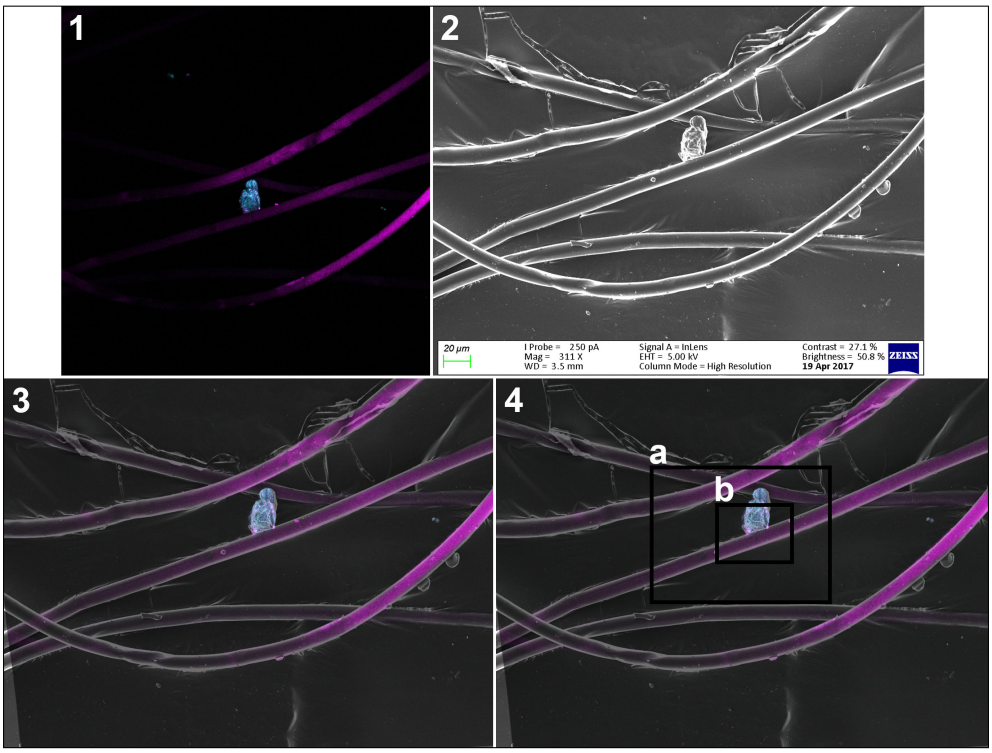

Figure 4.17: (1) Maximum intensity projected z-stack (40 × magnified) CFM images of PET-NH_2 treated with Con A, (2) SEM micrograph of the CFM image area, (3) correlative image produced from overlaying (1) & (2) and (4) marked areas of interest on (3).

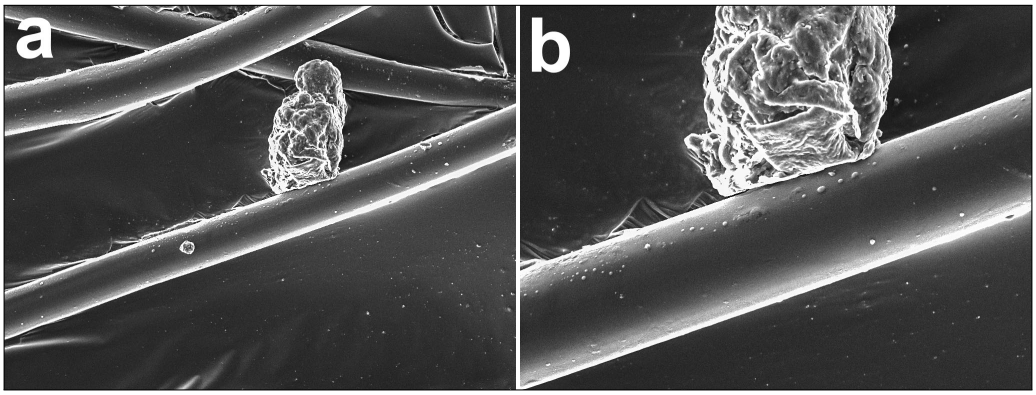

Figure 4.18: SEM micrographs of marked areas (a)-(c) on Figure 4.17.

The CLEM analysis study showed the limited potential of the method to be used as an analytic tool for detecting the presence of Con A on a fibre surface. While the method is adequate at detecting the presence of CLPA, it lacks specificity as well as sensitivity for detecting unistructural Con A. This is primarily due to shortcomings of the CFM data, which comes as a result of the convoluted emission spectra of the GA/Con-A complex and PET auto-fluorescence. The implication of which is an inverse proportionality

between specificity and sensitivity. Hence increasing the sensitivity of the CFM analysis would lead to false positive results.

It can be concluded that this technique is beneficial for confirming that the nodules observed on PET-NH-GA-Con A/CLPA fibres, in a SEM analysis, are in fact due to GA/Con A complexes. This technique however fails to give an indication of the degree of protein immobilisation. In addition to this, its low sensitivity limits its use to fibres which have high protein loadings on the surface.

4.3.2.5 Horseradish peroxidase assay

A HRP assay was performed to simultaneously confirm the successful immobilisation of Con A as well as preservation of its biological activity. This type of assay is convenient, since HRP is a glycoprotein and can accordingly bind to Con A. The presence of bound HRP is then detectable by a set of chromogenic substrates[34].

This assay was performed in the fashion of first incubating the relevant fibres in a PBS solution (PH 7.4) containing HRP, before introducing them into the ABTS substrate[13]. The presence of biologically active Con A on the fibre surface, resulted in a deepening of the substrates colour from light green to dark blue (Figure 4.19).

Both the PET-NH-GA-Con A and PET-NH-GA-CLPA fibres brought on a colour change of the ABTS substrate, thereby confirming the presence and biological activity of the immobilised Con A. The control fibres, however, did not result in any colour change of the substrate.

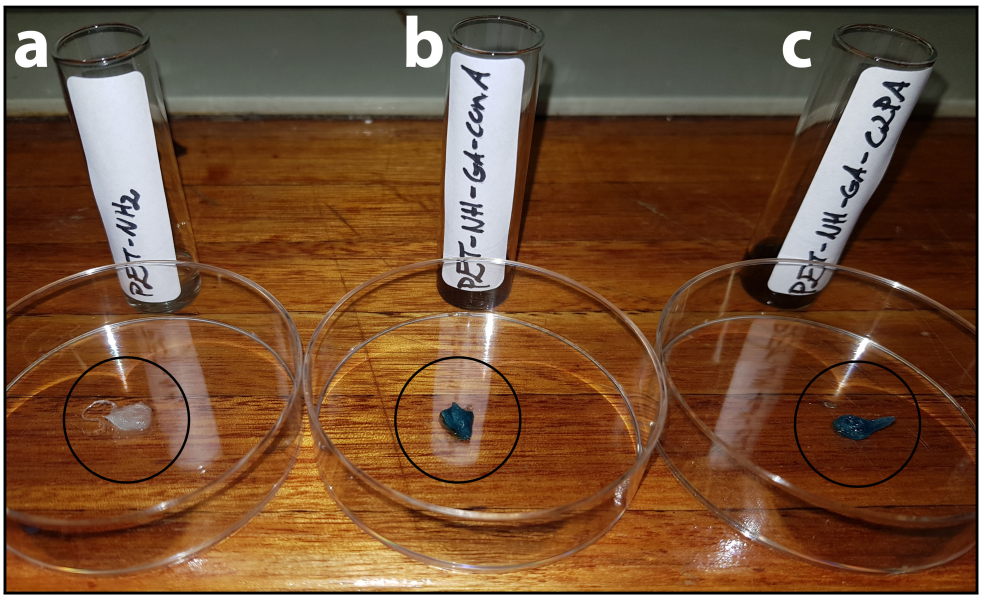

Figure 4.19: The colour change of an ABTS substrate observed for (a)PET-NH_2, (b) PET-NH-GA-Con A and (c) PET-NH-GA-CLPA.

4.3.3 DSC activation of PET-NH_2 (PET-NH-DSC)

DSC is a homobifunctional cross-linker, which is exceptionally reactive towards nucleophiles[35]. This reactivity emanates from the molecular structure of DSC (Figure 4.20), which consists of two NHS esters bound at a central carbonyl carbon. It follows that nucleophilic attack readily progresses at the carbonyl, due to the easy expulsion of N-hydroxysuccinimide[3]. The difunctional characteristic of the molecule then allows for subsequent reaction upon the introduction of a nucleophile. As such DSC could be used to activate both the amine and the hydroxyl groups created by the amination process (Scheme 4.7 and Figure 4.21).

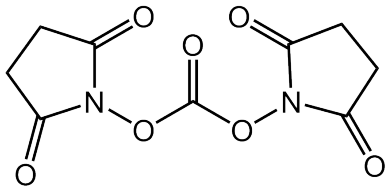

Figure 4.20: N,N'-Disuccinimidyl carbonate (DSC) molecular structure.

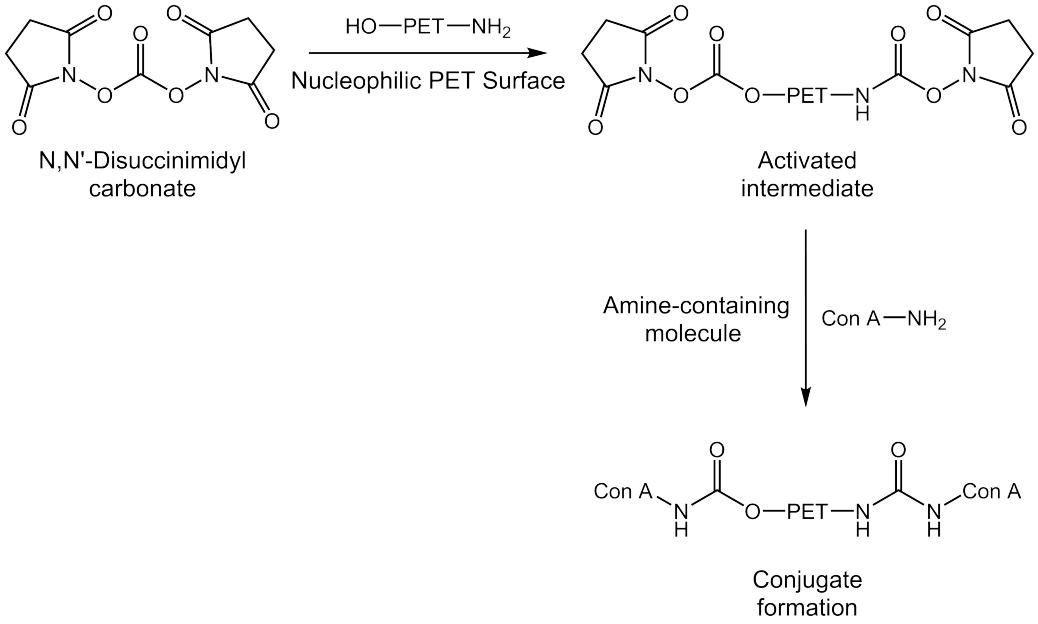

Scheme 4.7: DSC mediated activation of a hydroxyl and amine rich PET surface followed by an immobilisation event.

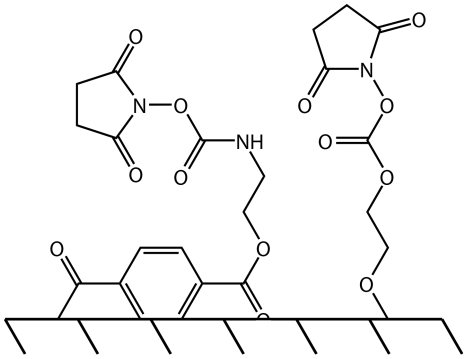

Figure 4.21: DSC activated PET-NH_2 surface (PET-NH-DSC).

4.3.4 PET-NH-DSC-Con A and PET-NH-DSC-CLPA

After the attachment of the DSC, the now electrophilic PET surface could be utilised for protein immobilisation as illustrated in Scheme 4.7. The introduction of primary amines present on Con A then gives rise to a second reaction of the now succinimidyl carbonate and carbamate rich surface, resulting in protein immobilisation (Figure 4.22). The immobilisation reaction is, however, impeded due to hydrolysis of the reactive groups in aqueous media. Although this is typically alleviated by using high concentrations of protein in the reaction mixture, this remedy was not feasible in this case[3]. As such not all of the active sites would be available for Con A immobilisation.

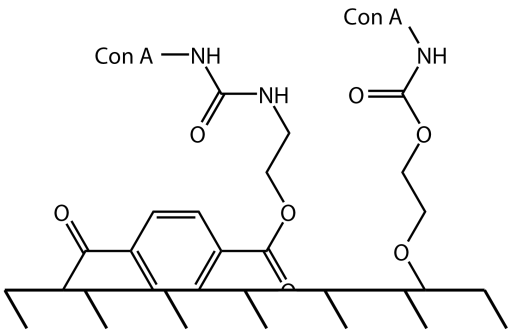

Figure 4.22: Con A immobilised onto a PET-NH-DSC surface (PET-NH-DSC-Con A).

FITC tagged Con A could not be used to confirm the presence of Con A by CFM, as was described in Section 4.3.2.2 (CFM detection of immobilised Con A). This is due to the ability of the nucleophilic functional groups present on the fluorescein molecule (Figure 4.7) to react with the DSC activated surface. Consequently, the fluorescence intensity comparison could not be used to compare the DSC immobilisation with GA immobilisation. For the detection of immobilised Con A using DSC as a surface activation, ATR-FTIR spectroscopy, SEM and a HRP assay was performed.

4.3.4.1 ATR-FTIR spectroscopy detection of immobilised Con A

The detection of immobilised Con A, mediated by a DSC activated surface, could be achieved by ATR-FTIR spectroscopy (Figure 4.23). This was done by identifying amide bands of Con A on the spectra of PET-NH-DSC-Con A and CLPA.

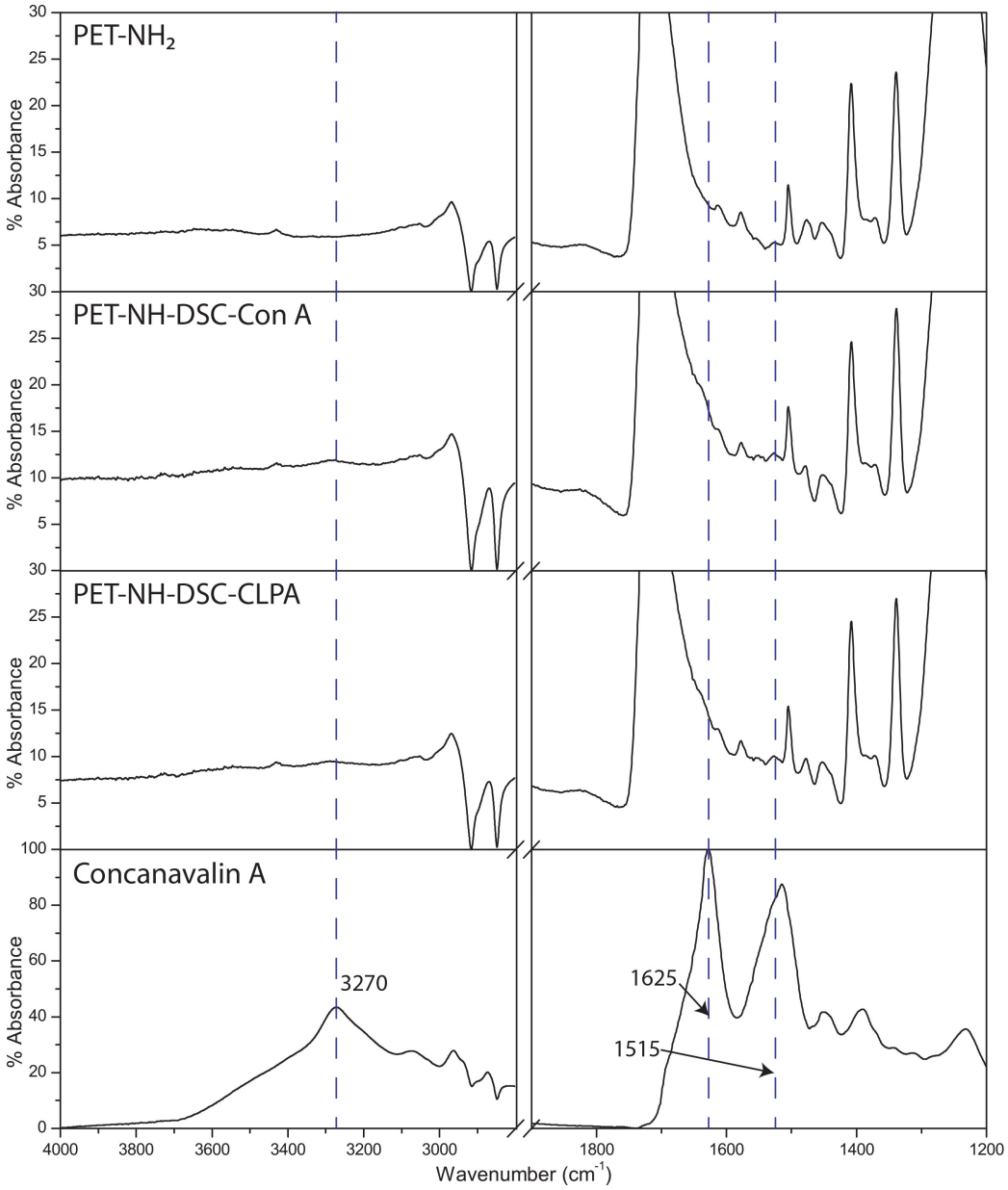

Figure 4.23: FTIR spectral correlation of Con A immobilisation by aid of DSC activation.

When comparing the spectra of the Con A functionalised fibres mediated by DSC in Figure 4.23 to those mediated by GA in Figure 4.5, the amide peaks typical of Con A are lower in intensity for the DSC activated fibres. This can be seen from the amide A band of Con A (3600-3100 cm^{-1}), which shows a weak absorption for the DSC derivative compared to the GA derivative. This result suggests that the immobilisation of Con A was less efficient when mediated by a DSC activated surface, than with a GA activated one.

4.3.4.2 SEM detection of immobilised Con A

Based on the SEM and CLEM results obtained from the GA derivatives, Con A immobilisation should result in nodulation of the fibre surface. Hence, the topography of the PET-NH-DSC-Con A and CLPA fibres were compared to that of PET-NH-DSC, as well as PET-NH_2 fibres which had been incubated in a protein coupling solution, in a SEM analysis (Figure 4.24).

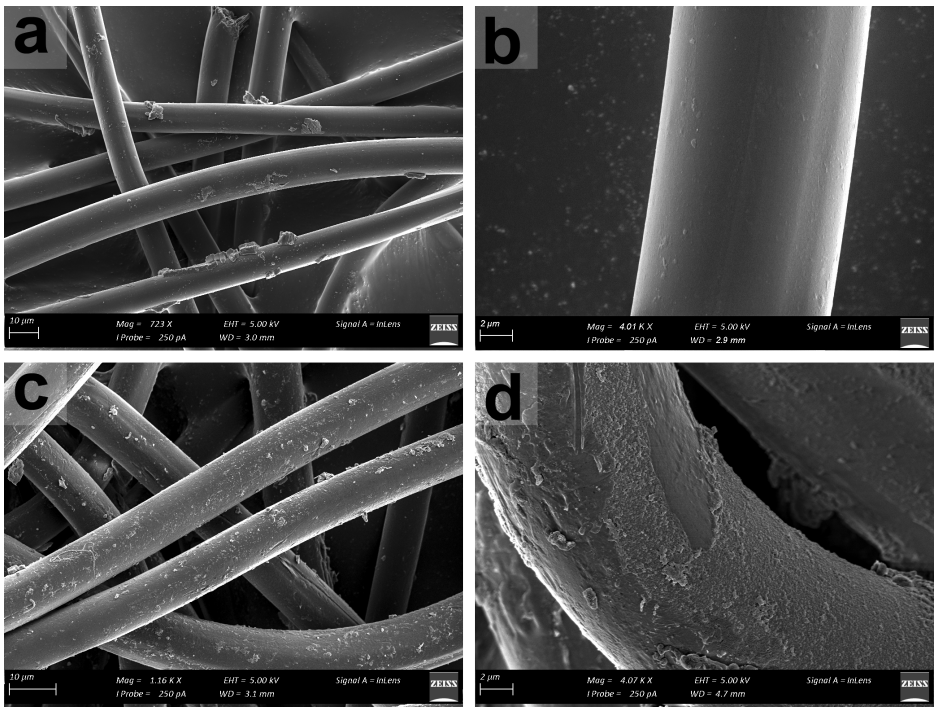

Figure 4.24: SEM micrographs of (a) PET-NH_2 treated with Con A (b) PET-NH-DSC, (c) PET-NH-DSC-Con A and (d) PET-NH-DSC-CLPA fibres.

Figure 4.24 (c) and (d) both show that the surfaces of the PET-NH-DSC-Con A and CLPA fibres were nodulated, in contrast with the PET-NH_2 and PET-NH-GA fibres (micrographs (a) and (b)). It is also clear that the nodules are larger with a denser distributed in the case of the CLPA derivative, compared to those of the unimolecular Con A. While all the key attributes of immobilised Con A could be observed from SEM micrographs (c) and (d), the structures were not as clearly defined as those of the GA activated fibres (Figure 4.9).

Figure 4.24 (a) shows objects on the surface of the PET-NH_2 fibres. Due to the regular fracture planes of these objects, they can be ascribed to salt crystals of the PBS.

4.3.4.3 Horseradish peroxidase assay

Implementation of the HRP assay on PET-NH-DSC-Con A and CLPA fibres, would indicate whether Con A had successfully been immobilised onto the activated substrate, with conservation of its biological activity (Figure 4.25).

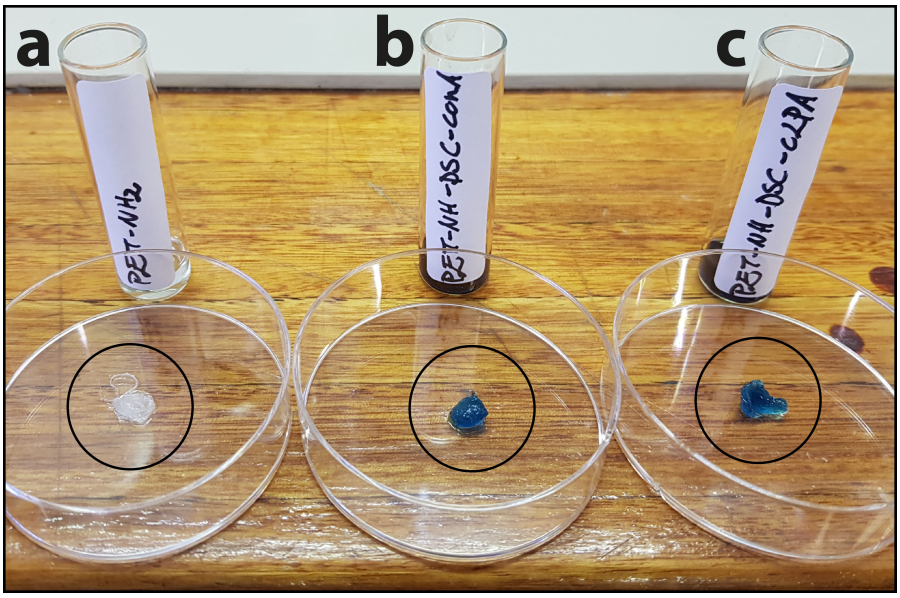

Figure 4.25: The colour change of an ABTS substrate observed for (a)PET-NH_2, (b) PET-NH-DSC-Con A and (c) PET-DSC-GA-CLPA.

Figure 4.25 shows a colour change of the ABTS substrate from light green to dark blue for the Con A and CLPA functionalised fibres. In contrast, the PET-NH_2 fibres which acted as a control study, did not induce a colour change. It can therefore be concluded from this study that biologically active Con A was immobilised on the DSC activated fibres.

4.4 Conclusion

From the aminated PET microfibre activation for Con A immobilisation study, it was found that Con A could be immobilised onto PET-NH_2 surfaces activated with either GA or DSC. In the case of GA activation, the auto-fluorescent property of GA allowed its detection by CFM. Immobilisation of Con A was confirmed for both types of surface activation by the use of ATR-FTIR spectroscopy, SEM and a HRP assay. Con A immobilised onto a GA activated surface, was additionally also detected by the use of CFM and CLEM.

4.5 References

1. Irena, G., Jolanta, B., Karolina, Z. & Pet, E. Applied Surface Science Chemical modification of poly (ethylene terephthalate) and immobilization of the selected enzymes on the modified film. Applied Surface Science 255, 8293-8298 (2009).

2. Jiang, X., Chai, C., Zhang, Y. & Zhuo, R. Surface-immobilization of adhesion peptides on substrate for ex vivo expansion of cryopreserved umbilical cord blood CD34 cells. Biomaterials 27, 2723-2732 (2006).

3. Harmanson, G. T.Audet, J., ed. Bioconjugate Techniques. London: Elsevier. 2013.

4. Locke, A. K., Cummins, B. M., Abraham, A. A. & Coteí, G. L. PEGylation of concanavalin a to improve its stability for an in vivo glucose sensing assay. Analytical Chemistry 86, 9091-9097 (2014).

5. Kim, J. J. & Park, K. Glucose-Binding Property of Pegylated Concanavalin A. Pharmaceutical Research 18, 794-799 (2001).

6. Hartmeier, W. Immobilized Biocatalysts An Introduction. Berlin Heidelberg: Springer. 1986.

7. Feng, Q., Chai, C., Jiang, X., Leong, K. W. & Mao, H. Expansion of engrafting human hematopoietic stem/progenitor cells in three-dimensional scaffolds with surface-immobilized fibronectin. Journal of Biomedical Materials Research Part A 76, 781-791 (2006).

8. Zhang, Y., Chai, C., Song, X., Hin, S. & Leong, K. W. Fibronectin immobilized by covalent conjugation or physical adsorption shows different bioactivity on aminated-PET. Materials Science and Engineering: C 27, 213-219 (2007).

9. Van Aken, B., Ledent, P., Naveau, H. & Agathos, S. N. Co-immobilization of manganese peroxidase from Phlebia radiata and glucose oxidase from Aspergillus niger on porous silica beads. Biotechnology Letters 22, 641-646 (2000).

10. Tukel, S. S. & Alptekin, O. Immobilization and kinetics of catalase onto magnesium silicate. Process Biochemistry 39, 2149-2155 (2004).

11. Magnan, E., Catarino, I., Paolucci-Jeanjean, D., Preziosi-Belloy, L. & Belleville, M. P. Immobilization of lipase on a ceramic membrane: Activity and stability. Journal of Membrane Science 241, 161-166 (2004).

12. Burteau, N., Burton, S. & Crichton, R. R. Stabilisation and immobilisation of penicillin amidase. Federation of European Btochemtcal Societtes Letters 258, 185-189 (1989).

13. Cloete, W. J., Adriaanse, C., Swart, P. & Klumperman, B. Supplementary Information: Facile immobilization of enzymes on electrospun poly (styrene-alt- maleic anhydride) nano fibres. Polymer Chemistry 2, 2-7 (2011).

14. Betancor, L., Lopez-Gallego, F., Hidalgo, A., Alonso-morales, N., Mateo, G. D. C., Fernandez-Lafuente, R. & Guisan, J. M. Different mechanisms of protein immobilization on glutaraldehyde activated supports: Effect of support activation and immobilization conditions. Enzyme and Microbial Technology 39, 877-882 (2006).

15. Swaminathan, C. P., Surolia, N. & Surolia, A. Role of Water in the Specific Binding of Mannose and Mannooligosaccharides to Concanavalin A. Journal of the American Chemical Society 120, 5153-5159 (1998).

16. Sato, K., Imoto, Y., Sugama, J., Seki, S., Inoue, H., Odagiri, T., Hoshi, T. & Jun-ichi, A. Sugar-Induced Disintegration of Layer-by-Layer Assemblies Composed of Concanavalin A and Glycogen. Langmuir 21, 797-799 (2005).

17. Kim, B. C., Nair, S., Kim, J., Kwak, J. H., Grate, J. W., Kim, S. H. & Gu, M. B. Preparation of biocatalytic nanofibres with high activity and stability via enzyme aggregate coating on polymer nanofibres. Nanotechnology 16, 382-388 (2005).

18. Cronje, L. PhD Thesis: Surface modification of styrene maleic anhydride nanofibers for efficient capture of Mycobacterium tuberculosis. Stellenbosch. 2012.

19. Girelli, A. M., Mattei, E. & Messina, A. Immobilized tyrosinase reactor for on-line HPLC application Development and characterization. Sensors and Actuators, B 121, 515-521 (2007).

20. Migneault, I., Dartiguenave, C., Bertrand, M. J. & Waldron, K. C. Glutaraldehyde: Behavior in aqueous solution, reaction with proteins, and application to enzyme crosslinking. BioTechniques 37, 790-802 (2004).

21. Makino, K., Maruo, S., Morita, Y. & Takeuchi, T. A study on the glutaraldehyde activation of hydrophilic gels for immobilized enzymes. Biotechnology and Bioengineering 31, 617-619 (1988).

22. Müller, M. Introduction to Confocal Fluorescence Microscopy. Washington: SPIE Press. 2006.

23. Monici, M. Cell and tissue autofluorescence research and diagnostic applications. Biotechnology annual review 11, 227-256 (2005).

24. Kubitscheck, U., editor. Fluorescence Microscopy From Principles to Biological Applications. Weinheim: Wiley-Blackwell. 2013.

25. Mörtelmaier, M., Kögler, E. J., Hesse, J., Sonnleitner, M., Huber, L. A., Schütz, G. J., Kepler, J. & Schtz, G. J. Single Molecule Microscopy in Living Cells: Subtraction of Autofluorescence Based on Two Color Recording. Single Molecules 4, 225-231 (2002).

26. Lee, K., Choi, S., Yang, C., Wu, H. & Yu Junhua. Autofluorescence generation and elimination: a lesson from glutaraldehyde. Chemical Communications 49, 3028-3030 (2013).

27. Krafft, C., Salzer, R., Seitz, S. & Schieker, M. Differentiation of individual human mesenchymal stem cells probed by FTIR microscopic imaging. Analyst 132, 647-653 (2007).

28. Invitrogen. Concanavalin A Conjugates Product documentation. 13 (2006).

29. Broadbent, A. D. Basic Principles of Textile Coloration. Yorkshire: Society of Dyers and Colourists. 2001.

30. Oktay, B., Demir, S.& Kayaman-apohan, N. Immobilization of α-amylase onto poly (glycidyl methacrylate) grafted electrospun fibers by ATRP. Materials Science & Engineering C 50, 386-393 (2015).

31. Müller-reichert, T. & Verkade, P., editors. Methods in Cell Biology Correlative Light and Electron Microscopy. Oxford: 2012.

32. Sun, M. A Review of Correlative Light and Electron Microscopy (CLEM) Methods, Markers, and Instrument Set Ups to Study Infectious Disease. EC Microbiology 5, 787-800 (2016).

33. Schirra, R. T. & Zhang, P. Correlative fluorescence and electron microscopy. Current Protocols in Cytometry 70, 1-15 (2015).

34. Hawkes, R. Identification of Concanavalin A-Binding Proteins after Sodium Dodecyl Electrophoresis and Protein Blotting. Analytical Biochemistry 123, 143-146 (1982).

35. Miron, T. & Wilchek, M. A Simplified Method for the Preparation of Succinimidyl Carbonate Polyethylene Glycol for Coupling to Proteins. Bioconjugate Chemistry 4, 568-569 (1993).

Chapter 5

Affinity studies between microfibrous substrates and mycobacteria

5.1 Introduction

In general, bacterial cells prefer to adhere and grow upon material surfaces, rather than in aqueous environments. Adhesion to a solid surface is a process which is governed by various physiochemical interactions, which may either favour or hinder the event[1]. The adhesion process as a whole can be considered to occur in two phases. The first is the initial and instantaneous, but also reversible phase (physical phase), which takes place prior to the time-dependant and irreversible second phase (molecular and cellular phase)[2].

During the physical phase of adhesion, bacterial cells are drawn towards material surfaces by means of physical forces, which include van der Waals forces, Brownian motion, electrostatic surface charge, gravitational pull and also hydrophobic interactions[1]. Along with these, chemotaxis and haptotaxis assists the diffusion[3]. This initial adhesion forms the foundation for the subsequent molecular and cellular phase adhesion process. The cellular phase adhesion process involves the formation of adhesive scaffolds by means of the polymeric entities on the bacterial surface. As such, molecular-specific reactions govern the permanent adhesion of the bacteria to the substrate surface in this phase[4-6].

The adhesion of bacteria to materials is governed by specific and non-specific interactions[7]. If the surface of the material can act as both an adhesin and a receptor, for complementary groups on the bacterial cell surface, specific interactions can be selectively promoted[2,8,9]. Throughout this study, this

was achieved by covalently binding the mannose specific binding protein, Concanavalin A (Con A) to a poly(ethylene terephthalate) (PET) fibre surface. This protein, in turn, is able to bind to the mannose capped lipoarabinomannan (LAM) present on the cell wall of *Mycobacterium tuberculosis* (*Mtb*)[10]. This is facilitated by the formation of direct hydrogen bonds and van der Waals interactions[11]. Accordingly, these surfaces would potentially gain the ability to limit the reversibility of the physical phase during the adhesion of *Mtb* to the substrate. Since the physical phase is a prerequisite for the molecular and cellular phase, the latter is also promoted.

5.2 Experimental

Modified PET microfibres were tested for their affinity towards *Mtb*. This affinity was approximated by making use of an *Mtb*-mimic, namely the bacillus of Calmette-Guérin (BCG). BCG is non-pathogenic, attenuated strain of Mycobacterium bovis, belonging to the *Mtb* complex[12-14]. Mycobacterium bovis itself is closely related to *Mtb* and the etiological factor of bovine tuberculosis[15]. Like *Mtb*, BCG also possesses α 1→2 mannose residue capped LAM, the compound known to affiliate with Con A[10]. Affinity studies were consequently performed to assess the interaction between BCG and the surface functionalised PET microfibrous substrates. Successful adhesion of bacterial cells will henceforth be referred to as capture.

The kanamycin-resistant BCG strain selected for this study, was cultured to contain a fluorescent protein reporter gene, namely mCherry. This allowed for the rapid detection of the bacilli on the fibre surface, without the need for staining. This also circumvented staining of the fibres, which was found to hamper accurate evaluation of the capture ability. Kanamycin in turn would be used during bacterial dilution in the affinity studies to inhibit the growth of contaminating bacteria on the polymeric substrates.

Bacterial adhesion is principally complex and affected by several factors, which include exposure period, surface area and surface characteristics, bacterial concentration and temperature amongst others[2]. Accordingly, affinity studies were conducted in a consistent manner. In broad terms, this included incubating the modified fibres in known serial dilutions of bacterial culture concentrations, followed by mechanically washing them in phosphate buffered saline (PBS). Thereafter, the ability of the substrates to capture bacteria were determined by means of confocal fluorescence microscopy (CFM). Any bacteria observed during the analysis were considered to have been captured by the fibre matrix (this being a result of chemical association between the fibre surface and the bacterial cell wall). The chemical surface structures of the substrates used for the affinity assessment are presented in Figure 5.1.

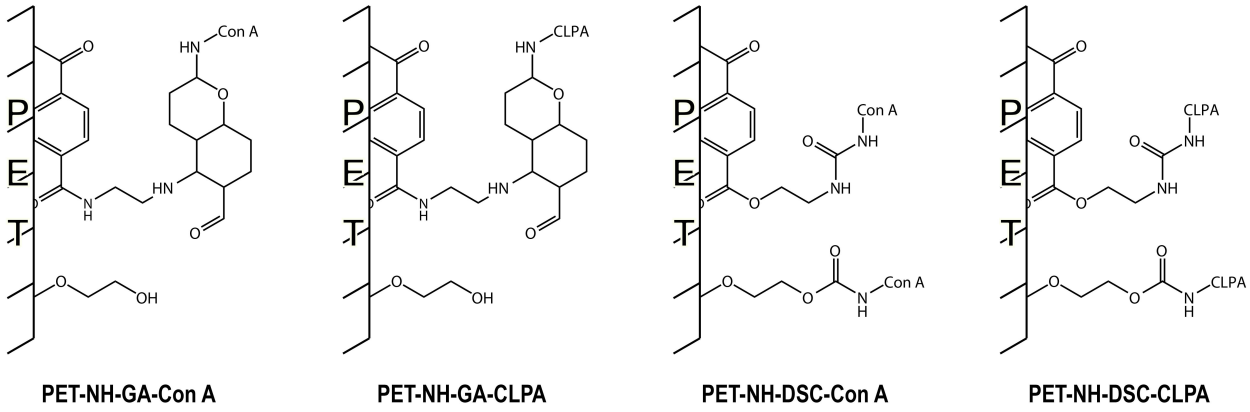

Figure 5.1: Chemical surface structures of the functionalised PET microfibres used for affinity tests with mCherry-BCG.

5.2.1 mCherry-BCG culture

mCherry-expressing BCG (mCherry-BCG) was cultured by transforming BCG Pasteur with pMSG432 (episomal plasmid encoding mCherry as well as conferring hygromycin resistance). Thereafter, BCG strains were grown at 37 °C in Middlebrook 7H9 growth medium supplemented with 10% albumin/dextrose/saline, 0.5% glycerol and 0.05% Tween-80 in the presence of 50 µg/mL hygromycin to an approximate optical density measured at 600 nm (OD_{600}) of 0.80.

5.2.2 mCherry-BCG affinity study

A fixed amount of each substrate (10 mg) was placed in a glass vial (30 mL), to which 5 mL of BCG culture dispersed in PBS (pH 7.4) at an OD_{600} of approximately 2.0 was added. The fibres were thoroughly wetted and incubated at 37 °C for one hour on an orbital shaker. As a control study, aminated precursor PET fibres were treated in the same fashion.

Thereafter, the fibres were removed from the culture solution and sequentially washed with three aliquots of PBS on a laboratory vortex shaker for two minutes at a time. This aided in removing most of the loosely adhering bacterial cells from the fibres. The washed fibres were then placed in sealed vials, and were submitted for immediate analysis.

5.2.3 mCherry-BCG dilution study

Following a procedure similar to the affinity trial study, the fibres were prepared for incubation with BCG culture solutions, which had been serially diluted by tenfold. The OD_{600} to which the samples had been diluted, was chosen to cover a range from 0 to 0.7. The same procedure was then followed for incubation and subsequent washing. The dilution study was repeated in duplicate to evaluate the affinity trends observed.

5.2.4 Average surface area calculation

The density of the cylindrical PET fibres were given to be 1.38 g.cm^{-3} by the supplier, and their diameter remained constant at 10 µm. From this, the surface area per 10 mg mass of fibre could be calculated as follows:

(a) By plugging the equation for the volume of a cylinder into the equation for the density of a material, the total fibre length of the sample could be determined.

$$\begin{aligned} \text{Length} &= \frac{\text{Mass}}{\text{Density} \times \text{Radius}^2 \times \pi} \\ &= \frac{0.01}{1.38 \times 0.0005^2 \times \pi} \\ &= 9226.37 \text{ cm} \end{aligned}$$

(b) Since the fibres were 3 cm in length, this meant that the sample was comprised of 3075.46 individual fibre strands. Given this, the exposed surface area could be calculated, not taking into account the increased surface area due to fissure formation nor protein aggregates.

$$\begin{aligned} \text{Area per fibre} &= (2 \times \pi \times \text{Radius} \times \text{Length}) + (2 \times \pi \times \text{Radius}^2) \\ &= (2 \times \pi \times 0.0005 \times 3) + (2 \times \pi \times 0.0005^2) \\ &= 9.426 \times 10^{-3} \text{ cm}^2 \\ \text{Total Area} &= 9.426 \times 10^{-3} \times 3075.46 \\ &= 28.99 \text{ cm}^2 \end{aligned}$$

5.3 Results and discussion

5.3.1 mCherry-BCG affinity study

For the various Con A modified fibres to be considered viable platforms for *Mtb* cell capture, they needed to show greater affinity for the *Mtb* mimic, BCG, than the precursor substrate (PET-NH_2). To assess this, an affinity study was conducted in triplicate. This entailed that the various substrates were exposed to cultures of mcherry-BCG with OD_{600} values of approximately 2.0, and subsequently analysed with CFM and scanning electron microscopy (SEM). CFM was the preferred method of the two, as it allows direct visualisation of both the fibres and the bacteria. Fibres were observed as broad, uniform strands, while the bacteria could easily be detected by the mCherry fluorophore it possessed. mCherry was excited by a 561 nm laser and its emission detected at 622 nm. SEM analysis would provide topographical information with regards to the association between the fibres and the bacteria. From both the CFM and SEM analyses, the bacilli were observed as short rod-shaped cells dispersed on and amongst fibres as individual bacilli or clusters (Figure 5.2a, 5.2b and 5.3).

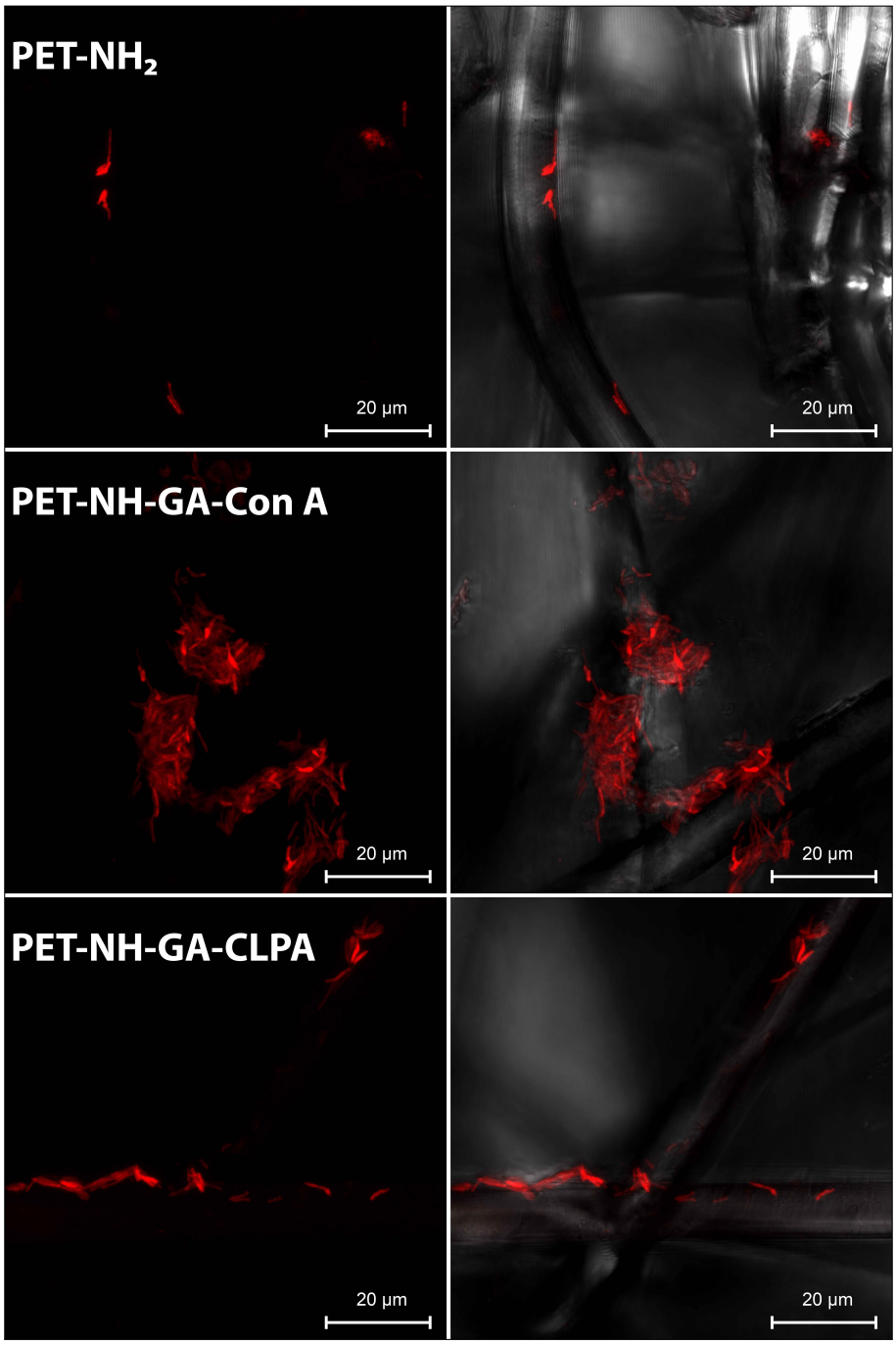

Figure 5.2a: Maximum intensity projected z-stack (100 × magnified) CFM images of PET-NH_2, PET-NH-GA-Con A and PET-NH-GA-CLPA incubated with mCherry-BCG with an OD_{600} of 2.0. Left hand side images represent fluorescent signals produced by excitation with a 561 nm laser and detected at 622 nm. Right hand side images represent the combination of residual signals detected by the T PMT filter as well as the images on the left.

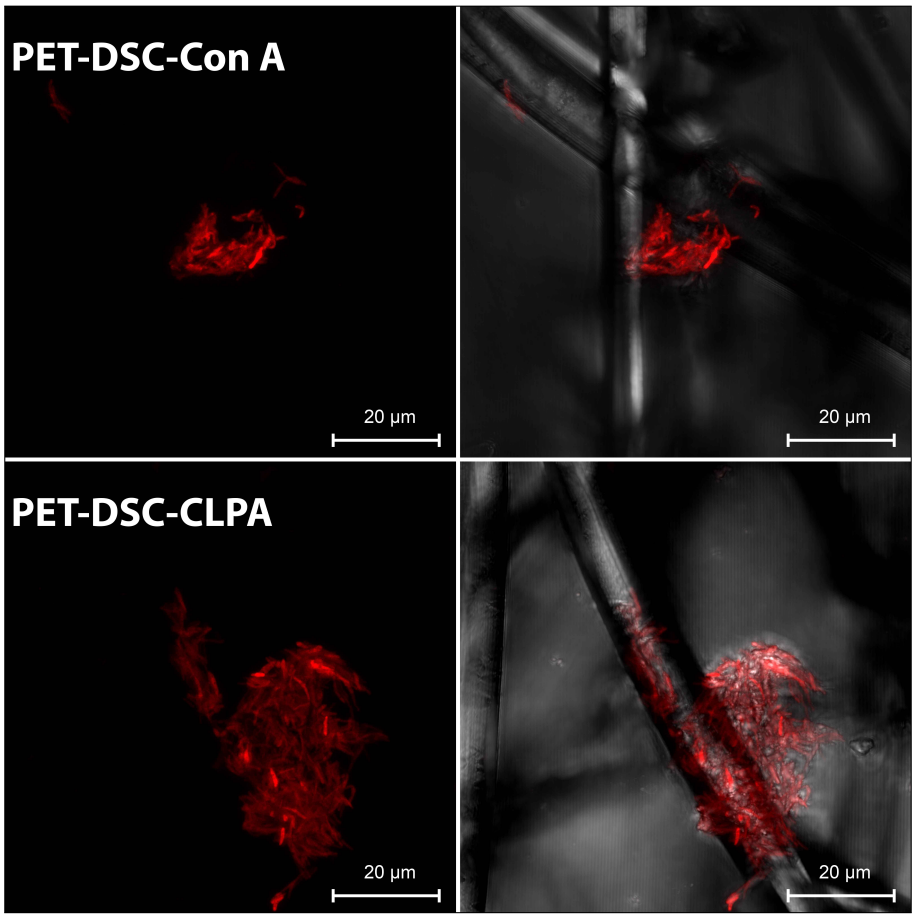

Figure 5.2b: Maximum intensity projected z-stack (100 × magnified) CFM images of PET-NH-DSC-Con A and PET-NH-DSC-CLPA incubated with mCherry-BCG with an OD_{600} of 2.0. Left hand side images represent fluorescent signals produced by excitation with a 561 nm laser and detected at 622 nm. Right hand side images represent the combination of residual signals detected by the T PMT filter as well as the images on the left.

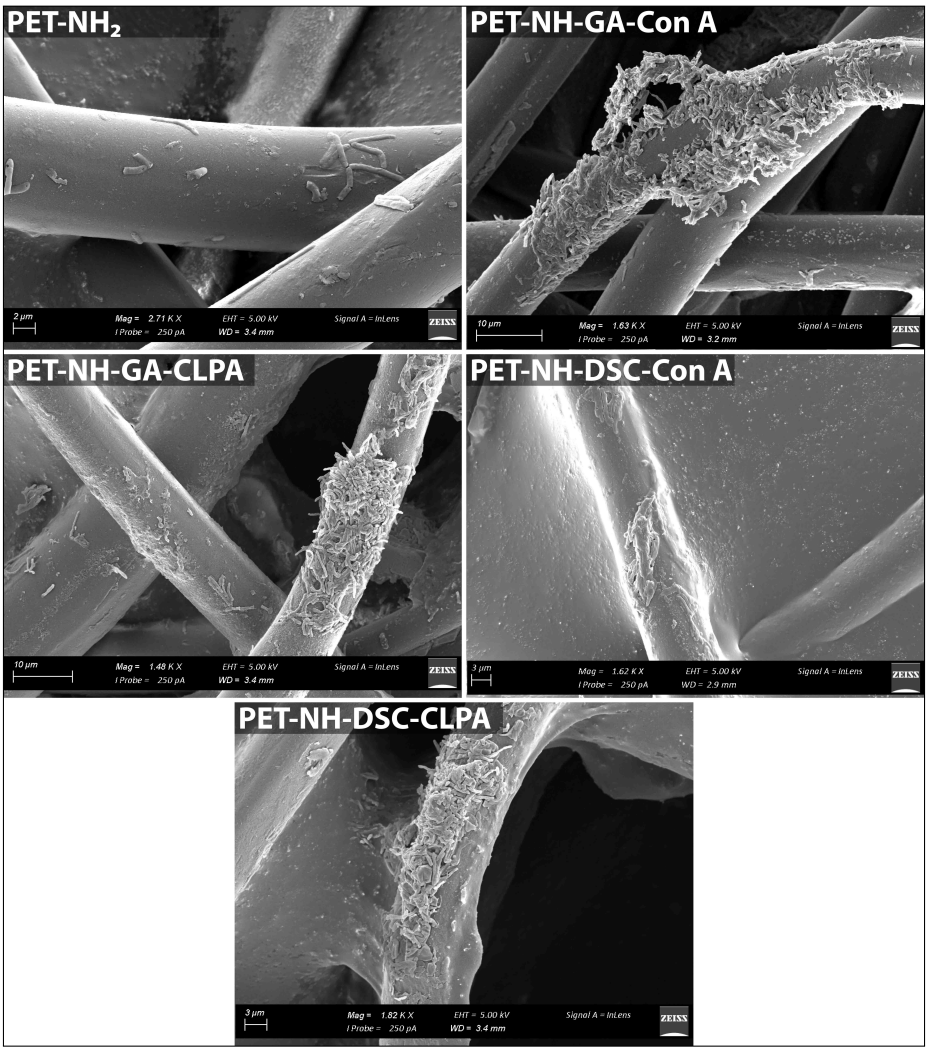

Figure 5.3: SEM micrographs of PET-NH_2, PET-NH-GA-Con A, PET-NH-GA-CLPA, PET-NH-DSC-Con A and PET-NH-DSC-CLPA incubated with mCherry-BCG with an OD_{600} of 2.0.

Figures 5.2a, 5.2b and 5.3 show the presence of BCG on all of the fibre substrates, including the PET-NH_2 control study fibres. This is to be expected, and occurs due to the ability of the fibres to act as a filter medium when removing it from the culture solution. As such, cells become trapped in the matrix and are not easily removed by washing. While the concentration of these cells was low throughout the sample, they were purposefully imaged for comparison purposes. With regards to the Con A functionalised fibres, both the CFM and SEM micrographs indicate that these fibres were able to avidly capture BCG bacteria.

The CFM micrographs (Figures 5.2a and 5.2b) show that the amounts of bacteria captured by the Con A derivatives, are far greater than that trapped by the PET-NH_2 fibres. Additionally, the bacteria are observed to be distributed along the length of the fibres as single cells or clumps of several cells. This is indicative of adhesion based interaction, rather than physical entrapment[1,16]. Similar attributes can be seen in the SEM

micrographs (Figure 5.3), with the added advantage that the topographical aspects of the bacterial capture could be resolved. The SEM micrographs show that the BCG bacteria were inclined to accumulate and form clusters around the circumference of the Con A functionalised fibres. In the case of the control fibres, small groups of bacteria can be seen, although bacterial clusters are absent.

The clumping of the BCG bacilli as seen from the CFM and SEM micrographs (Figures 5.2a, 5.2b and 5.3) is an inherent property of the mycobacteria, which is due the hydrophobic outer layers of the organisms[17,18]. It is however likely that the capture platform promotes clump formation. This can occur as a result of initial cell capture, followed by a hydrophobic clustering formation[1]. To add to this, the analysis is prejudiced towards visualization of clusters of bacteria, due to the vast sample area which is analysed. The surface area per sample exposed to the BCG culture was approximately 29 cm^2, whereas the imaging of the sample surface is limited to around 7×10^{-5} cm^2 at a hundred times magnification. So, while ample amounts of single or small clusters of bacilli were present on the protein modified fibre derivatives, for the sake of clarity, larger groups of the bacteria were selected for imaging.

From this study, a general trend in BCG capture ability for the various substrates could be observed and expressed as follows: PET-NH-GA-CLPA > PET-NH-DSC-CLPA > PET-NH-GA-Con A > PET-NH-DSC-Con A > PET-NH_2. This trend slightly deviates from that suggested by Figures 5.2a, 5.2b and 5.3, from which it seems that PET-NH-GA-CLPA captured the third least bacteria. This deviation occurs since mycobacterial cell capture is an accumulative fibre property, while analysis was performed on a per fibre basis. This is due to physical bulk and irregular surfaces of the fibres bundles which had to be analysed. Consequently, only the fibres closest to the surface could be imaged, resulting in a facile representation of the materials BCG capture ability.

The observed ability of the Con A modified fibres to interact with BCG bacilli is likely mediated by the carbohydrate-binding ability, and mannose specificity of the protein[11,21]. This proved to be effective on the BCG bacterial cells, due to the presence of mannose caps on their cell walls[10]. It follows, that the adhesion between the Con A functionalised fibre surface and the mannose caps of BCG, is likely achieved by means of direct hydrogen bond formation, as well as van der Waals interactions[11].

It could also be observed from the BCG affinity trend that the CLPA derivatives displayed greater affinity for the BCG bacilli than the unistructural Con A derivatives. This was likely the causative effect of greater protein loadings per unit area of fibre surface, as well as improved protein activity and stability[22].

From this study, it can be concluded that the Con A functionalised PET substrates were able to perform as viable platforms for BCG cell capture. All of the protein bearing fibres captured the bacterial cells with high avidity. These captured cells could also be seen to be intimately associated with the fibre surfaces.

5.3.2 mCherry-BCG dilution study

Most children infected with TB develop a paucibacillary form of the disease, where the count of *Mtb* bacilli in their sputum is very low[21]. Hence, the ability of the various substrates to aid in the detection of *Mtb*, was assessed by conducting a dilution study. From this, the sensitivity of the substrates for BCG baccili, as *Mtb* mimic, could be determined. The study entailed that the fibres were exposed to serial dilutions (1:10 OD_{600}) of bacteria, whereafter their capture ability was analysed by CFM.

Paucibacillary cases of TB, correspond to bacilli counts which approach zero colony-forming units per millilitre (CFU/mL) of sputum[12,22]. Therefore, the series of dilutions at which this study was performed, were selected to fall within a range respective of paucibacillary TB. The OD_{600} values of the *Mtb* bacilli corresponding to this range, was obtained from literature. This was found be OD_{600} values of less than 0.5[23]. The CFM dilution study results presented in Figures 5.4a and 5.4b correspond to a dilution set of 0.3 to 0.003. These micrographs display the BCG affinity of the various fibre types and their ability to operate

as capture media, down to bacteriological concentrations representative of paucibacillary TB.

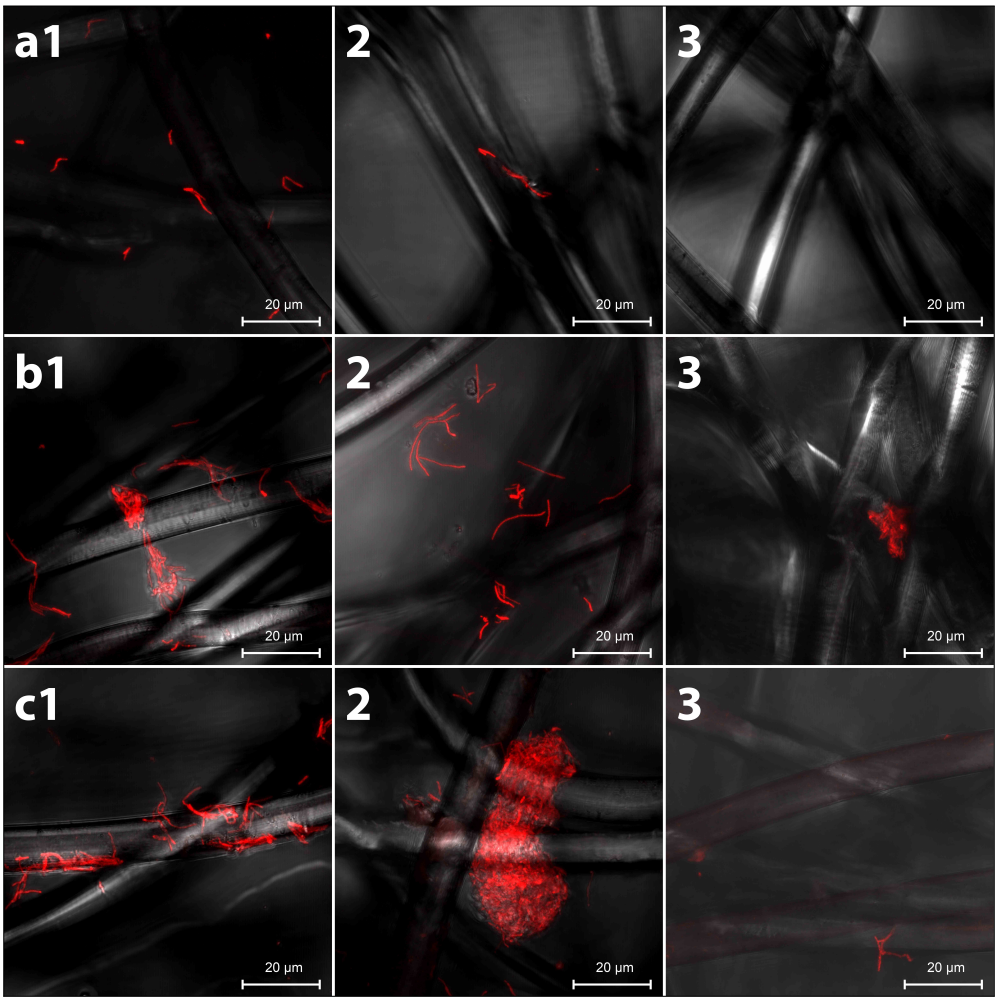

Figure 5.4a: Maximum intensity projected z-stack (100 × magnified) CFM images of (row a) PET-NH_2, (row b) PET-NH-GA-Con A and (row c) PET-NH-GA-CLPA incubated with mCherry-BCG with an OD_{600} of 0.3 (column 1), 0.03 (column 2) and 0.003 (column 3). All images represent fluorescent signals produced by excitation with a 561 nm laser and detected at 622 nm, overlaid with T PMT filter data.

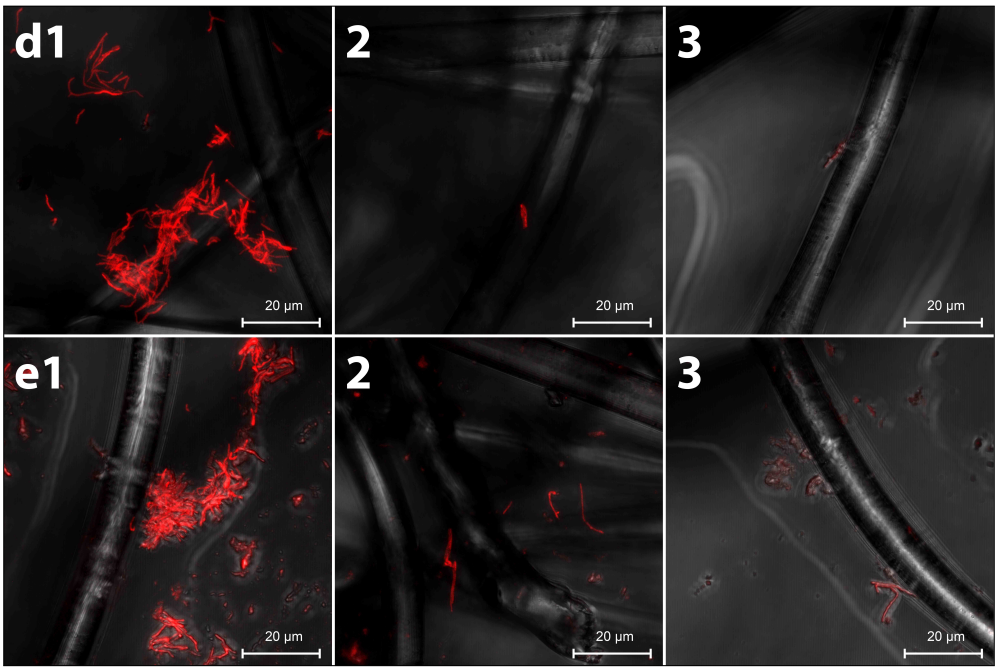

Figure 5.4b: Maximum intensity projected z-stack (100 × magnified) CFM images of (row d) PET-NH-DSC-Con A and (row e) PET-NH-DSC-CLPA incubated with mCherry-BCG with an OD_{600} of 0.3 (column 1), 0.03 (column 2) and 0.003 (column 3). All images represent fluorescent signals produced by excitation with a 561 nm laser and detected at 622 nm, overlaid with T PMT filter data.

The micrographs of columns (1-3) of Figures 5.4a and 5.4b, show the enhanced BCG affinity of the Con A modified fibres, compared to the control study fibres. The localisation of the bacteria onto the surfaces of these fibres, illustrates their ability to also concentrate bacteria from solution. In addition, all of the Con A derivatives show the ability to capture significant amounts of bacilli at an OD_{600} of 0.3. These amounts are then seen to decrease as the concentration of the bacteria in solution decrease. From the decline in captured bacilli, per individual fibre type, an agreement with the trend described in in Section 5.3.1 can be observed. This, in brief, implies that the CLPA functionalised and glutaraldehyde (GA) activated fibres show superior BCG capture ability.

Figures 5.4a and 5.4b, suggest that the lowest limit of detection of BCG bacteria on the Con A functionalised fibres, by aid of CFM, is approached at an OD_{600} of 0.003. Since such an OD_{600} value corresponds to a theoretical CFU/mL value of zero[23], this technique suggests a possible increase in the detection threshold for acid fast sputum smear microscopy of 10^4 CFU/mL[12,24]. This is however a strongly theoretical statement, based on detection of an *Mtb* mimic at correlated culture concentrations and ideal experimental parameters.

The control study fibres of columns (1) and (2) (row (a) of Figures 5.4a and 5.4b), show bacilli concentrations which appear much greater than they actually were. This was done for comparison reasons, as discussed

in Section 5.3.1. However, from the control studies, it can be observed that the fibrous matrix plays a significant role in aiding bacterial capture, with the fibres being able to physically entrap bacilli down to an OD_{600} value of 0.03.

It can be concluded from this study that the Con A functionalised fibres were able to perform as BCG capture and concentration platforms. They were able to do so at OD_{600} values, which correlate to the concentration of bacteria in the sputum of paucibacillary TB patients. It was also seen that the fibre matrix plays a significant role in aiding BCG capture, by entrapment of bacteria in the fibre matrix.

5.4 Conclusion

An *Mtb* mimic, mCherry-BCG, was successfully captured onto the PET-NH-GA-Con A, PET-NH-GA-Con A, PET-NH-GA-CLPA and PET-NH-DSC-CLPA microfibre surfaces. This was evaluated and confirmed with CFM and SEM analysis, by comparing it against a controlled study precursor. In all instances, the lectin functionalised fibres outperformed the control study samples. This can be ascribed to the adhesion based interactions between the adhesin functionalised fibres and the mannose receptor groups on the BCG cell wall.

From a dilution study, it was found that all of the Con A functionalised substrates were able to capture and concentrate mCherry-BCG from low concentration culture solutions. This study also indicated the importance of the fibrous morphology, in aiding mycobacterial cell capture.

The general trend observed in capture ability, was that the CLPA derivatives had the greatest affinity for BCG bacteria, and that overall, the fibres which had been activated with GA were best suited for mycobacterial adhesion.

From the results obtained from this chapter, it can be concluded that PET microfibres, surface modified to bear Con A, are capable of capturing mycobacterial BCG cells. These substrates were able to perform admirably down to culture concentrations which are characteristic of paucibacillary cases. As such, the substrates investigated could prove to assist with the detection of *Mtb* by means of buccal swabbing.

5.5 References

1. Katsikogianni, M. & Missirlis, Y. F. Concise review of mechanisms of bacterial adhesion to biomaterials and of techniques used in estimating bacteria-material interactions. European Cells and Materialsterials 8, 35-37 (2004).

2. An, Y. H. & Friedman, R. J. Concise Review of Mechanisms of Bacterial Adhesion to Biomaterial Surfaces. Journal of Biomedical Materials Research Part A 43, 338-348 (1998).

3. Kirov, S. M. Bacteria that express lateral flagella enable dissection of the multifunctional roles of flagella in pathogenesis. FEMS Microbiology Letters 224, 151-159 (2017).

4. O'Gara, J. P. & Humphreys, H. Staphylococcus epidermidis biofilms: importance and implications. Journal of Medical Microbiology 50, 582-587 (2017).

5. Mack, D. Molecular mechanisms of Staphylococcus epidermidis biofilm formation. Journal of Hospital Infection 43, 113-125 (1999).

6. Götz, F. MicroReview Staphylococcus and biofilms. Molecular Microbiology 43, 1367-1378 (2002).

7. Morra, M. & Cassinelli, C. Bacterial adhesion to polymer surfaces: A critical review of surface thermodynamic approaches. Journal of Biomaterials Science, Polymer Edition 9, 55-74 (1997).

8. Tojo, M., Yamashita, N., Goldmann, D. A. & Pier, G. B. Isolation and Characterization of a Capsular Polysaccharide Adhesin from Staphylococcus epidermidis. The Journal of Infectious Diseases 157, 713-722 (1988).

9. Hasty, D. L., Ofek, I., Courtney, H. S. & Doyle, R. J. Multiple Adhesins of Streptococci. Infection and Immunity 60, 2147-2152 (1992).

10. Dinadayala, P., Kaur, D., Berg, S., Amin, A. G., Vissa, V. D., Chatterjee, D., Brennan, P. J. & Crick, D. C. Genetic Basis for the Synthesis of the Immunomodulatory Mannose Caps of Lipoarabinomannan in *Mycobacterium tuberculosis*. Journal of Biological Chemistry 28, 20027-20035 (2006).

11. Naismith, J. H. & Field, R. A. Structural Basis of Trimannoside Recognition by Concanavalin A. The American Society for Biochemistry and Molecular Biology 271, 972-976 (1996).

12. Starke, J. R. & Donald, P. R., editors. Handbook of child and adolescent tuberculosis. New York: Oxford University Press. 2016.

13. Sanso, K. T. & Medlar, M. D. Studies of the Bacillus-Calmette-Guerin strain of the tubercle bacillus. Tubercle 12, 214-219 (1931).

14. Cronje, L. PhD Thesis: Surface modification of styrene maleic anhydride nanofibers for efficient capture of *Mycobacterium tuberculosis*. Stellenbosch. 2012.

15. Buddle, B. M., Parlane, N. A., Keen, D. L., Aldwell, F. E., Pollock, J. M., Lightbody, K. E. N. & Andersen, P. Differentiation between Mycobacterium bovis BCG-Vaccinated and M. bovis - Infected Cattle by Using Recombinant Mycobacterial Antigens. American Society for Microbiology 6, 1-5 (1999).

16. Mullis, S. N. & Falkinham, J. O. Adherence and biofilm formation of Mycobacterium avium, Mycobacterium intracellulare and Mycobacterium abscessus to household plumbing materials. Journal of Applied Microbiology 115, 908-914 (2013).

17. Jarher, V. & Nikaido, H. Mycobacterial cell wall: Structure and role in natural resistance to antibiotics. FEMS Microbiology Letters 123, 11-18 (1994).

18. Lambrecht, R. S., Carriere, J. F. & Collins, M. T. A Model for Analyzing Growth Kinetics of a Slowly Growing Mycobacterium sp. Applied and Environmental Microbiology 54, 910-916 (1988).

19. Hirabayashi Jun & Walker, J. M., editors. Lectins Methods and Protocols. Humana Press. 2014.

20. Kim, B. C., Nair, S., Kim, J., Kwak, J. H., Grate, J. W., Kim, S. H. & Gu, M. B. Preparation of biocatalytic nanofibres with high activity and stability via enzyme aggregate coating on polymer nanofibres. Nanotechnology 16, 382-388 (2005).

21. Newton, S., Brent, A., Anderson, S. & Whittaker, E. Paediatric Tuberculosis. The Lancet Infectious Diseases 8, 498-510 (2010).

22. Frieden, T. Toman's Tuberculosis Case detection, treatment and monitoring - questions and aswers. Geneva: World Heath Organisation. 2004.

23. Peñuelas-urquides, K., Villarreal-treviño, L., Silva-ramírez, B., Rivadeneyra-espinoza, L., Said-fernández, S. & Len, M. B. De. Measuring of *Mycobacterium tuberculosis* growth. A correlation of the optical measurements with colony forming units. Brazilian Journal of Microbiology 1, 287-290 (2013).

24. Patin, S., Alamo, L., Cimino, M., Casart, Y., Bartoli, F., García, M. J. & Salazar, L. Autofluorescence of Mycobacteria as a Tool for Detection of *Mycobacterium tuberculosis*. Journal of Clinical Microbiology 46, 3296-3302 (2008).

Chapter 6

Conclusions and recommendations

6.1 Conclusions

The surface modification and characterisation of poly(ethylene terephthalate) (PET) microfibrous substrates were presented in this thesis. Specifically, these substrates were altered to express the adhesin, Concanavalin A (Con A) on their surface. The ability of these fibres to entrap and capture *Mycobacterium tuberculosis* (*Mtb*) was evaluated by conducting an affinity study with bacillus Calmette-Guérin (BCG), an attenuated strain of Mycobacterium bovis.

The objectives, as defined in Chapter 1, have predominantly been met. As such, it can be concluded that PET microfibres are a suitable starting material to utilise for the preparation of *Mtb* capture platforms.

6.1.1 Selective degradation of PET

PET microfibres were subjected to hydrolysis or amination reactions, to generate hydroxyl or a combination of primary amine and hydroxyl groups respectively, on the fibre surfaces. These modified surfaces could then act as precursor scaffolds for subsequent modification reactions, utilising the newly introduced functionalities.

While characterisation of the functionalities was aided by means of staining tests, quantitative assessment of the yields could only be approached semi-quantitatively for the aminated fibres.

6.1.2 Surface activation with glutaraldehyde and subsequent Con A immobilisation

The primary amine groups of the aminated PET fibres were activated with glutaraldehyde (GA). Due to the auto-fluorescent properties of GA, its presence on the surface of the fibres was confirmed by confocal fluorescence microscopy (CFM).

Con A was immobilised onto the activated PET fibre surfaces. Its presence was confirmed by attenuated total reflectance Fourier transform infrared (ATR-FTIR) spectroscopy and scanning electron microscopy (SEM). By making use of a Con A-fluorescein isothiocyanate conjugate, the presence of the immobilised protein could be visually confirmed by CFM. By subjecting the protein functionalised fibres to a horseradish peroxidase (HRP) assay, the presence of biologically active Con A on their fibre surfaces was confirmed.

The use of correlative light-electron microscopy (CLEM) as a means of detecting immobilised Con A, was assessed. It was not found to be a viable technique for evaluating the degree of protein immobilisation, and its ability to detect the immobilised protein was limited to high protein loadings.

6.1.3 Surface activation with N,N'-Disuccinimidyl carbonate and subsequent Con A immobilisation

N,N'-disuccinimidyl carbonate (DSC) was used to activate the hydroxyl and primary amine groups on the surfaces of aminated PET fibres. This activated surface could then mediate the immobilisation of Con A.

The presence of Con A on the fibre surfaces was confirmed by ATR-FTIR spectroscopy and SEM. From a HRP assay, both the presence and the biological activity of the protein was confirmed.

6.1.4 Affinity studies

Affinity studies between the functionalised fibres and BCG were performed to determine whether or not the substrates could perform as capture platforms for *Mtb*. The interaction between the fibres and the bacteria were observed and evaluated by means of SEM and CFM.

From the affinity study, it could be concluded that BCG capture ability was greater for fibres with a Con A surface functionality, compared to PET-NH_2 control study fibres. It was also found that the cross-linked protein aggregate (CLPA) derivatives showed the greatest affinity for BCG.

From the dilution study it was found that the Con A bearing fibres were able to efficiently capture and concentrate BCG bacteria down to culture concentrations with an optical density measured at 600 nm (OD_{600}) value of 0.003.

6.2 Recommendations for future research

The work presented in this study was performed in a manner which makes its results comparable to a number of similar studies. The methods and tests were standardised, producing applicable as well as valid data. The study, however, remains unique in several regards and holds great potential for future iterations. There exist parameters which may benefit from slight adjustments.

6.2.1 Analysis

The greatest challenge associated with this study was the limited solubility of PET. Hence, surface analysis techniques proved to be the best means of acquiring data, with concern to modifications to the PET materials.

A technique which has the potential to be particularly proficient at tracking changes to the material chemistry is CFM. While it does require fluorophore tagging of functionalities, the produced effect is a honed in image of only the tagged compounds.

The electrophilic activation of PET is an area of the study which would particularly benefit from such an analysis. By using fluorophores which contain primary amine groups, the presence and reactivity of the activating groups can be assessed by CFM.

6.2.2 Material selection

Another challenge encountered, was the use of unbound microfibres. While their use was integral to the final substrates produced, and likely increased their efficiency as capture platforms, they are not well suited for analysis. To circumvent this, a material with similar properties might be considered. A well-suited candidate is spunbond nonwoven PET. This will allow for better microscopy analysis of the material, as well as permit quantitative elemental surface analysis.

6.2.3 Affinity studies

In addition to affinity studies performed, a real-world case study should be conducted. This should include realistic incubation and preparation procedures typically followed during mainstream diagnosis of tuberculosis.

The importance of this point comes to bear when considering the eventual intent of the materials created in this study. While the affinity studies performed are applicable, they are highly theoretical and ideal. Moving closer to a real-world scenario would provide additional parameters which need to be considered. This is especially important in relation to the form factor and durability of the substrates, since changes to the material structure and morphology could influence the adhering ability of the bacteria.